X-RAY STUDY OF DYNAMICS OF GROWING WETTING FILMS

A THESIS

PRESENTED TO THE

SCHOOL OF GRADUATE STUDIES

ADDIS ABABA UNIVERSITY

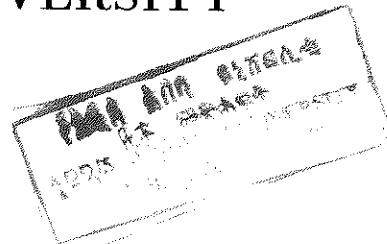

IN PARTIAL FULFILLMENT OF

THE REQUIREMENTS FOR THE DEGREE OF

MASTER OF SCIENCE IN PHYSICS

BY

HAGOS WOLDEGHEBRIEL

ADDIS ABABA

June 1996

Acknowledgement

I am extremely grateful to my advisor Prof. Dr. Werner Press who has enabled me to join the research group at the Institute of Experimental Physics. University Kiel. Germany and for his constant assistance. invaluable guidance and for his friendly encouragement without any reservation during the whole period of my research work at the Institute.

My experiments were done together with Mr. Peter-Mueller-Buschbaum. a PhD student in the group. It is my pleasure to express my heartfelt gratitude to him for his immediate advice. guidance and friendly encouragement throughout the work.

I would like to express my due thanks to all members of the group for their unreserved assistance while I was carrying out my experiments. I am particularly grateful to Dr. M. Tolan. Dr. B. Asmussen. M. Mueller. O. Seeck. M. Strzelczyk. J. Stettner. M. Seeger. D. Hupfeld. O. Bahr. M. Kalning and M. Luett for their valuable suggestions and useful advises accounted in dealing my research.

I am also greatly indepted to my advisor Dr. Ulrich Stutenbaeumer. Addis Ababa University, for his helpful comments and suggestions.

Finally, I would like to thank DAAD for financing the work.

Abstract

NRC ARMY SYSTEMS LIBRARIES

The dynamics of growing wetting films is studied by the method of x-ray scattering in the region of total external reflection. With a short pulse disturbance caused by a temperature difference between the substrate and the vapour in the x-ray cell, the wetting film thickness is reduced. Afterwards the time dependence of the growing film is monitored by x-ray reflectivity measurements. The examined sample systems are H_2/Si, CH_3/Si, Ge/Si and a quartz glass wetted by a liquid film of CCl_4. The observed growth kinetics of the wetting layers are discussed in the framework of a model which is adapted to the experimental conditions, particularly the finite temperature stability of the experimental set-up. From the growth law $l(t) \propto 1 - \exp[-(t/\tau)^n]$ fitted to the data, the time constants τ and the dynamic exponent n are determined. The quantity n depends on the dimension of the growth mechanism.

Contents

LIBRARIES

Acknowledgement i

Abstract ii

1 Introduction 1

2 Theory of X-Ray Scattering 3

2.1 X-Ray Scattering in the Region of Total External Reflection 3

2.2 Specular Scattering 5

2.3 Diffuse Scattering 10

3 Theory of Growing Wetting Films 13

3.1 Wettability 13

3.2 Van der Waals Force and the Hamaker Constant 14

3.3 Film Thickness 17

3.4 Kolmogorov Model for Film Growth 22

4 Sample Systems 25

4.1 The Substrates 25

4.1.1 Silicon Wafer 25

4.1.2 Quartz Glass 26

4.2 The Adsorbate 26

5 Experimental Set-up and Scattering Geometry 28

5.1 Experimental Set-up 28

5.2 Scattering Geometry 29

6 Measurements and Evaluation 31

6.1 Dry Substrates 31

6.1.1 H_2/Si Substrate 33

6.1.2 CH_3/Si Substrate 34

6.1.3 Ge/Si Substrate 36

6.1.4 Quartz glass 37

6.2 Wetting Experiments 39

6.2.1 CCl_4 on H_2/Si 40

6.2.2 CCl_4 on CH_3/Si 47

6.2.3 CCl_4 on Ge/Si 54

6.2.4 CCl_4 on a Quartz Glass 58

7 Discussion 65

7.1 Adaption of the growth measurements to the Kolmogorov Model 65

7.2 Concluding Remarks 68

A Appendix 70

References 77

Chapter 1

Introduction

Much recent work, both theoretical and experimental, for example see reviews[8,11], has been devoted to the study of wetting transitions; most of them focus on the properties of wetting layers in thermal equilibrium. It is also of interest, however, to study how such layers approach equilibrium, i.e., growth of liquid films, if they are far away from it. A liquid film is adsorbed on a substrate surface leading to an interface between the adsorbed liquid phase and the gas phase in the bulk. A solid surface in contact with a vapour in coexistence with its liquid can be classified as completely or incompletely wet, depending on whether the surface-adsorbed liquid film is macroscopically thick or microscopically thin. In the case of complete wetting the film grows only in one direction, which means that the thickness of the liquid layer monotonously increases with time.

In this paper the growth of liquid CCl_4 film on a Si coated with H_2, Ge and CH_3 and on a quartz glass substrates is investigated. All these substrates provide the case of complete wetting with a build up of stable film thickness. The thickness was first reduced by a short pulse disturbance and afterwards the evolution of a stable film was observed over days.

To study the dynamics of growing films we use x-ray specular reflectivity scans near total external reflection. With Parratt's approach[28], the resulting film thickness as a function of time is obtained by fitting the x-ray reflectivity data. The experiment was done in the "Institute of Experimental Physics of the Christian-Albrechts-University" Kiel -Germany, with a three-crystal diffractometer and a laboratory x-ray tube.

The paper is structured in the following sequence: After the introduction a brief

description of the theory of x-ray scattering, with more emphasis on specular reflection, is given. In chapter three the film thickness as a function of a differential heating temperature is derived based on van der Waals interaction with the Hamaker constant therein. Also, the Kolmogorov growth model is explained in this chapter. Chapter four deals with the properties of the sample systems used in the experiment. Next to this chapter the experimental set-up and the scattering geometry are given. In chapter six we present the x-ray determined parameters of the bare substrates and their corresponding wetting systems. The adaption of the experimentally determined film thickness with the time dependent growth model is left for chapter seven. Afterwards, a discussion with a concluding remark finishes the work.

Chapter 2

Theory of X-Ray Scattering

Electromagnetic waves scatter, diffract and interfere. Reflection is the result of the constructive interference of many scattered or diffracted waves originating from scattereres in a stratified medium. The reflection of a monochromatic wave can be analyzed as that of a superposition of general electromagnetic waves. For a given angular frequency, ω, the time dependence of all fields is carried in the factor exp(-iωt).

2.1 X-Ray Scattering in the Region of Total External Reflection

The propagation of an electromagnetic plane wave $\vec{E}(\vec{r}) = \vec{E}_0 \exp\{i(\vec{k} \cdot \vec{r} - \omega t)\}$ in a medium characterized by an index of refraction n follows from Maxwell's equations to obey the Helmholtz equation:

$$\vec{\nabla}^2 \vec{E}(\vec{r}) + \vec{k}^2 n^2 \vec{E}(\vec{r}) = 0 \qquad (2.1)$$

where $|\vec{k}| = \omega/c$ is the wavevector and ω and c are the frequency and speed of the electromagnetic wave, respectively.

The index of refraction is given in[18] by

$$n = 1 - \frac{N_a r_o \lambda^2 \rho}{2\pi A} \sum_j f_j, \qquad (2.2)$$

where

λ is the wavelength of photons, ρ the density of substance, N_a the Avogadro's number,

A the molecular weight, r_o the classical electron radius, and f_j the atomic scattering factor.

The effective number of electrons contributing to the scattering is affected by the presence of absorption edges. Denoting the form factor of the atom by

$$f_j = Z_j + f'_j(\lambda) + i f''_j(\lambda), \tag{2.3}$$

the index of refraction n can be expressed as

$$n = 1 - \delta - i\beta \tag{2.4}$$

where

$$\delta = \frac{N_a r_o \lambda^2 \rho}{2\pi A} \sum_j (Z_j + f'_j) \tag{2.5}$$

is called the dispersion, and

$$\beta = \frac{N_a r_o \lambda^2 \rho}{2\pi A} \sum_j f''_j \tag{2.6}$$

the absorption (extinction) coefficient. The parameters δ and β are of the order of 10^{-7} to 10^{-5} (dimensionless quantities).

Because the refractive index of a substance for x-rays is less than unity it is possible to obtain total external reflection from a surface, since the x-rays, on entering the substance from the air (vacuum), are going into a medium of smaller refractive index. Then, the laws of refraction lead to the result that x-rays should be totally reflected from a plane surface at all glancing angles smaller than a certain critical angle α_c, given by

$$\cos\alpha_c = 1 - \delta. \tag{2.7}$$

Since δ and α_c are small, on expanding the cosine we get

$$\alpha_c = \sqrt{2\delta}. \tag{2.8}$$

We consider now the situation of a plane x-ray wave in vacuum impinging on a flat surface of a crystal (at z=0) under a shallow angle α_i which is in the vicinity of the critical angle α_c. The linearly polarized incident x-ray wave field $\vec{E}_i(\vec{r}) = \vec{E}_o \exp\{i\vec{k}\cdot\vec{r}\}$ reads in the coordinate system of Fig. 2.1 as

$$\vec{E}_i = E_{i\parallel} \begin{pmatrix} \sin\alpha_i \\ 0 \\ -\cos\alpha_i \end{pmatrix} + E_{i\perp} \begin{pmatrix} 0 \\ 1 \\ 0 \end{pmatrix} \tag{2.9}$$

and

$$\vec{k}_i = k \begin{pmatrix} \cos\alpha_i \\ 0 \\ \sin\alpha_i \end{pmatrix} \tag{2.10}$$

where $E_{i\parallel}$ and $E_{i\perp}$ denote the components of the electric field vector parallel and perpendicular to the plane of incidence (x-z plane).

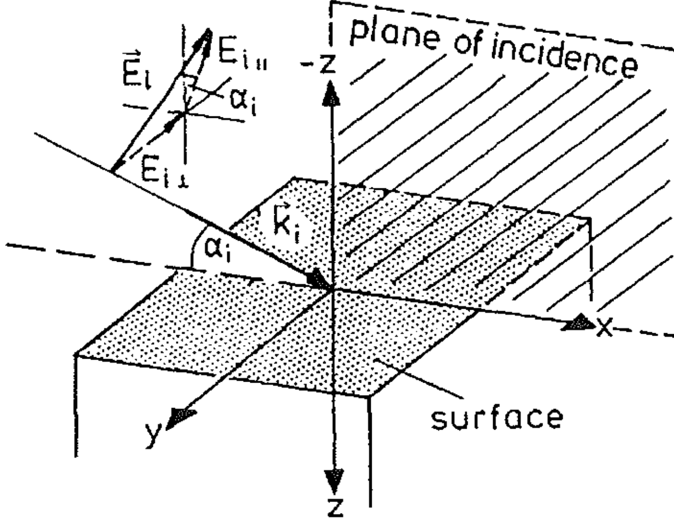

Figure 2.1: *Monochromatic x-ray with wave vector $\vec{k}_i$ and field vector $\vec{E}_0$ impinging onto an interface (at z = 0) at an incidence angle α_i[9].*

2.2 Specular Scattering

Specular scattering is the result of the constructive interference of many scattered or re-radiated waves. In the specular case the angle of incidence is equal to the angle of scattering ($\alpha_i = \alpha_f$).

Assuming a system consisting of N layers $j = 1, 2, ..., N$, such that, the refractive index n_j of layer j is $n_j = 1 - \delta_j - i\beta_j$ with the dispersion δ_j and the absorption β_j, the Fresnel-reflection and transmission coefficients for each (smooth) interface [27] are

$$r_{j-1,j} = \frac{k_{z,j-1} - k_{z,j}}{k_{z,j-1} + k_{z,j}} \tag{2.11}$$

and

$$t_{j-1,j} = \frac{2k_{z,j-1}}{k_{z,j-1} + k_{z,j}} \tag{2.12}$$

respectively. Here $k_{z,j}$ is the z component of the wavevector in medium j. The jth interface lies between the $(j-1)^{th}$ and the $(j)^{th}$ layers where layer 0 is assumed to be vacuum.

and the interface j=1 is the free surface (see Fig. 2.2).The z-axis is perpendicular to the surface and its origin lies at the surface ($z_1 = 0$); the x-axis lies in the incidence plane.

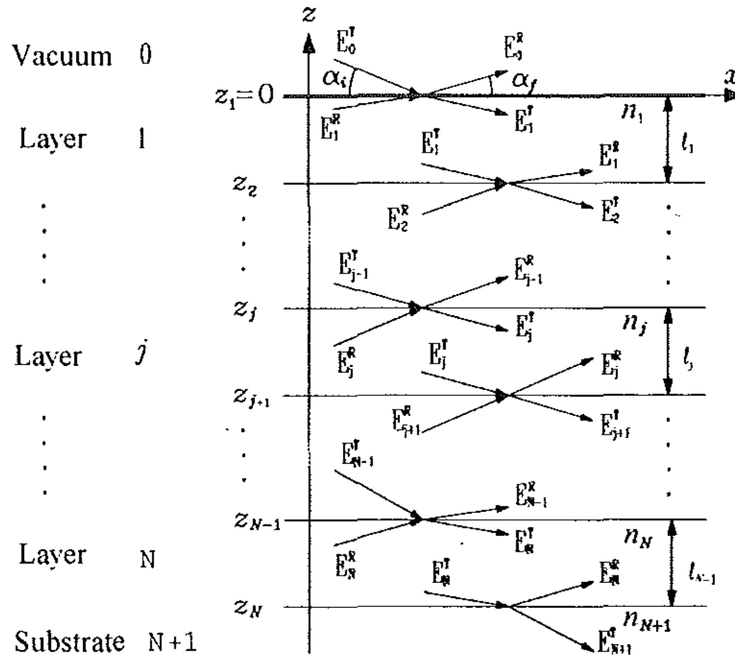

Figure 2.2: *A model of an x-ray scattering in a multilayer system.*

In each layer of thickness $l_j (l_j = |z_{j+1} - z_j|)$ the component of the wavevector normal to its surface, which is determined by the law of refraction, is

$$k_{z,j} = k_j \sin(\alpha_j) \approx k_i(n_j^2 - \cos^2 \alpha_i)^{1/2} = \frac{2\pi}{\lambda}\sqrt{\alpha_i^2 - 2(\delta_j + i\beta_j)}. \qquad (2.13)$$

This expression is valid only for small incident angles α_i. The optical constants δ_j and β_j of each layer j are defined by the complex index of refraction, eq. (2.4). They are proportional to the density ρ_j of each layer. The glancing angle of incidence is α_i and $k_i = k_f = 2\pi/\lambda = k_1$ denotes the modulus of the incoming wavevector (and λ is the x-ray wavelength).

To calculate reflectivity curves for single and multiple layered systems, we follow the treatment of Parratt[28] first formulated for the case of metal-dielectric layers. This formalism is based on Maxwell's theory applied to a system of N parallel layers from which x-rays undergo multiple reflection and refraction. The reflectivity of a layered system as a function of the incident angle α_i and the layer thickness l_j (between interfaces at z_j and z_{j+1}) can be expressed in terms of a recursive formula as

$$R_{j-1}(l_j) = \frac{r_{j-1,j} + R_j(l_{j+1})\exp[2ik_{z,j}l_j]}{1 + r_{j-1,j}R_j(l_{j+1})\exp[2ik_{z,j}l_j]} \qquad (2.14)$$

with the Fresnel-reflectivity of one smooth interface $r_{j-1,j}$ given by eq. (2.11). Here $R_j = E_j^R/E_j^T$ is the ratio of the amplitudes of outgoing and incoming x-ray waves.

In the case of rough interfaces, the Fresnel coefficient, eq. (2.11), has to be replaced by that of a rough interface in the recursion formula. Numerical tests show, however, that in the case of relatively small roughnesses ($\sigma \sim 10$Å) this procedure is indistinguishable from fitting a density profile of the whole system to the reflectivity data [27]. If a probability density function in z-direction

$$P_{\tanh}(z) = \frac{1}{\sqrt{2\pi}\cosh^2(\sqrt{2/\pi}\,z/\sigma)} \tag{2.15}$$

for the roughness distribution is chosen, an analytical solution for the tanh-refractive index profile between media $j-1$ and j is found [21] as

$$n(z) = \frac{n_j + n_{j-1}}{2} + \frac{n_j - n_{j-1}}{2}\tanh(\sqrt{2/\pi}\frac{z}{\sigma_j}), \tag{2.16}$$

where σ_j is the root-mean square roughness of the $(j)^{th}$ layer. Figs. 2.3 and 2.4 show

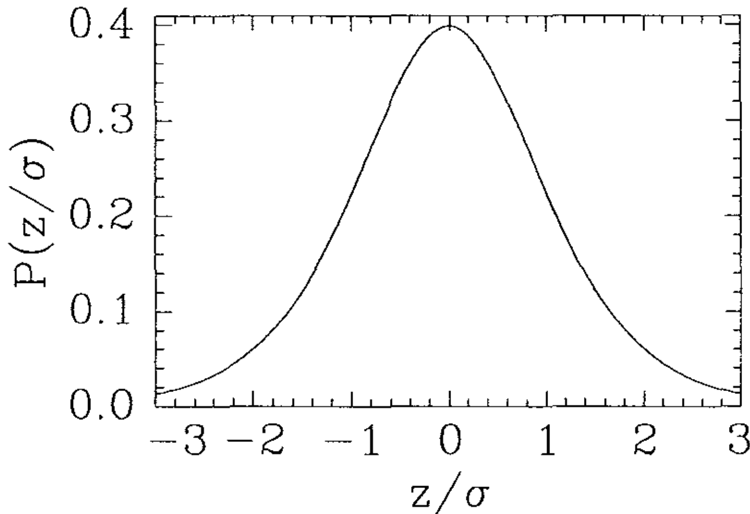

Figure 2.3: *Assumed Gaussian roughness distribution function.*

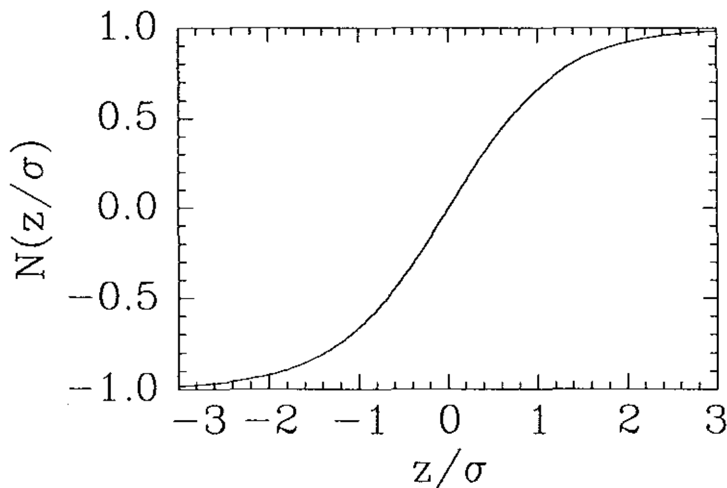

Figure 2.4: *Tanhyperbolic density profile.*

the assumed Gaussian roughness distribution function and the tanhyperbolic density profile, respectively, with

$$\mathcal{N}(z/\sigma) = \frac{(n(z/\sigma) - n_{j-1}) + (n(z/\sigma) - n_j)}{n_j - n_{j-1}}. \tag{2.17}$$

Eq. (2.16) has the advantage that the Helmholtz eq. (2.1) of the electromagnetic field can be solved analytically. The resulting reflection coefficient of one rough interface with the above roughness distribution now leads to [21]

$$r_{j-1,j} = \frac{\sinh[\sigma_j(\pi/2)^{3/2}(k_{z,j-1} - k_{z,j})]}{\sinh[\sigma_j(\pi/2)^{3/2}(k_{z,j-1} + k_{z,j})]} G(k_{z,j-1}, k_{z,j}, \sigma_j). \tag{2.18}$$

where $G(k_{z,j-1}, k_{z,j}, \sigma_j)$ is a relatively complicated expression in $k_{z,j-1}, k_{z,j}, \sigma_j$. But numerical tests show that the factor G is equal to one for roughnesses σ_j up to 100Å [31].

When a thick film is grown on the substrate, the experiment shows that a dip, Fig. 2.5, is observed at a certain incident angle between the critical angles of the substrate and the adsorbate, provided that the critical angles fulfill the condition

$$\alpha_{fc} \leq \alpha_{dip} \leq \alpha_{sc} \tag{2.19}$$

where α_{fc} and α_{sc} are the critical angles of the film and substrate, respectively.

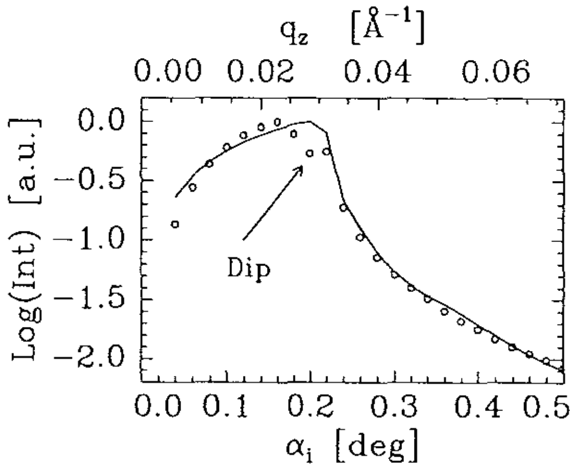

Figure 2.5: *A reflectivity scan taken from the system CCl_4 on CH_3/Si which shows an intensity dip at a film thickness of 270Å.*

For a thick film of thickness l, incident angle α_1 and angle of refraction α_2, the recursion formula reduces to[35]

$$R = \left| \frac{r_1 + r_2 \exp(2ik_1\alpha_2 l)}{1 + r_1 r_2 \exp(2ik_1\alpha_2 l)} \right|^2. \tag{2.20}$$

The quantities k_1 and k_2 are the wavevector of the incident and refracted waves, respectively, and r_1 and r_2 are the Fresnel-reflectivities at the two interfaces (z_1 and z_2), see Fig. 2.6. At an angle of incidence $\alpha_{dip}(\alpha_1 = \alpha_{dip})$ between the critical angles of the film and the substrate, the Fresnel-coefficient reduces to

$$r_1 = \frac{\alpha_{dip} - \alpha_2}{\alpha_{dip} + \alpha_2}. \tag{2.21}$$

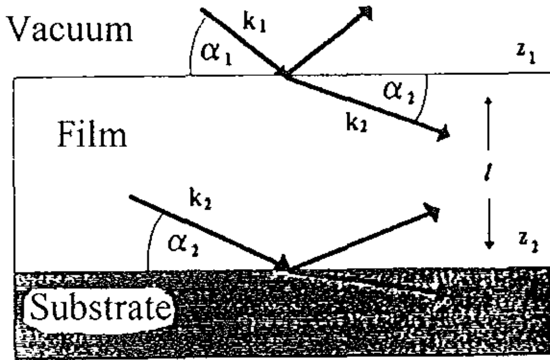

Figure 2.6: *Representation of x-ray scattering from a one layer structure[35].*

Here we consider radiation from a non-absorbing medium (real n_1) onto an absorbing medium (complex n_2). Thus the angle of refraction is complex, and has a formal meaning only and we write

$$\alpha_2 = \alpha_r + i\alpha_I. \tag{2.22}$$

The real and imaginary parts, α_r and α_I, can be expressed in terms of the dispersion δ and the absorption β of the film as[25]

$$\alpha_r = \frac{1}{\sqrt{2}}\left[\sqrt{(\alpha_{dip}^2 - 2\delta)^2 + 4\beta} + (\alpha_{dip}^2 - 2\delta)\right]^{1/2}, \tag{2.23}$$

$$\alpha_I = \frac{1}{\sqrt{2}}\left[\sqrt{(\alpha_{dip}^2 - 2\delta)^2 + 4\beta} - (\alpha_{dip}^2 - 2\delta)\right]^{1/2}. \tag{2.24}$$

Eq. (2.20) can now be transformed into a relation between the reflectivity R and the film thickness l of the wetting layer:

$$l = C\frac{R(\alpha_{dip}) - 1}{R(\alpha_{dip}) + 1}. \tag{2.25}$$

Here R is the reflectivity at the angular position α_{dip} of the intensity dip, and C a constant which is given by:

$$C = \frac{\lambda}{8\pi}\frac{1 + |r_1|^2 + 2|r_1|\cos(\Delta\alpha)}{|r_1|[\alpha_r \sin(\Delta\alpha) + \alpha_I \sin(\Delta\alpha)]}. \tag{2.26}$$

The Fresnel-reflectivities of the vacuum-layer and layer-substrate interfaces are denoted by r_1 and r_2, respectively, and the angles $\alpha_{1,2}$ are defined via the eq: $r_j = |r_j|\exp(i\alpha_j)$ with $j = 1,2$ and ($\Delta\alpha = \alpha_1 - \alpha_2$).For a film thickness $l < 500$Å the dependence of l on the reflectivity at the dip eq. (2.25) is linear[35].

2.3 Diffuse Scattering

X-ray reflection has frequently been used for structure studies of crystalline and amorphous layers and multilayers. By measuring the specular reflectivity, the thickness and electron densities of the layers can be determined and the root-mean-square (rms) roughnesses of the interfaces can be estimated. From the non-specular reflectivity (diffuse scattering), the correlation function of the interface roughness profile can be reconstructed. The specular reflected wave consists of the coherent wave and of the part of the incoherent wave propagating in the direction of specular reflection ($q_r = 0$). The non-specularly reflected wave is incoherent. If we neglect the divergence of the primary beam irradiating the sample, the coherent wave is plane and the incoherent wave is divergent (diffuse). The diffuse scattering can be described using the formalism of the differential scattering cross-section[31].

$$
\begin{aligned}
\left(\frac{d\sigma}{d\Omega}\right)_{diffuse} &= \frac{\Upsilon k_1^2}{16\pi^2}\sum_{j,k=1}^{N}(n_j^2 - n_{j+1}^2)(n_k^2 - n_{k+1}^2)^* \,\widetilde{C}_{jk}(q_r). \\
&\sum_{m,n=0}^{3} \widetilde{G}_j^m \,\widetilde{G}_k^{n^*} \exp[-\tfrac{1}{2}((q_{z,j}^m\sigma_j)^2 + (q_{z,k}^{n^*}\sigma_k)^2)] \\
&= \frac{\Upsilon k_1^2}{16\pi^2}\Big(\sum_{j=1}^{N} |n_j^2 - n_{j+1}^2|^2 \,\widetilde{C}_j(q_r). \\
&|(\widetilde{G}_j^o + \widetilde{G}_j^3)\exp[-\tfrac{1}{2}(\sigma_j q_{z,j}^o)^2] + (\widetilde{G}_j^1 + \widetilde{G}_j^2)\exp[-\tfrac{1}{2}(\sigma_j q_{z,j}^1)^2]|^2 \\
&+ \sum_{\substack{j,k=1 \\ k\neq j}}^{N} (n_j^2 - n_{j+1}^2)(n_k^2 - n_{k+1}^2)^* \,\widetilde{C}_{jk}(q_r). \\
&\sum_{m,n=0}^{3} \widetilde{G}_j^m \,\widetilde{G}_k^{n^*} \exp(-\tfrac{1}{2}((q_{z,j}^m\sigma_j)^2 + (q_{z,k}^{n^*}\sigma_k)^2))\Big)
\end{aligned}
\tag{2.27}
$$

The illuminated area of the sample is denoted by Υ, $q_j^m = (q_r, q_{z,j}^m)^T$ is the momentum transfer within each layer, and $\widetilde{C}_j(q_r)$ and $\widetilde{C}_{jk}(q_r)$ are the Fourier-transforms of the auto- and cross- correlation functions of the interface[31]. Furthermore, the factors $\widetilde{G}_j^m$ are defined by

$$
\widetilde{G}_j^m = G_j^m \exp[-iq_{z,j}^m z_j] \tag{2.28}
$$

with the respective expressions for G_j^m given in [35].

To analyze x-ray diffraction data, particular correlation functions for the interface and the strength of the correlations between different layers have to be assumed. The correlation functions contain the information about the morphology of the surface.

The shape of the interface j at the position $z_j(R) = z_j + \phi_j(R)$ [31] can be statistically described via the so-called height-height correlation function $C_j(R)$ which is defined by

$$C_j(\vec{R}) = < \phi_j(r)\phi_j(\vec{r}+\vec{R}) >_r = \int d\vec{r}\phi_j(\vec{r})\phi_j(\vec{r}+\vec{R}). \qquad (2.29)$$

Here $\vec{R} = (x, y)^T$ and $\vec{r}$ are vectors within the surface and $< ... >_r$ means the average over the (x,y)-plane. The (single valued) function $\phi_j(\vec{R})$ is the height fluctuation of the interface z_j at a lateral position $\vec{R}$ with roughness $\sigma_j = \sqrt{C_j(0)}$ and vanishing mean value $< \phi_j(\vec{r}) >_r$.

For the solid-solid and solid-liquid interfaces $C_j(\vec{R})$ is represented by the correlation function[32] of a self-affine fractal surface [33]

$$C_j(R) = \sigma_j^2 \exp[-(R/\xi_j)^{2h_j}] \qquad (2.30)$$

with the correlation length ξ_j and the Hurst-parameter h_j of the respective interfaces[33]. The quantity ξ_j describes the lateral length scale on which the interface begins to look rough. For $R < \xi_j$ the surface is self-affine rough where as for $R \geq \xi_j$ the surface looks smooth. The parameter h_j is restricted to the region $0 < h_j \leq 1$ and defines the fractal box-dimension $D_j = 3 - h_j$ of the interface. Small values of h_j produce extremely jagged surface while values close to one lead to interfaces with smooth hills and valleys. For clarity see Fig. 2.7, which shows possible real structures which are calculated assuming the correlation function given by eq. (2.30) with different ξ_j and h_j values respectively.

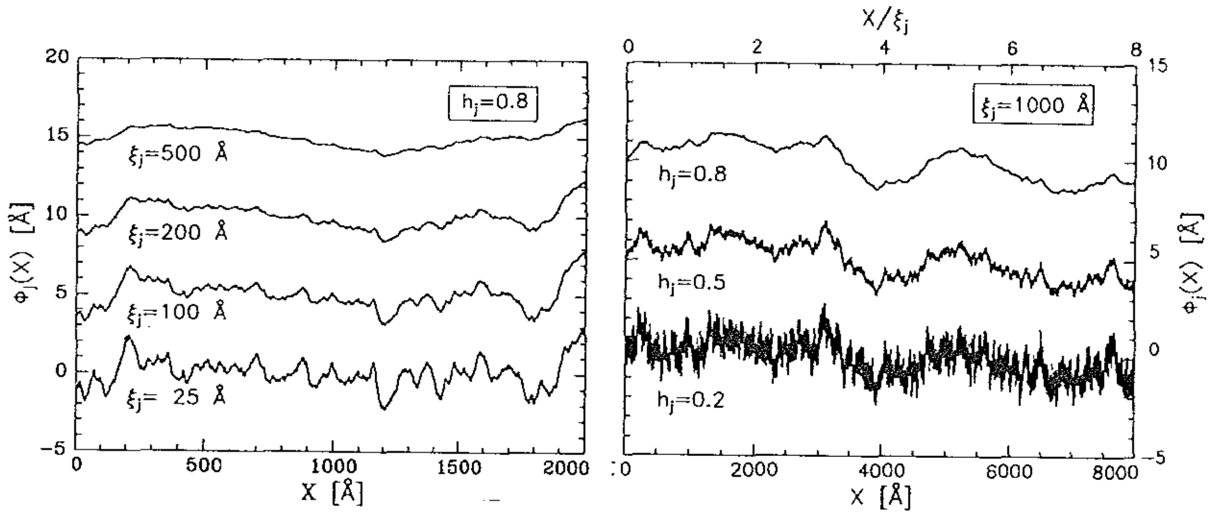

Figure 2.7: *Calculations of possible one -dimensional surface structures using the correlation function given by eq. (2.30) for various kinds of the parameters ξ and h[30]. Always a rms -roughness of σ =1Å was assumed[31].*

Chapter 3

Theory of Growing Wetting Films

3.1 Wettability

The formation of liquid drops on a substrate is a common phenomenon. What makes it interesting is the fact that the macroscopic shape of such a drop is intimately related to the three surface tensions(energy per unit area) associated with the three interfaces meeting at the contact line between the drop and the substrate: γ_{LS} the liquid-substrate. γ_{VS} the gas-substrate, and ($\gamma_{VL} = \gamma$) the gas-liquid surface tensions. These parameters describe adequately the energy content of the interfaces in the far field (far from the line of contact). In equilibrium the energy must be stationary with respect to any shift (dx) of the line position. Hence the contact angle is related as[41]

$$\gamma_{VS} - \gamma_{LS} - \gamma \cos \Theta = 0, \tag{3.1}$$

where Θ refers to the contact angle at equilibrium. Eq. (3.1) shows that the contact angle is entirely defined in terms of thermodynamic parameters.

When a small liquid droplet is put in contact with a flat solid surface, three distinct equilibrium regimes may be found. The contact angle Θ permits a classification for the wettability of a substrate by an adsorbate: for Θ=0 the substrate is called wet, for $\Theta < \pi$ non-wet, and for $\Theta = \pi$ dry (see Fig. 3.1). For complete wetting (Θ=0) we have

$$\gamma = \gamma_{VS} - \gamma_{LS}. \tag{3.2}$$

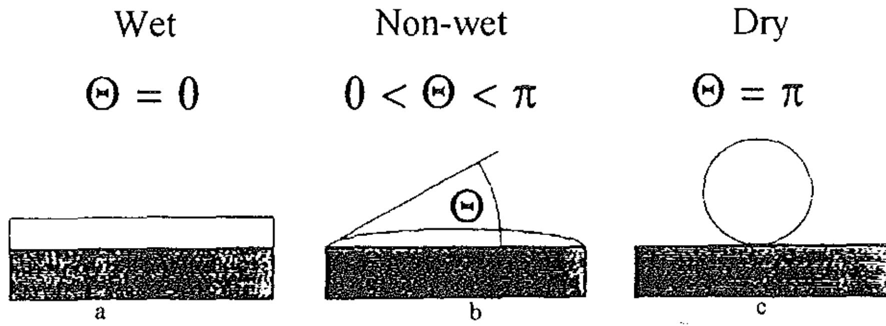

Figure 3.1: *A small droplet in equilibrium over a horizontal surface: a, b and c correspond to complete wetting, partial wetting and dry with Θ=0, (0,π) and π, respectively[11].*

3.2 Van der Waals Force and the Hamaker Constant

This paper is mainly concerned with intermolecular forces essentially electrostatic in origin. Once the spatial distribution of the electron clouds has been determined by solving the Schroedinger equation, the intermolecular forces may be calculated on the basis of classical electrostatics.

Thus, for two charges, we have the familiar inverse- square Coulomb force, while for moving charges we have electromagnetic forces, and for complex fluctuating charge distributions occurring in and around atoms, we obtain the various interatomic and intermolecular bonding forces.

There are three distinct types of forces contributing to the van der Waals force: namely, the induction force, the orientation force and the dispersion force, each of which has an interaction free energy that varies with the inverse sixth power of the distance. Thus, the total van der Waals interaction energy is given by

$$W_{VDW}(r) = -\frac{C_{VDW}}{r^6} = -\frac{(C_{ind} + C_{orient} + C_{disp})}{r^6}. \tag{3.3}$$

In 1963 McLachlan[24] presented a generalized theory of van der Waals forces, which included in one equation the induction, orientation and dispersion forces. McLachlan's expression for the van der Waals free energy of two molecules or small particles 1 and 2 in medium 3 is given by the series [17]

$$w(r) = -\frac{6kT}{(4\pi\varepsilon_o)^2 r^6} \sum_{n=0,1,2,\cdots}^{\infty}{}' \frac{\alpha_1(i\nu_n)\alpha_2(i\nu_n)}{\varepsilon_3^2(i\nu_n)}. \tag{3.4}$$

where $\alpha_1(i\nu_n)$ and $\alpha_2(i\nu_n)$ are the polarizabilities of molecules 1 and 2 and $\varepsilon_3(i\nu_n)$ the dielectric permitivity of medium 3 at imaginary frequencies $i\nu_n$, with

$$\nu_n = \frac{2\pi kT}{h}n \approx 4 \times 10^{13} n s^{-1} \tag{3.5}$$

at 300K and where the prime over the summation indicates that the zero frequency $n = 0$ term is multiplied by 1/2.

Dispersion forces generally exceed the dipole -dependent induction and orientation forces except for small highly polar molecules, such as water. In the interaction between two dissimilar molecules of which one is non -polar, the van der Waals energy is almost completely dominated by the dispersion contribution.

The van der Waals interaction energy between two dissimilar molecules A and B is usually intermediat between the values for A-A and B-B. In fact, the coefficient C_{VDW} for A-B is often close to the geometric mean of A-A and B-B.

When two atoms are an appreciable distance apart, the dispersion energy between them begins to decay faster than $-1/r^6$, approaching a $-1/r^7$ dependence at r >800Å[27]. This is called the retardation effect, and the dispersion forces between molecules and particles at large separations are called retarded forces. That is, at a greater separation the time taken for the electron field of the first atom to reach the second and return can become comparable with the period of the fluctuating dipole itself. When this happens the field returns to find that the direction of the instantaneous dipole of the first atom is now different from the original and less favorably disposed to an attractive interaction.

In this paper, since the film thickness is smaller than 800Å, the non -retarded case is assumed. At a smaller distance the dispersion interaction energy ($\sim -1/r^6$) is superior over the induction and the orientation energies.

Van der Waals forces play a central role in all phenomena involving intermolecular forces, for while they are not as strong as Coulomb or H-bonding interactions, they are always present. By assuming a non -retarded interaction for an interatomic van der Waals pair potential of the form w(r) = -C/r^6 one may sum (integrate) the energies of all the atoms in one body with all the atoms in the other and thus obtain the two -body potential for an atom near a surface, for a sphere near a surface, or for two flat surfaces. The resulting interaction laws are given in terms of the conventional Hamaker

constant[14] (which measures the strength of the dispersive forces)

$$A = \pi^2 C \rho_1 \rho_2. \tag{3.6}$$

where ρ_1 is the number of molecules per unit volume in material 1, ρ_2 is the number of molecules per unit volume in material 2 and C is the coefficient of r^{-6} in the expression for the dispersion energy between isolated molecules 1 and 2, separated by a distance r.

For the assumed case, non -retarded and dispersion, the Hamaker constant for an interaction of two media 1 and 2 across a third medium 3 is expressed based on the Lifshitz theory[22] as

$$A = \frac{3h}{4\pi}\int_{\nu_1}^{\infty}\left(\frac{\varepsilon_1(i\nu)-\varepsilon_3(i\nu)}{\varepsilon_1(i\nu)+\varepsilon_3(i\nu)}\right)\left(\frac{\varepsilon_2(i\nu)-\varepsilon_3(i\nu)}{\varepsilon_2(i\nu)+\varepsilon_3(i\nu)}\right)d\nu, \tag{3.7}$$

with

$$\rho_i \alpha_i = 2\varepsilon_o \varepsilon_3 \left(\frac{\varepsilon_i - \varepsilon_3}{\varepsilon_i + \varepsilon_3}\right) \tag{3.8}$$

for C eq. (3.4), and i = 1,2 (media 1 and 2, respectively,), where ε_1 ,ε_2 and ε_3 are the static dielectric constants of the three media, $\varepsilon(i\nu)$ are the values of ε at imaginary frequencies.

To obtain the Hamaker constant for any system we first need to know how the dielectric permitivity of the media vary with frequency, after which we can integrate eq. (3.7) to obtain A. The dielectric permitivity $\varepsilon(i\nu)$ can usually be represented by a function of the form[23]

$$\varepsilon(i\nu) = 1 + \frac{(n^2-1)}{(1+\nu^2/\nu_e^2)}, \tag{3.9}$$

where ν_e is the mean electronic absorption frequency in the UV typically around $3 \times 10^{15}s^{-1}$, and n is the refractive index of the medium in the visible (i.e., $n^2 = \varepsilon_{vis}(\nu)$). Note that $\varepsilon(i\nu)$ of eq. (3.9) is a real function of ν.

For interactions dominated by dispersion forces, combining relations (or combining laws) are frequently used for obtaining approximate values for unknown Hamaker constants in terms of known ones. The non -retarded Hamaker constant for media 1 and 2 interacting across vacuum is approximated by[17]

$$A_{12} \approx \sqrt{A_{11}A_{22}} \tag{3.10}$$

and for media 1 and 2 interacting across medium 3 is given by

$$A_{123} \approx (\sqrt{A_{11}} - \sqrt{A_{33}})(\sqrt{A_{22}} - \sqrt{A_{33}}). \tag{3.11}$$

In order to calculate Hamaker constants for materials of practical interest it is necessary to have information on the relevant intermolecular forces and a means of calculating the constant C. Different expressions[7,38] of the Hamaker constant are given based on different assumptions, for example based on the assumption of additivity of intermolecular dispersion forces and on the macroscopic approach. The Hamaker constant for two interacting similar media[13] on the assumption of short-range macroscopic treatment is given by

$$A = 0.23h\nu_\nu \frac{(\varepsilon_o - 1)^2}{(\varepsilon_o + 1)^{3/2}(\varepsilon_o + 2)^{1/2}} \tag{3.12}$$

where ν_ν is the characteristic frequency, h is Plank's constant and ε_o is a limiting dielectric constant.

3.3 Film Thickness

A growth of wetting films is studied as a function of time t in the framework of effective interface models. The thickness of such a wetting film depends on a temperature difference ΔT, due to differential heating of the substance relative to the temperature of the liquid reservoir. An expression for the relation between the film thickness l and the temperature difference ΔT now is following.

The disjoining pressure[37], $\Pi(l)$ provides a convenient formalism for the discussion of wetting. By definition

$$\Pi(l) = -\frac{dG^\sigma(l)}{dl}, \tag{3.13}$$

where $G^\sigma(l)$ is the excess real free energy density of an adsorbed film of thickness l. Phenomenologically, the disjoining pressure is the thermodynamic force per unit area between the free surface of the wetting film and the adsorbing substrate. The excess free energy per unit area of the film can be split into a thickness dependent part $F(l)$ and a part which only depends on the surface tension[27] as

$$G^\sigma(l) = F(l) - S, \tag{3.14}$$

where $F(l)$ is the thickness-dependent part of the excess free energy of the liquid film and S is the total surface tension between interfaces(LV, SL, SV). For a volatile liquid

in thermal equilibrium and above the wetting transition temperature S is always zero due to Antonoff's rule[27].

Considering only the van der Waals interactions between the adsorbed molecules and a uniform substrate, the thickness -dependent part of the excess free energy of the liquid[17] can be expressed as

$$F(l) = \begin{cases} A_{eff}/(12\pi l^2) & l < \lambda_c; \\ B/(3l^3) & l > \lambda_c; \end{cases} \quad (3.15)$$

where A_{eff} is the Hamaker constant of the whole system. The first part of eq. (3.15) is for the case of non-retarded van der Waals forces and the second part is for the retarded case. A van der Waals interaction energy between molecules of the form $w(r) = -C_{ij}/r_{ij}^n$ is assumed, where n depends whether the interaction is retarded or non-retarded, and the definition for the Hamaker constant $A_{ij} = \pi^2 \rho_i \rho_j C_{ij}$, with $\rho_{i,j}$ as the molecular density. The constants A_{eff} and B are assumed to be positive (complete wetting). This means that the van der Waals forces tend to thicken the liquid film. The critical length λ_c is of the order of 800Å. Therefore, the non-retarded case is considered in this paper. The disjoining pressure for the non-retarded case is then given by

$$\Pi_o(l) = \frac{A_{eff}}{6\pi l^3}. \quad (3.16)$$

A more general approach given by Dietrich[8] is

$$F(l) = al^{-k} + bl^{-\eta} + ... \quad l \gg d_\omega. \quad (3.17)$$

which is exact for $T = 0K$. For distances smaller than a microscopic distance d_ω the density of the liquid near the wall vanishes[27] (in the case of CCl_4, $d_\omega < 7Å$). Here d_ω is a hard-core radius that takes into account the fact that, owing to the finite size of the adsorbate and substrate molecules, they cannot come arbitrarily close to each other. $k = 2$ corresponds to the non-retarded case and $k = 3$ to the retarded one. $\eta > k$ is the exponent of the first correction term and usually $\eta = k + 1$. For T>0K the coefficients a and b become temperature dependent. Under the assumption that this temperature dependence is only weak and that only a small temperature interval is regarded, the following expression is obtained

$$F(l) = \frac{A_{eff}}{12\pi l^2} + \frac{\tilde{B}}{3l^3} + O(l^{-4}). \quad (3.18)$$

and the disjoining pressure is

$$\Pi_o(l) = \frac{A_{eff}}{6\pi l^3} + \frac{\widetilde{B}}{l^4} + O(l^{-5}). \tag{3.19}$$

It should be mentioned that a thin layer between the substrate and the liquid CCl_4 film also may cause an l^{-4} term in the disjoining pressure as pointed out in[37]. Inclusion of a substrate surface layer in the Hamaker formalism yields an effective adsorbate substrate Hamaker constant with an l dependence:

$$A_{eff}(l) = (A_{FL} - A_{LL}) + (A_{SL} - A_{FL})(1 + d/l)^{-3}. \tag{3.20}$$

where L, S, and F denotes the liquid film, the substrate and the solid layer between liquid and substrate with thickness d, respectively. Inserting eq. (3.20) into eq. (3.16) and expanding $\Pi_o(l)$ in powers of (d/l) up to first order yields,

$$\Pi_o(l) = \frac{H_3}{l^3} + \frac{H_4}{l^4} + O(l^{-5}) \tag{3.21}$$

where

$$H_3 = -\frac{A_{SL} - A_{LL}}{6\pi}, \tag{3.22}$$

$$H_4 = -d\frac{A_{SL} - A_{FL}}{2\pi}, \tag{3.23}$$

and

$$O(l^{-5}) = d^2\frac{(A_{SL} - A_{FL})}{\pi l^5}. \tag{3.24}$$

In general, the wetting properties depend on the magnitude and sign of H_3, H_4, etc. For example, if H_3 and H_4 are both positive (i.e., $A_{FL} > A_{SL} > A_{LL}$) the wetting is complete; however, if H_3 is positive and H_4 negative (i.e., $A_{SL} > A_{FL} > A_{LL}$), the surface is either incompletely or completely wet, depending on the precise value of H_3/H_4[37].

The temperature difference, ΔT, represents only a slight perturbation of the thermodynamic equilibrium. Therefore, the related film thickness can be calculated by an expansion in the vicinity of thermodynamic equilibrium. With the pressure p_v, the temperature T_v and the chemical potential $\mu(p_v, T_v)$ of the vapour and the respective quantities for the liquid wetting film (indices $v \to l$), the equilibrium conditions at the gas-liquid coexistence line are

$$p_v = p_l, \qquad T_v = T_l, \qquad \mu_v(p_v, T_v) = \mu_l(p_l, T_l). \tag{3.25}$$

The chemical potential gives the total free energy per molecule: it includes the interaction energy as well as the contribution associated with its thermal energy. Introducing a temperature difference between the vapour and the liquid, the equilibrium is perturbed, thus,

$$p_v = p_l, \qquad T_v + \Delta T = T_l \tag{3.26}$$

and

$$\mu_v(p_v, T_v) + \Delta\mu = \mu_l(p_l, T_v + \Delta T) = \mu_l(p_l, T_l). \tag{3.27}$$

Here the reservoir provides isobaric conditions. A Taylor expansion of the chemical potential together with the definitions of the heat capacity $C_{p,l}$ and latent heat of vaporization per molecule q leads to the following expression[10]:

$$\left(\frac{\partial\mu}{\partial T}\right)_p = \frac{q}{T} - \frac{C_{p,l}}{N_A}\frac{\Delta T}{T}. \tag{3.28}$$

With the introduction of a temperature differential, the thickness-dependent part of the excess free energy of the adsorbed liquid film is

$$F(l) = F_o(l) + \Delta F. \tag{3.29}$$

where ΔF is an additional contribution to the excess free energy density, F, caused by the temperature difference ΔT. The term ΔF is proportional to $\Delta\mu$ and represents the energy cost (per unit area) associated with forming a liquid layer of thickness l at a temperature ΔT off the liquid-vapour coexistence line. Thus, it can be expressed[25] as

$$\Delta F = \rho_i l \left(\frac{\delta\Delta\mu}{\delta T}\right)_p \Delta T \tag{3.30}$$

and eq. (3.29) is given by

$$F(l) = \frac{A_{eff}}{12\pi l^2} + \frac{\tilde{B}}{3l^3} + \rho_i l \left(\frac{\partial\Delta\mu}{\partial T}\right)_p \Delta T + O(l^{-4}) \tag{3.31}$$

Omitting higher terms in the expansion of eq. (3.27) and using eqs. (3.19), (3.28) and (3.31) we obtain the following expression for the disjoining pressure

$$\Pi(l) = \Pi_o(l) - \rho_i q \frac{\Delta T}{T}(1 - \varepsilon(\Delta T)). \tag{3.32}$$

where $\varepsilon(\Delta T) = (\bar{c}/q)\Delta T$ with $\bar{c} = C_{p,l}/N_a$. In the case of CCl_4, the latent heat of vaporization per molecule is $q = 4.8209 \times 10^{-20}$ J/particle[12] and the heat capacity per

molecule is of the order of $\bar{c} = 2.1870 \times 10^{-25}$J/(particle.K)[20]. Hence the second term in eq. (3.32) is of the order of $\varepsilon(\Delta T) = 10^{-5}$, even if a temperature difference as large as $\Delta T = 10$K is taken. Thus, this term can be neglected. Therefore, with the condition $\Pi(l_0) = 0$ for an equilibrium film thickness l_0 eq. (3.32) is transformed to

$$\Pi_o(l_o) = \frac{A_{eff}}{6\pi l_o^3} + \frac{\tilde{B}}{l_o^4} = \rho_i q \frac{\Delta T}{T}. \tag{3.33}$$

And finally we get an implicit formula for the change in temperature as

$$\Delta T = \frac{T}{q\rho_i}\left(\frac{A_{eff}}{6\pi l_o^3} + \frac{\tilde{B}}{l_o^4}\right). \tag{3.34}$$

From eq. (3.34), we can see that, introducing a temperature differential changes the condition for the film thickness from $\Pi(l) = \Pi_o(l_o) = 0$ at liquid-vapour coexistence to $\Pi_o(l_o) = (\rho_i q\Delta T)/T$ and a measurement of the film thickness l_o as a function of the temperature difference ΔT between the liquid wetting film and the vapour is well-suited to determine the microscopic constants A_{eff} and $\tilde{B}$.

For the case of the non-retarded van der Waals force, the thickness as a function of temperature difference is given by

$$l(\Delta T) = \left(\frac{A_{eff}}{6\pi q\rho_i}\frac{T}{\Delta T}\right)^{1/3}. \tag{3.35}$$

The temperature behaviour for small time t is approximated by the Newton law of cooling[3]. Mathematically,

$$-\frac{d\Delta T}{dt} \propto \Delta T \tag{3.36}$$

which gives

$$\Delta T = \Delta T_0 \exp(-ct). \tag{3.37}$$

Eq. (3.37) shows an exponential decay of the temperature difference to zero as $t \to \infty$. But, the experimental result is quit different, the change in temperature ΔT decreases exponentially against a final value ΔT_∞, (see Fig. 3.2). Thus, eq. (3.37) is transformed to

$$\Delta T = \Delta T_0 \exp(-ct) + \Delta T_\infty. \tag{3.38}$$

and the ΔT dependence thickness, eq. (3.35) is given by

$$l(t) = \left(\frac{A}{6\pi q\rho_i}\frac{T}{\Delta T_0 \exp(-ct) + \Delta T_\infty}\right)^{1/3}. \tag{3.39}$$

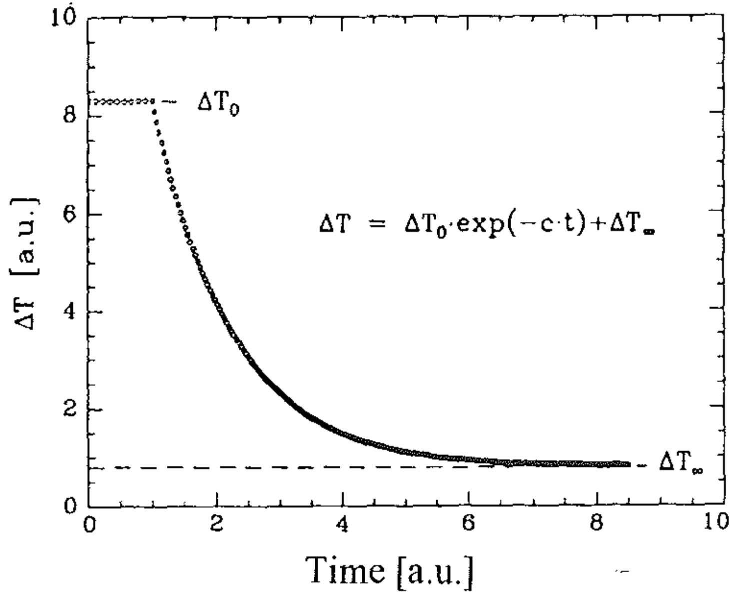

Figure 3.2: *Schematic drawing of the temperature difference between the vapour and the substrate as a function of time eq. (3.67)[41].*

Eq. (3.39) shows that the maximum film thickness depends on the change in temperature, ΔT_∞, achieved in the experiment as $t \to \infty$. Accordingly the film thickness is limited by the temperature difference between the substrate and the vapour.

3.4 Kolmogorov Model for Film Growth

In recent years there has been renewed interest in the process of nucleation and growth at first-order phase transformation[15]. The Kolmogorov model[19] (also called the Johnson-Mehl-Avrami model[1,2,39]) was developed to describe a first order phase transformation from a metastable phase A into a stable phase B. In this section the model is discussed first in its general sense and then as applied to our film growth process.

The assumptions of the model are as follows. At an initial time t=0 infinitesimal grains of stable phase are randomly produced throughout the initially homogeneous metastable phase at a constant rate, Γ, per unit volume. The nucleation rate thus decreases with time in direct proportion to the volume fraction of metastable remaining. Once formed, the grains grow isotropically with constant domain wall velocity v until the wall is impeded by impinging on neighboring grains.

Let V be a certain volume. Initially (at t=0) it is occupied by the mother phase A. After time t a certain part $V_1(t)$ of the volume V is occupied by another phase B. The

volume $V_1(t)$ grows with time t. A necessary and sufficient condition for a point to be in the transformed field at time t is that at some previous time $t_o > 0$ there be a grain nucleated within the free propagation range $v(t - t_o)$ of p. where p is a random point in the transformed region. The volume occupied by a hypothetical "free" grain (one that does not impinge on a neighboring grain) at time $t' = t - t_o$ after nucleation is given by

$$V(t') = C_d[vt']^d. \quad (3.40)$$

C_d is a constant, which depends on the dimension d, for $d = 1, 2, 3$, $C_d = 2, \pi, 4\pi/3$ [14]. The probability that such a nucleus has formed in the volume $V(t')$ during an infinitesimal time interval $\Delta t'$ around t'_j can be expressed as

$$Q = \Gamma V(t'_j)\Delta t', \quad (3.41)$$

and thus the probability that such a nucleus has not found in the volume during the infinitesimal time $\Delta t'$ around t'_j is

$$P_j = 1 - Q = 1 - \Gamma V(t'_j)\Delta t'. \quad (3.42)$$

The probability that such a nucleus has not been transformed throughout the entire time interval $0 \leq t'_j \leq t$ is

$$P(t) = \prod_{t'_j=0}^{t}(1 - \Gamma V(t'_j)\Delta t'). \quad (3.43)$$

Taking the logarithm of eq. (3.43), we obtain

$$\ln[P(t)] = -\sum_{t'_j=0}^{t}\Gamma V(t'_j)\Delta t'. \quad (3.44)$$

For $\Delta t' \to 0$, we get

$$\ln[P(t)] = -\int_0^t \Gamma V(t')dt'. \quad (3.45)$$

On substituting eq. (3.40) into eq. (3.45) and taking the antilogarithm we find

$$P(t) = \exp\left[-\int_0^t C_d\Gamma(vt')^d dt'\right]. \quad (3.46)$$

Assuming Γ, and v as constants in the integration, eq. (3.46) is transformed to

$$P(t) = \exp\left[-\frac{C_d\Gamma v^d}{d+1}t^{d+1}\right]. \quad (3.47)$$

Eq. (3.47) gives the probability of a nucleus in its first phase A. Thus, the probability of transforming in to phase B in time t will be

$$X(t) = 1 - P(t) = 1 - \exp[-ct^n], \tag{3.48}$$

with $n = d + 1$ and $c = \Gamma(C_d v^d)/(d+1)$.

Since the model is completely characterized by the parameters Γ-(with dimension $t^{-1}L^{-d}$ in a d -dimensional space) and v (dimension $t^{-1}L$), it follows that there exists a single characteristic length scale and time scale[4] given by

$$\xi = \left(\frac{\Gamma}{v}\right)^{-\frac{1}{d+1}} \tag{3.49}$$

and

$$\tau = \left(\Gamma\frac{C_d v^d}{d+1}\right)^{-\frac{1}{d+1}}. \tag{3.50}$$

Thus, eq. (3.48) reduces to a simple, but general, exponential growth law

$$X(t) = 1 - \exp[-(t/\tau)^n]. \tag{3.51}$$

Let us see how this global model works to the dynamics (special case) of growing wetting films. Assume $V_1(t)$ be the volume of a liquid film adsorbed in the interval between [0,t] and V_2 be the volume in the interval [0,t→ ∞]. Then, the volume fraction adsorbed in the interval [0,t] can be expressed as

$$X(t) = \frac{V_1(t)}{V_2} = \frac{Ol_1(t)}{Ol_2}, \tag{3.52}$$

where O is the surface area. Substituting eq. (3.51) in to eq. (3.52) gives

$$l_1(t) = l_2\{1 - \exp[-(t/\tau)^n]\}. \tag{3.53}$$

But the actual thickness of the film, at time t, is $l_1(t) + l_o$ where l_o is the thickness at t=0. Thus, eq. (3.53) is transformed to

$$l(t) = l_o + (l_{max} - l_o)\{1 - \exp[-(t/\tau)^n]\} \tag{3.54}$$

with $l_{max}(l_{max} = l_2 + l_o)$ the maximum equilibrium thickness, τ as the time constant of the film growth process, and $n = d + 1$, d being the growth dimension. Eq. (3.54) gives the thickness of the film at time t.

Chapter 4

Sample Systems

4.1 The Substrates

Two substrates were used to study the wetting process: Silicon and a quartz glass. Each has been carefully characterized by x-ray techniques. The details are given in chapter 6.

4.1.1 Silicon Wafer

The first type of substrate was an optically polished silicon(111) wafer. Polished silicon(100) wafers with a thin native oxide layer on top have a high surface tension which leads to a spreading parameter greater than zero[26]. Furthermore, polished silicon wafers are well-suited for x-ray reflectivity measurements because they are smooth on an angstrom-scale. This is very important because the wetting behaviour might be strongly influenced by the surface roughness of the substrate[30]. Therefore, a homogeneous liquid film covers the substrate and variation of the density of the film will only concern the direction normal to the surface. Table 4.1 shows the theoretically obtained (optical) parameters of the silicon wafer.

The Hamaker constant of Si is found[38] ranged from 22.1×10^{-13}erg to 25.6×10^{-13}erg and in reference[27] it is found as 24×10^{-13}erg.

Absorption($\beta \cdot 10^7$)	Dispersion ($\delta \cdot 10^6$)	Critical angle (α_c)
1.73	7.56	0.223°

Table 4.1: Absorption β, Dispersion δ and the critical angle α_c of the silicon substrate calculated for the wavelength 1.54056Å(CuK_α)[16].

4.1.2 Quartz Glass

Quartz is a crystalline form of silica. It has a hexagonal structure. Each silicon atom is surrounded by four oxygen atoms and each oxygen by two silicon atoms. Quartz is hard and has a high melting point. about 1600°C. This is hundreds of degrees above the melting point of an ordinary glass.

4.2 The Adsorbate

Adsorption is the accumulation of a gas or a solute at the interface. hence it is a surface phenomenon. In this paper the adsorbate used is carbon tetrachloride(CCl_4) which is liquid at room temperature.

Over a limited range of temperature the dependence of the vapour pressure of liquids on temperature may be represented by a formula of the form

$$\log_{10} p = A - \frac{B}{T} \tag{4.1}$$

in which A and B are constants over a temperature range and T denotes temperature on the absolute scale. A plot of $\log_{10} p$ versus $1/T$ gives a straight line. The vapour pressure is a function of the substance and of the temperature.

For the liquid CCl_4 in equilibrium with its vapour. the $p-T$ relation is given by the following expression[25] within the indicated range of temperature.

$$p = 10^{6.89406 - \frac{1219.58}{227.16+t}} \quad : \quad t\epsilon[19.00\ ,\ 80.00] \tag{4.2}$$

where t and p are in °C and Torr. respectively.

The vapor pressure of CCl_4(at 293K) is sufficiently high (p_g=120hPa) which is highly volatile and provides transport of molecules from the liquid in the reservoir through the

vapor to the wafer. So, a liquid film on top of the substrate can quickly be formed[26]. The structure of CCl_4 is a nearly tetrahedral molecule which can be assumed as spherical if one takes its (rotational) motion at room temperature into account. The interaction between CCl_4 and silicon is predominantly of the van der Waals type, atleast in the temperature range of the experiment. The van der Waals diameter of CCl_4 is 7.0Å[27]. Some physical/thermodynamic constants of CCl_4 are given in table 4.2.

Van der Waals diam.	7.0Å	Hamaker constant	(33.7→ 57.0)
V.pressure(at 293K)	120hPa		$\times 10^{-13}$erg
Molecular mass	153.84g/mol	Critical temp.	283.15°C
Density of gas(75°C)	0.0051g/cm^3	Critical pressure	44.98atm
Density of liquid $\rho(T)$	1.63372-0.00199T+	Critical density	0.577g/cm^3
	0.0000005T^2g/cm^3	Bond length C−Cl	1.766Å
Surface tension	(2.921-0.01259T)×	B.angle Cl−C−Cl	109.5°
	$10^{-2} J/m^2$	dissociation energy	
Melting point	-23.0°C	(CCl_3−Cl)	67.9kcal/mol
Boiling point	76.7°C	Dielectric constant	2.24
Triple point	-22.9°C(10.9mbar)	Critical angle(α_c)	0.181°
Heat capacity(at 25°C)	131.7J/g.mol (liquid)	Dispersion(δ)	5.008×10^{-6}
Heat capacity(at 25°C)	83.4J/g.mol (gas)	Absorption(β)	1.871×10^{-7}

Table 4.2: Some physical/thermodynamic constants of CCl_4 taken from refs.[6,38]. In[27] the Hamaker constant of pure CCl_4 is found as 45×10^{-13}erg.

Chapter 5

Experimental Set-up and Scattering Geometry

5.1 Experimental Set-up

The x-ray measurements were carried out by a high - resolution three crystal diffractometer whose general set up is given in[5]. A 12kW rotating anode generator with a copper target was used as an x - ray source. The schematic diagram is shown in Fig. 5.1. Two slits and a perfect, symmetrically cut Si(111) monochromator which picks out the CuK_α-lines are placed infront of the sample. The widths of the slits are 0.2mm and heights are 10mm which defines the height of the x - ray beam and they also define the illuminated area of the sample. A Si (111) analyzer crystal (which gives a better resolution) and a NaI(Tl) scintillation counter were used as detector unit. Lead shields around the monochromator and the detector system reduce the background radiation.

The x-ray cell is designed as a two chamber arrangement with an inner chamber (height h = 65mm and diameter d = 60mm) made of copper defining the surrounding of the substrate. It contains the CCl_4 atmosphere with a gas of volume 166.5ml. The wafer is mounted vertically onto a thermoelectric device. It is placed 25mm above a reservoir containing 5ml of CCl_4 which defines isobaric conditions. A controlled dry air cycle was designed for stabilization of the vapour temperature. A glass tube furnace which serves as a heat source of the cycle and a small membrane pump maintains the air flow. Kapton windows in the sample cell allows the analysis with x - ray radiation.

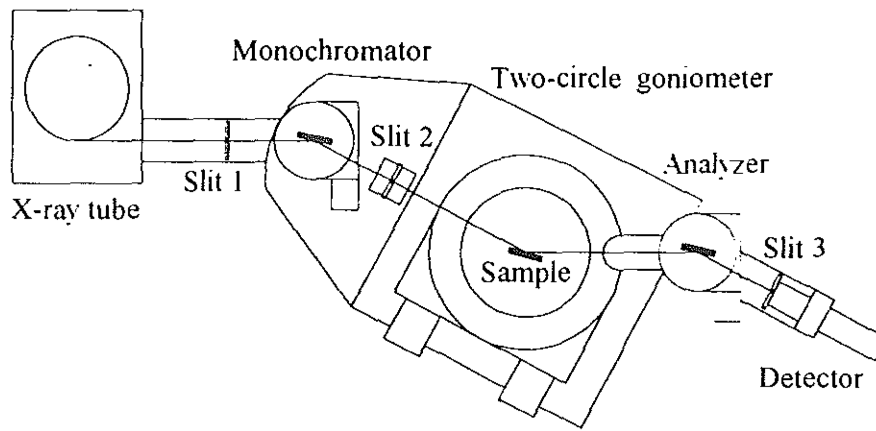

Figure 5.1: *Schematic drawing of the three -crystal diffractometer[5].*

With the heating principle of a thermostated air stream which surrounded the inner chamber, a uniform, smooth heating is realized and the CCl_4 atmosphere is nearly free of temperature gradients. The thermoelectric device in contact with the wafer allows changes of the temperature difference between the wafer and the surrounding vapour on short time scales. The best temperature stability achieved with this set-up was 2mK[27].

5.2 Scattering Geometry

In the experiment different scans were performed. When the angle of incidence is represented by α_i and the excite angle by α_f in all scans and the wavevector of the incident and scattered x-rays are k_i and k_f respectively, with the scattering angle sc$(=\alpha_i + \alpha_f)$, the momentum transfer $\vec{q} = \vec{k_f} - \vec{k_i} = (q_x, 0, q_z)^T$ is given by

$$q_x = k_i(\cos\alpha_f - \cos\alpha_i) \approx \frac{k_i}{2}(\alpha_i - \alpha_f)sc \tag{5.1}$$

$$q_z = k_i(\sin\alpha_f + \sin\alpha_i) \approx k_i sc \tag{5.2}$$

Therefore, a reflectivity-scan $(\alpha_i = \alpha_f)$ corresponds to a q_z (Bragg) - scan, Fig. 5.2, with $q_x = 0$.

By performing a detector scan, which means a scan with fixed angle of incidence α_i and varying the scattering angle sc, the q_x - and the q_z -components of the scattering vector, Fig. 5.3, are changed simultaneously.

A rocking - scan is performed by rotating the sample at a fixed detector position. Thus the incidence angle α_i varies and the scattering angle $sc = \alpha_i + \alpha_f$ is constant.

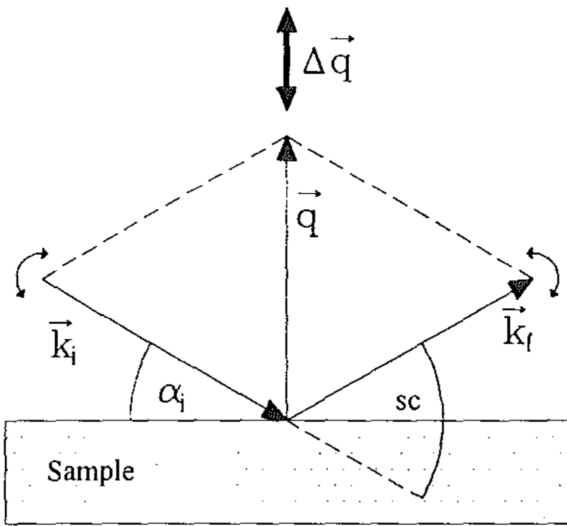

Figure 5.2: *Geometry of the specular Bragg scan:* $\alpha_i = \alpha_f$ *with* $q_x = 0$.

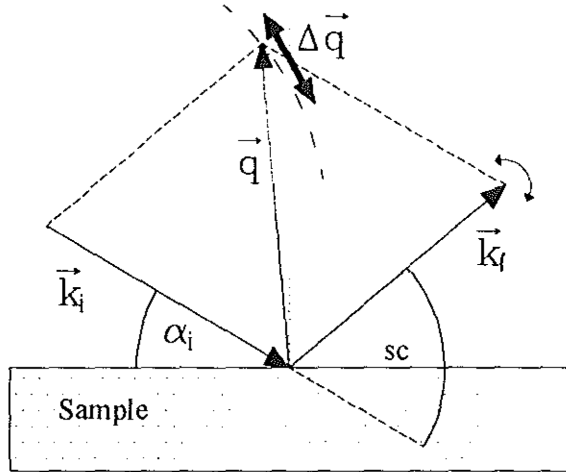

Figure 5.3: *Detector scan: A scan with fixed* α_i *and varying the scattering angle. sc.*

Rocking scans are (nearly) q_x-scans. Fig. 5.4, at a fixed q_z-position.

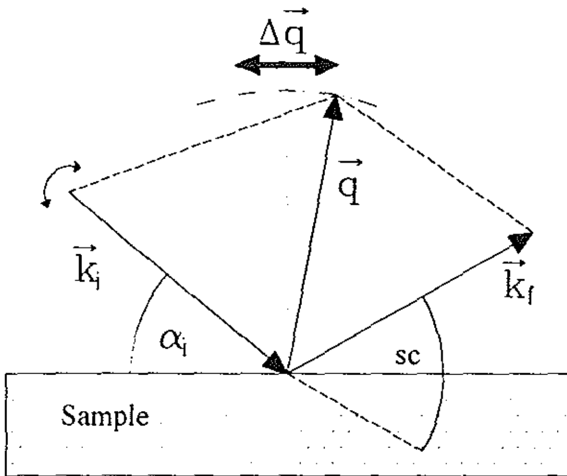

Figure 5.4: *Rocking scan: The incidence angle* α_i *varies. with the scattering angle. sc. fixed.*

All these different scan modes were performed during the experiments of all the dry substrates. and of the liquid film after maximum equilibrium thickness is reached. but the wetting process was analyzed using the Bragg-scan.

Chapter 6

Measurements and Evaluation

In the previous chapters the theoretical explanation of the x-ray reflectivity and the film growth model were given. In this chapter the experimental results are analyzed using Parratt's formalism and the model given in section 3.4. The parameters in the fit were controlled by the least square value of the quadratic function χ^2:

$$\chi^2 = \sum_{i=1}^{N} \left[\frac{\log y_i^{Meas} - \log y_i^{Theo}}{\triangle y_i} \right]^2 . \quad (6.1)$$

$\triangle y_i$ is the difference between the ith measured value and the ith theoretical value and the least square value of χ^2 was taken during the fit. The bare substrates were fitted with the specular, and the diffuse scattering models given in chapter 2 (where too much time, over days, was expended to fit a single scan). Wetting experiments were controlled by a differential temperature ΔT which decreases with time but never equals to zero and the fitting was carried out using the specular model where the time taken to fit a single scan was up to hrs.

6.1 Dry Substrates

X-ray diffraction within the region of total external reflection is a powerful tool for obtaining detailed information about the structure of thin solid and liquid films[32]. Whereas specular reflectivity samples the averaged electron density perpendicular to the surface, the non-specular diffuse intensity contains information about the in-plane structure of the sample.

The sources of the diffusely scattered intensity are lateral inhomogeneities. The most prominent inhomogeneity is the interface roughness which can be regarded as a (small) perturbation of an otherwise smooth interface.

To study the wetting behaviour of a liquid CCl_4 we characterized four bare sample systems: H_2/Si, CH_3/Si, Ge/Si and a quartz glass, using x-ray reflectivity measurements. The reflectivity data were explained using a one layer model, (j=1); where the starting point of the recursion formula ,eq. (2.14), is the substrate (j=2). There R_2=0 because the substrate is assumed as a semi-infinite. The theoretically obtained optical constants of the bulk silicon were kept fixed during the fit, and all fit parameters of bare substrates are shown in tables 6.1 and 6.2. In the measurement, the detector scan and the rocking scans were performed at α_i =0.4^o and sc =0.8^o fixed, respectively.

System	$\delta \cdot 10^6$	σ[Å]	l_{layer}[Å]	δ/β	System	$\delta \cdot 10^6$	σ[Å]	l_{layer}[Å]	δ/β
Si	7.6	5.0	−−	40	Si	7.6	11.6	−−	40
H_2	2.8	0.7	11.9	261	Ge	11.0	17.1	39.8	35
Si	7.6	15.0	−−	40	Glass	7.5	37.9	−−	40
CH_3	3.2	4.8	6.0	990	Layer	5.8	12.6	28.8	36

Table 6.1: Parameters obtained fitting specular reflectivity data of bare substrates eq.(2.14).

Sys.	$\delta 10^6$	σ [Å]	ξ[Å]	h	l[Å]	Sys.	$\delta 10^6$	σ [Å]	ξ[Å]	h	l[Å]
Si	7.6	4.0	7000	0.30	-	Si	7.6	13.6	1770	0.99	-
H_2	2.8	0.7	900	0.17	12.5	Ge	12.3	17.4	1160	0.14	38.2
Si	7.6	14.6	5500	0.20	-	Glass	7.5	36.0	1230	0.11	-
CH_3	3.1	4.8	2000	0.99	6.0	Layer	5.4	14.5	1380	0.13	27.3

Table 6.2: Parameters obtained fitting the bare substrates with the diffuse scattering model. The δ/β values given in table 6.1 were taken fixed in fitting the diffuse scattering.

6.1.1 H_2/Si Substrate

The H_2/Si sample was prepared, such that, a Si-substrate is covered (coated) by a thin H_2-layer. The preparation steps were rinsing with deionized water taking a desoxidation step of 90 to 120 sec iteratively. The thick oxide fabrication time was 3 min at 80°C and the thin oxide fabrication time 5 to 10 min at 80°C.

Before the wetting experiment the dry substrate was characterized by an x -ray reflectivity. Fits of the specular reflectivity data yield the optical constants of bulk-Si and the H_2-layer, table 6.1. It was tried to fit the data without layer (only substrate), but, since the H_2-layer was open to the atmosphere some foreign atoms may adhere to it, for example adsorption of water molecules from the surrounding since the density of water ($\delta_{H_2O} = 2.85 \times 10^{-6}$)[18] is almost the same as the value obtained from the fit, and hence affects the reflectivity.

Fig. 6.1 shows the measured reflectivity of the system, open circles denote the measurement and the solid line gives the best fit with the specular model. Figs. 6.2 and 6.3

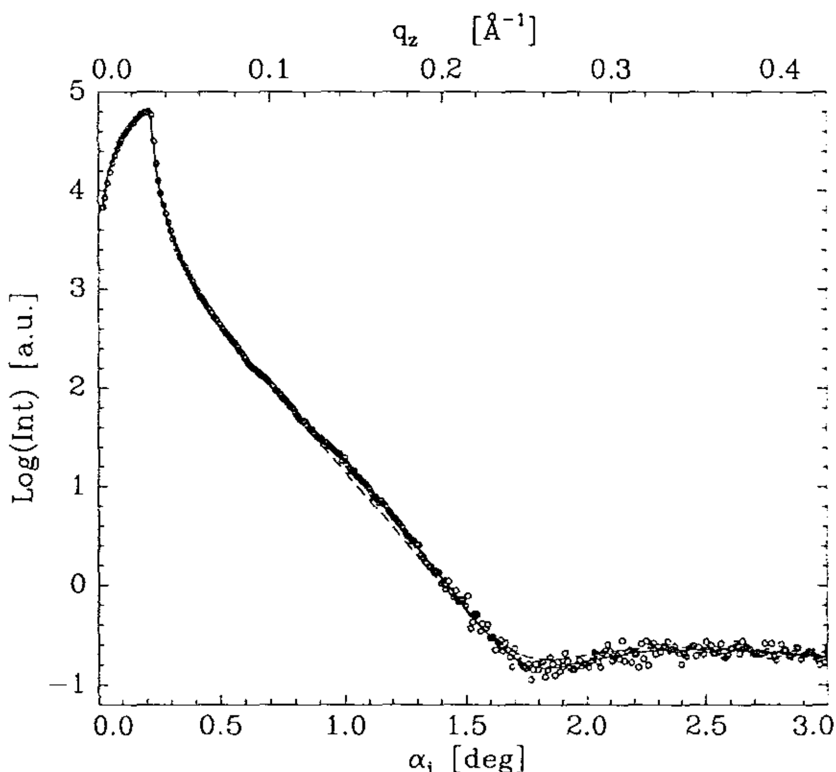

Figure 6.1: *A reflectivity scan of the bare H_2/Si substrate . Circles denote measurement, solid line fit result using the specular model and the broken line a fit result using the diffuse scattering model.*

show the measured diffuse scattering intensity; namely, detector scan and the rocking scans, respectively. A specular peak at $\alpha_i = \alpha_f$ is observed in the diffuse scattering and Yoneda peaks[40] at $\alpha_f = \alpha_{c,Si}$ in the rocking scan, where

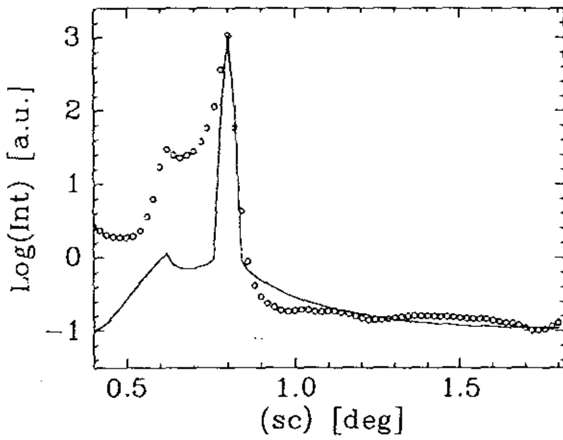

Figure 6.2: *Detector scan of the substrate H_2/Si at $\alpha_i = 0.4°$ (solid line is a fit and circles are measured values).*

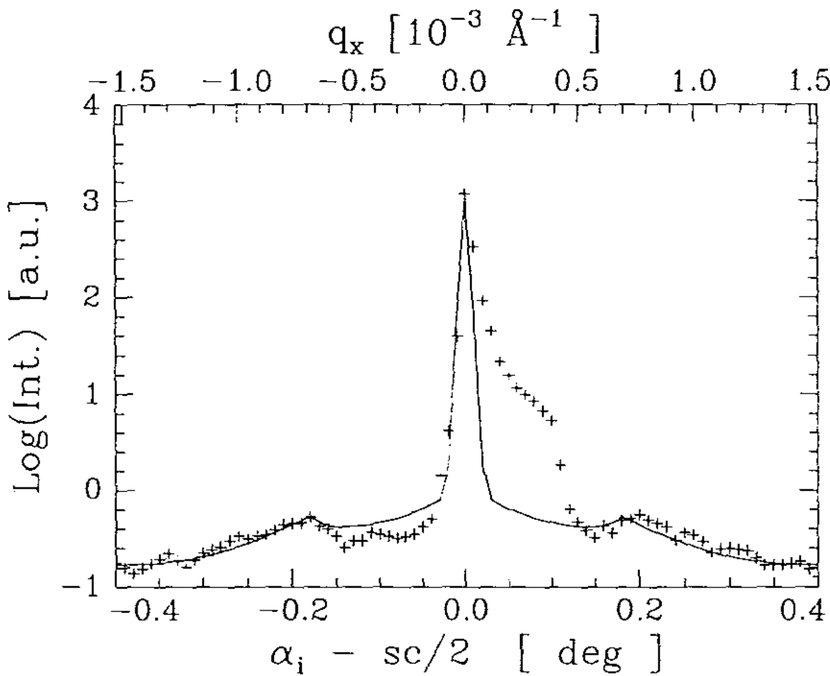

Figure 6.3: *Rocking curve of the bare H_2/Si substrate. The plus sign denotes measurement and the solid line a fit result with the diffuse scattering model at sc=0.8°.*

$\alpha_{c,Si}$ is the critical angle of the bulk silicon substrate. The measurement of the rocking scan shows non-symmetry, Fig. 6.3, perhaps due to a deformation of the sample during the installation. Nevertheless, the wetting experiment was expected not to be affected by the non-symmetric form of the diffuse scattering.

6.1.2 CH_3/Si Substrate

Using the procedure of section 6.1.1 we characterized the bare substrate of CH_3/Si. A thin layer of CH_3 coats the bulk-Si substrate. The optical parameters are given in table 6.1 where the theoretical value of the dispersion (fixed on fitting) was calculated[16] using the close-packing model taking the bond length[6] between Si-C 1.875Å C-H 1.115Å and

the bond angle between Si-C-H as 110°[36].

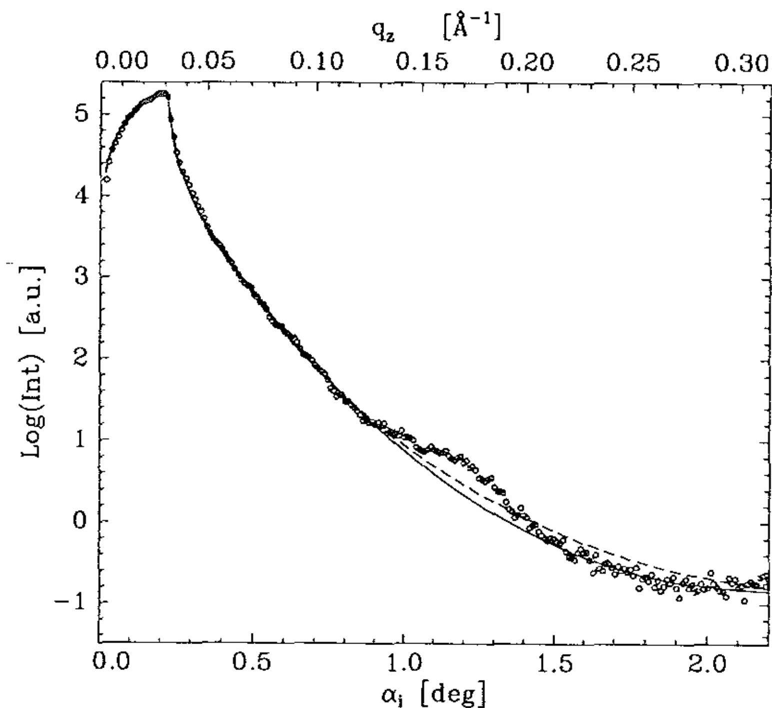

Figure 6.4: *Measured reflectivity scan of the bare CH_3/Si substrate . Circles denote measurement. solid line fit result using the specular model and the broken line a fit result using the diffuse scattering model.*

A bump is seen in the specular reflectivity measurement, Fig. 6.4, which can be resulted from the coating procedure and was not succeeded to fit that region. Figs. 6.7 and 6.8 show the diffuse scattering measurements: namely, detector and rocking scans, respectively.

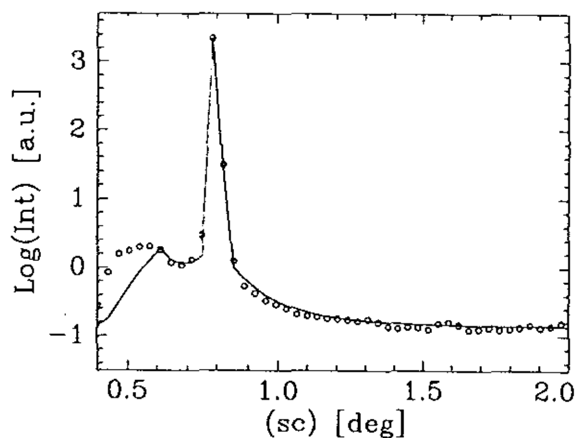

Figure 6.5: *Detector scan of the substrate CH_3/Si at $\alpha_i = 0.4°$. Circles are measured values and the solid line denotes fit result with the diffuse scattering model.*

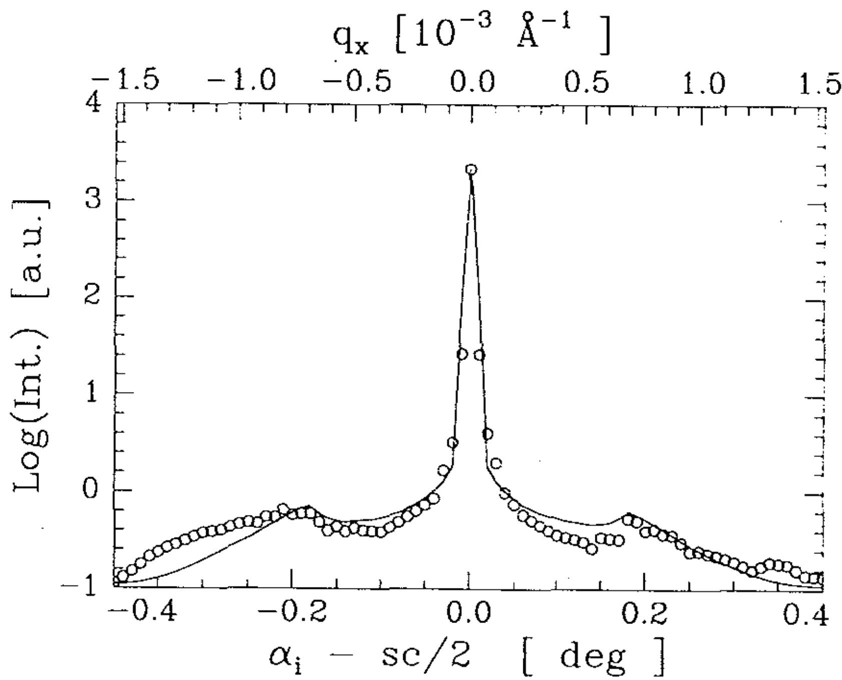

Figure 6.6: *Rocking curve of the bare CH_3/Si substrate. Circles denote measurement and the solid line a fit result of the diffuse scattering model at sc=0.8°.*

6.1.3 Ge/Si Substrate

This sample was prepared by evaporating a Ge layer on a bulk Si substrate. Before the wetting experiment the dry sample was characterized by x-ray reflectivity. The fit parameters of the one layer system, Ge layer on a silicon substrate, are given in table 6.1. From the fit we observe that the density of the Ge layer was reduced by 23% as compared to its theoretical value (14.44×10^{-6})[16]. The density reduction of the Ge layer can be explained such that the molecules of the Ge (thin) layer are not as close packed as the molecules of bulk germanium.

Figs. 6.7, 6.8 and 6.9 show the detector, specular reflectivity and the rocking scans, respectively. In the rocking scan (diffuse scattering), a specular peak at $\alpha_i = \alpha_f$ and Yoneda peaks at $\alpha_f = \alpha_{c,Si}$ are observed.

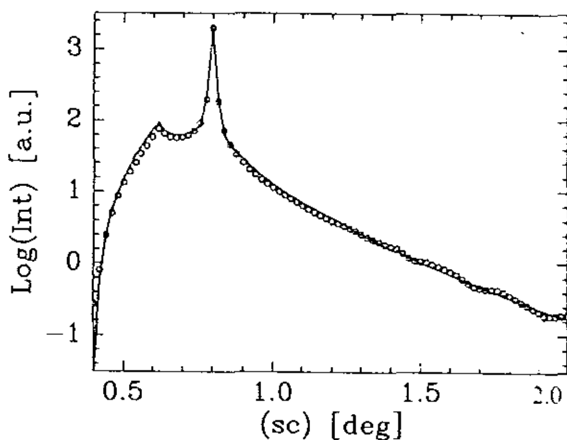

Figure 6.7: *Detector scan for the Ge/Si system at $\alpha_i = 0.4°$. Circles denote measured values and the solid line is a fit result with the diffuse scattering model.*

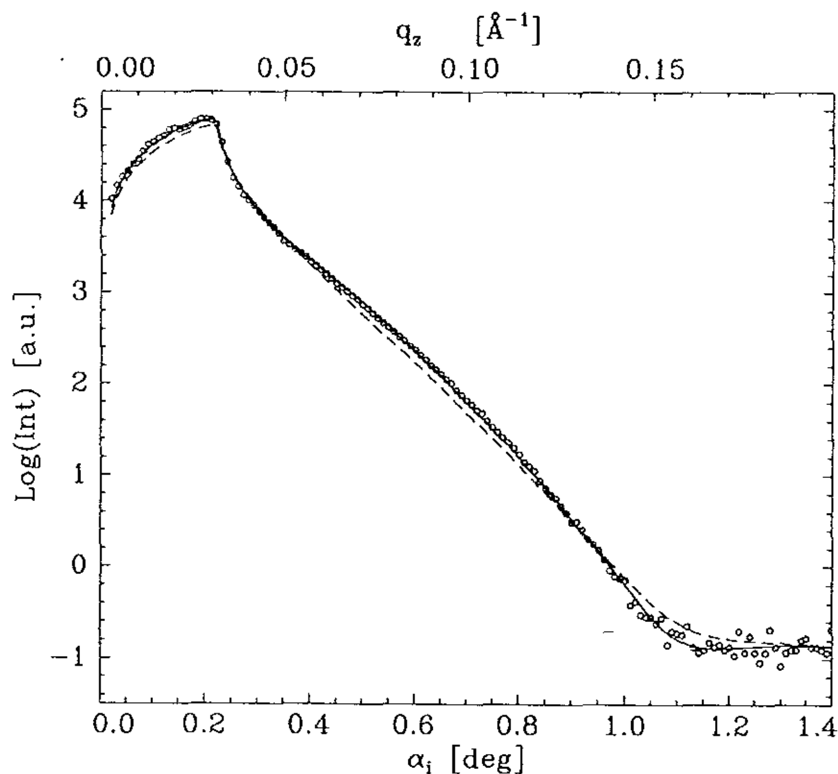

Figure 6.8: *A reflectivity scan of the bare Ge/Si substrate. Circles denote measurement, solid line fit result using the specular model and the broken line a fit result using the diffuse scattering model.*

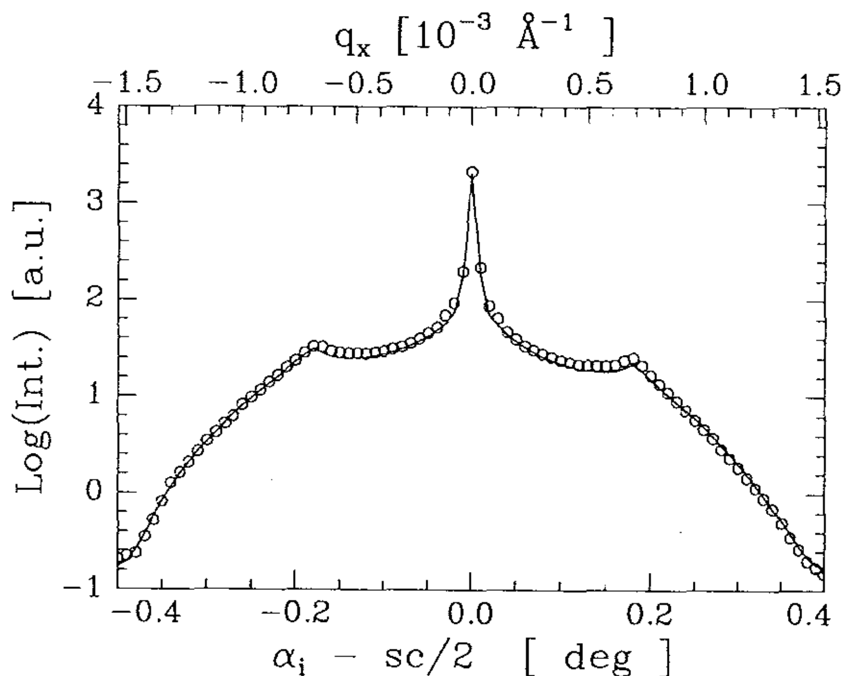

Figure 6.9: *Rocking curve of the bare Ge/Si substrate. Circles denote measurement and the solid line a fit result using the diffuse scattering model at sc=0.8°.*

6.1.4 Quartz glass

We examined this sample before we inject the liquid, and the fit parameters are given in table 6.1. The measured reflectivities are shown in: Fig. 6.10 specular reflectivity, Fig. 6.11 the detector scan and Fig. 6.12 the rocking scan. The fit was performed assuming a one layer model.

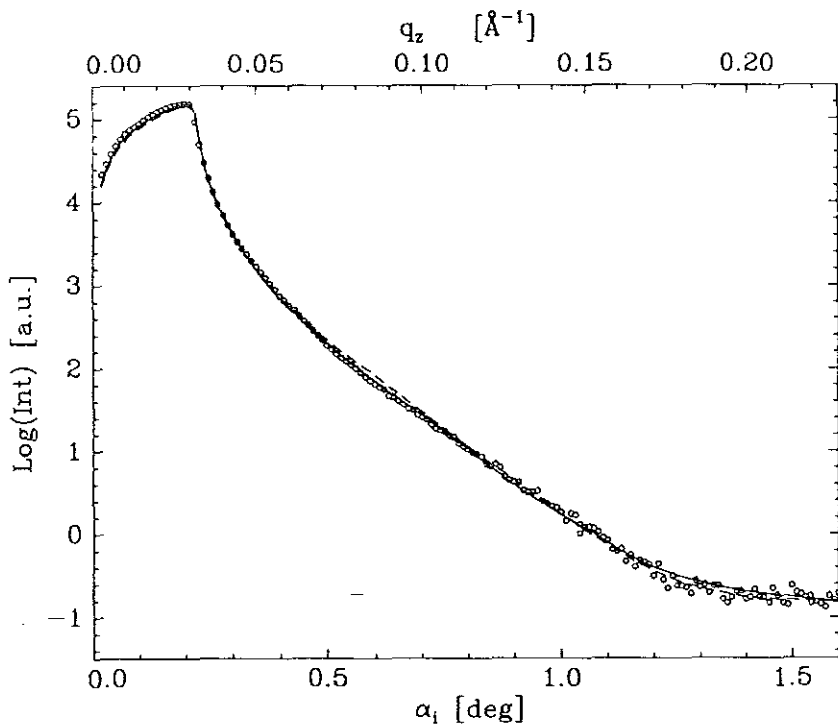

Figure 6.10: *A reflectivity scan of the bare glass substrate. Circles denote measurement. solid line fit result using the specular model and the broken line a fit result using the diffuse scattering model.*

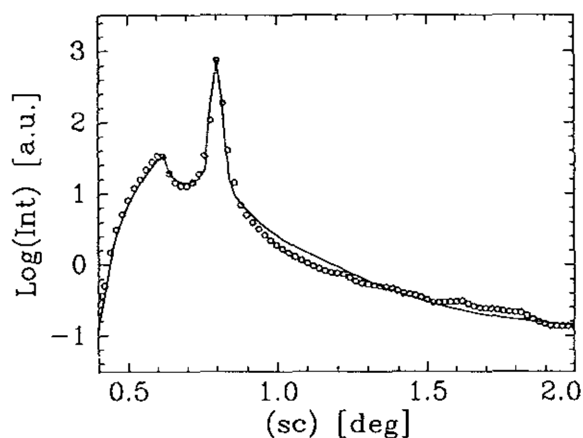

Figure 6.11: *Detector scan of the glass wafer at* α_i = 0.4°. *Circles denote measurement and the solid line is a fit result using the diffuse scattering model.*

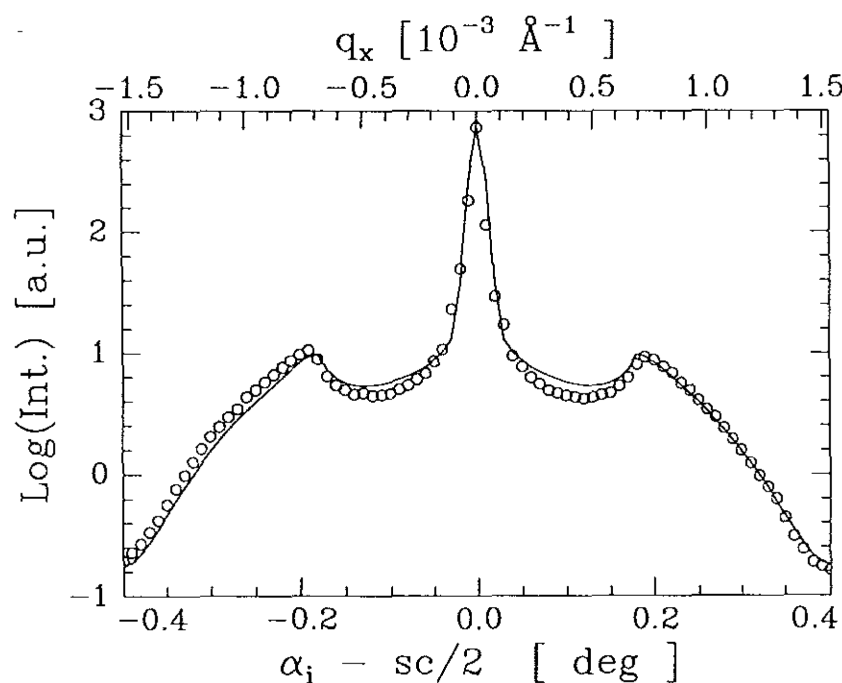

Figure 6.12: *Rocking curve of the bare glass substrate. Circles denote measurement and the solid line a fit result of the diffuse scattering model at sc=0.8°.*

An examination of the bare substrates after the wetting experiments lead to the same curves, i.e., the surface of the wafers was not affected by the wetting process.

6.2 Wetting Experiments

X-ray specular reflection was used to study the wetting of liquid CCl_4 on top of the bare substrates considered in section 6.1. After injecting the liquid into the reservoir of the evacuated x-ray cell, a stable wetting film was formed on top of the respective substrates. Then, the liquid film which builds up after the injection was monitored by a short rocking scans and, then, removed from the wafer introducing a disturbance of the thermodynamic equilibrium by a short temperature pulse ΔT between the substrate and the vapour phase, see Fig. 6.13. The perturbation was monitored with transverse-scans (i.e., q_x-scans at a fixed position of q_z=0.03Å^{-1}). After a short time the temperature at the glass tube furnace was set to the desired value. The switching-off of the heating source sets the zero point of the time axis and the beginning of the growth. With in-situ measured reflectivities the growth process was monitored.

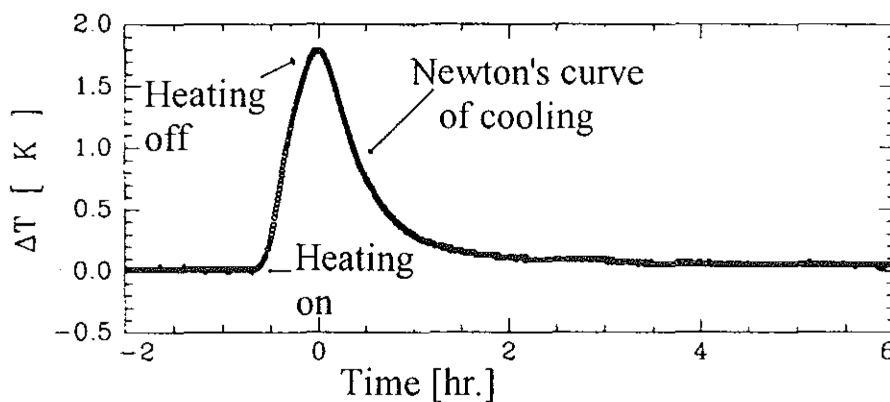

Figure 6.13: *Example of a heating and cooling systems for a growing film of CCl_3Br on Si [35]. The zero time corresponds to the starting point of the film growth.*

All reflectivity curves of the wetted wafer were measured in the range of $q_z = 5.7 \times 10^{-3}$Å^{-1} and q_z=0.22Å^{-1} for each scan with a step width of $\Delta q_z = 5.7 \times 10^{-3}$Å^{-1} between the points which denotes a good compromise between time resolution and counting statistics.

6.2.1 CCl_4 on H_2/Si

The reflectivities were fitted with the theory of section 2.2. assuming a two-layer model. The starting point of the recursion formula is the silicon substrate ($j=3$). Since the silicon substrate was assumed as a semi-infinite the reflectivity R_3 is equal to zero. During the fit the parameters of the dry substrate were kept constant.

Due to the fact that the film thickness changes during the measurements, only averaged parameters over the time resolution of 0.522hr can be obtained. Therefore, the fit yields the mean density profile of the system. The fit results are given in table 6.3. From the table one can see that the roughness increases with increasing thickness and the density of the adsorbed film varies from 42.1% to 64.9% of its bulk value $\delta_{CCl_4} = 5.01 \times 10^{-6}$[15].

An example of the density profile found during the fit is shown in Fig. 6.14. Fig. 6.15 shows the measured reflectivities over a time range of 25hrs and the film is stable after this time. The x-ray determined film thickness of CCl_4 on H_2/Si layer is shown in Figs. 6.16. 6.17. 6.18 and 6.19 for a time length of 6.27hrs each: open circles and triangles denote specular reflectivities and solid lines represent fit results. For clarity the curves are shifted by a 0.8-unit order of magnitude (log-scale) against each other. The measurement starts with the reflectivity curve at the bottom. and the time increases. from t=0. by a step of 0.522hrs from bottom to top.

Sc.No	$\delta 10^6$	$\sigma[\AA]$	$l[\AA]$	Sc.No	$\delta 10^6$	$\sigma[\AA]$	$l[\AA]$	Sc.No	$\delta 10^6$	$\sigma[\AA]$	$l[\AA]$
1	3.0	5.2	20.5	17	3.1	15.6	56.0	33	2.9	24.0	80.6
2	3.2	8.2	26.7	18	3.2	16.6	58.2	34	2.9	25.5	83.0
3	3.3	9.6	30.0	19	3.1	17.4	61.0	35	3.0	26.1	81.0
4	3.2	10.4	32.4	20	3.1	18.2	63.1	36	2.9	25.2	82.0
5	3.2	11.0	33.8	21	3.1	17.8	64.6	37	2.9	27.4	84.0
6	3.2	11.8	37.0	22	3.2	18.9	66.0	38	2.8	26.2	85.5
7	3.2	12.2	38.8	23	3.1	19.4	67.7	39	2.7	27.0	87.0
8	3.2	13.4	40.0	24	3.1	19.0	68.5	40	2.8	27.2	83.0
9	3.1	12.9	41.8	25	3.1	19.6	66.9	41	3.0	27.9	86.0
10	3.2	13.6	44.4	26	3.1	20.2	69.7	42	3.0	31.2	89.0
11	3.1	14.0	46.5	27	3.1	21.5	71.1	43	2.7	28.3	87.9
12	3.1	14.0	48.0	28	3.1	21.6	72.0	44	2.7	29.9	88.9
13	3.1	14.6	49.0	29	3.1	24.0	76.3	45	2.7	30.7	86.4
14	3.1	15.1	52.0	30	3.0	24.0	78.3	46	2.5	26.4	90.0
15	3.2	15.3	51.5	31	2.1	25.3	80.2	47	2.6	27.0	88.6
16	3.1	15.1	53.2	32	3.0	25.3	81.0	48	2.6	27.8	87.0

Table 6.3: Fit parameters of the growing wetting film CCl_4 on the substrate H_2/Si.

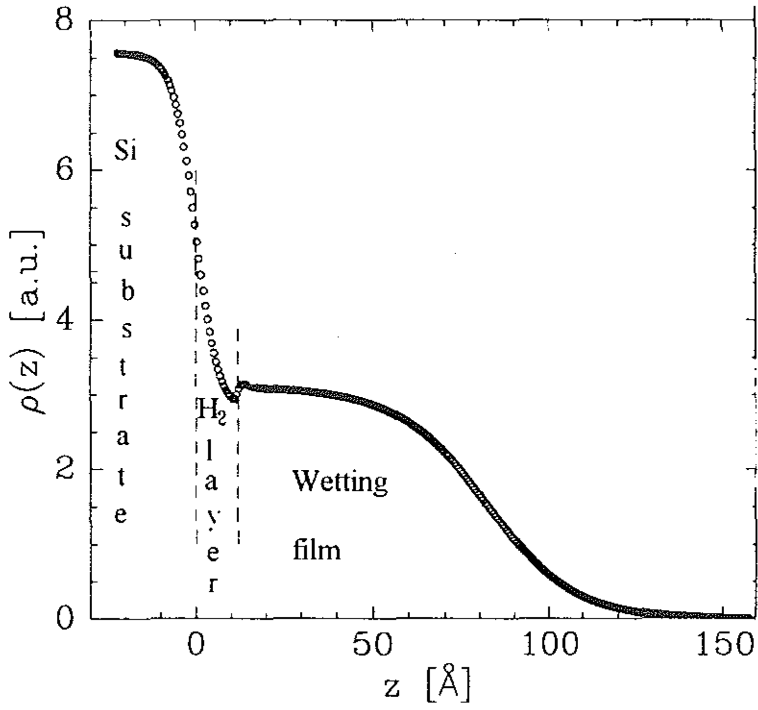

Figure 6.14: *An example of a density profile of the wetting film CCl_4 on H_2/Si.*

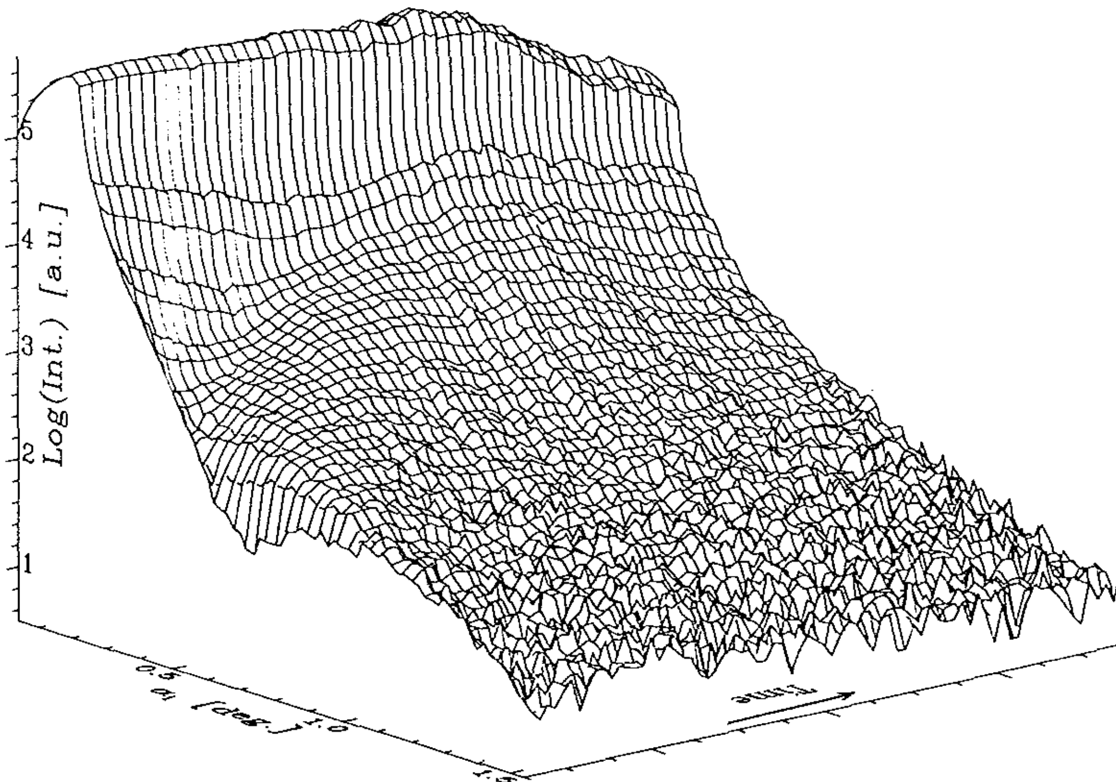

Figure 6.15: *Measured reflectivities over 25hrs for the system CCl_4 on H_2/Si. The arrow indicates the time direction.*

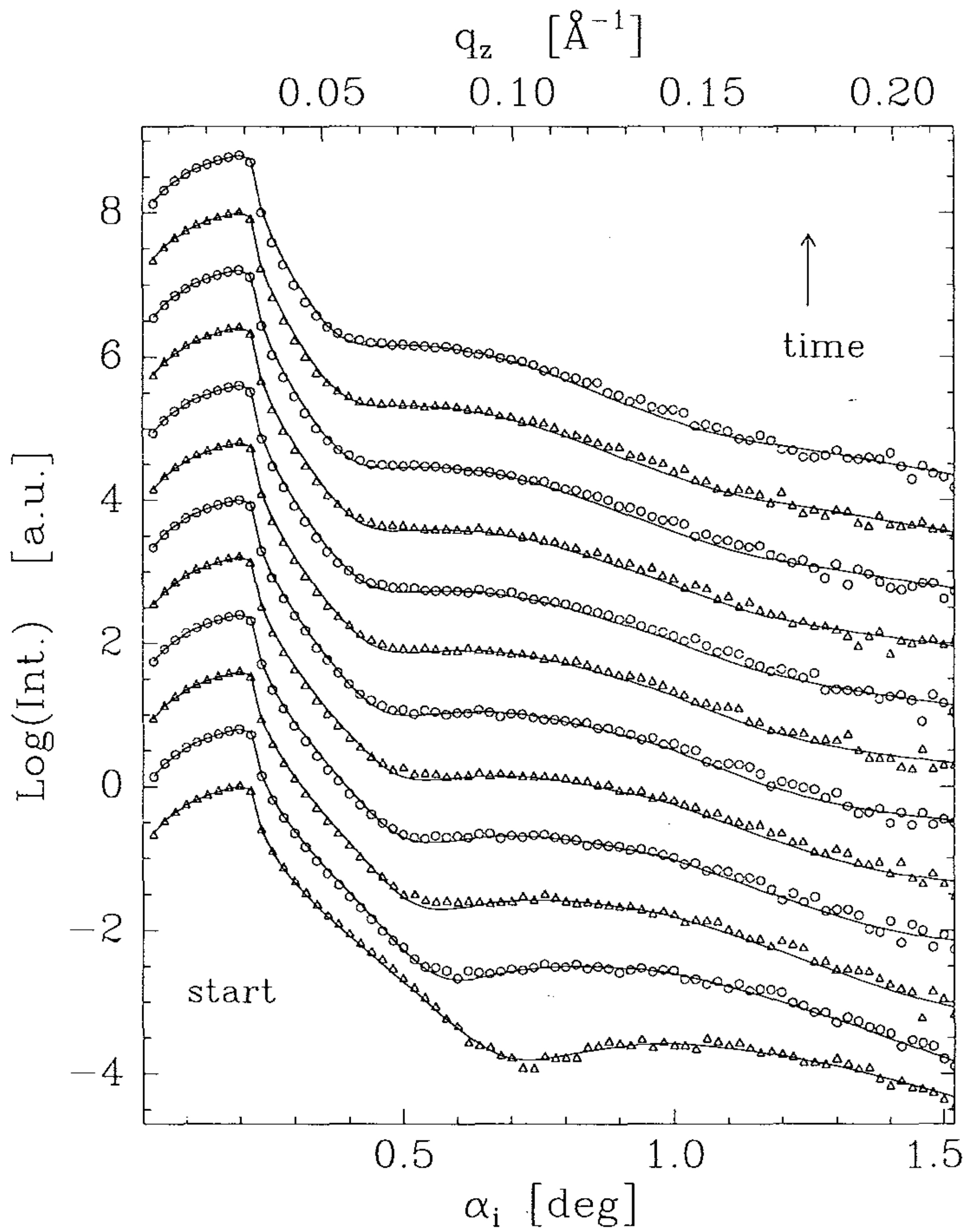

Figure 6.16: *Specular reflectivities (open circles and triangles) and fit results (solid lines) during the growth process for the system CCl_4 on H_2/Si.*

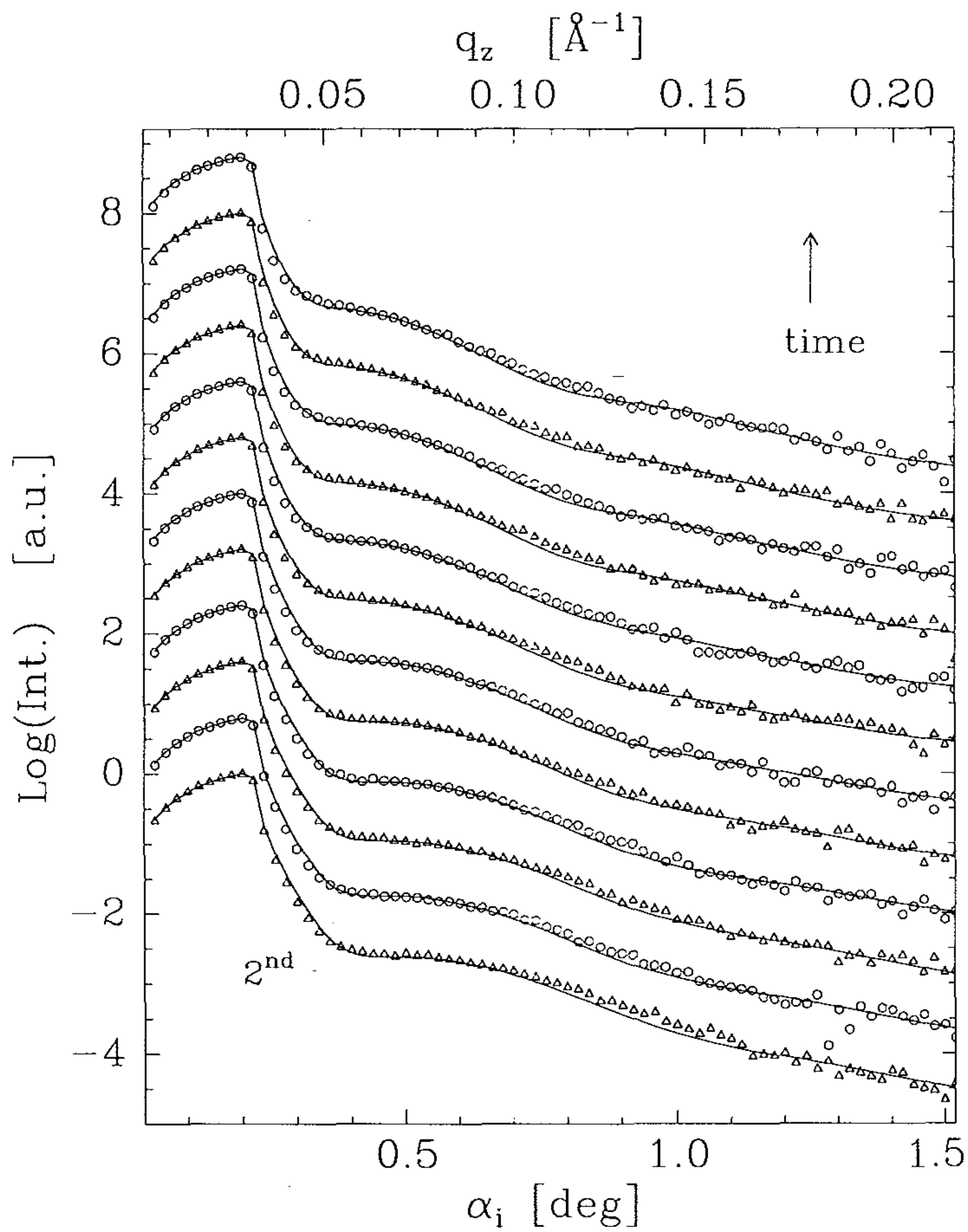

Figure 6.17: *Continuation of Fig.6.16.*

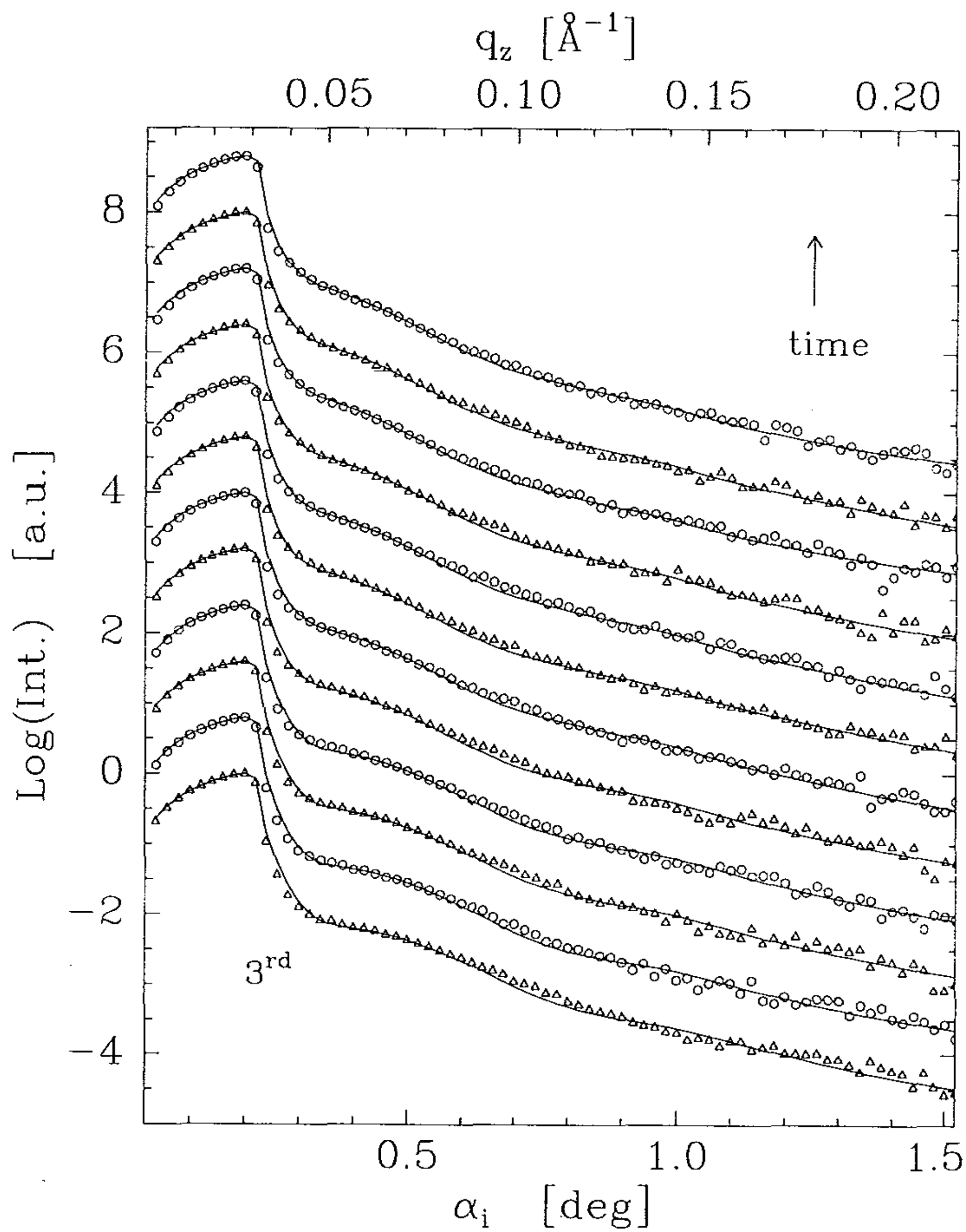

Figure 6.18: *Continuation of Fig.6.17.*

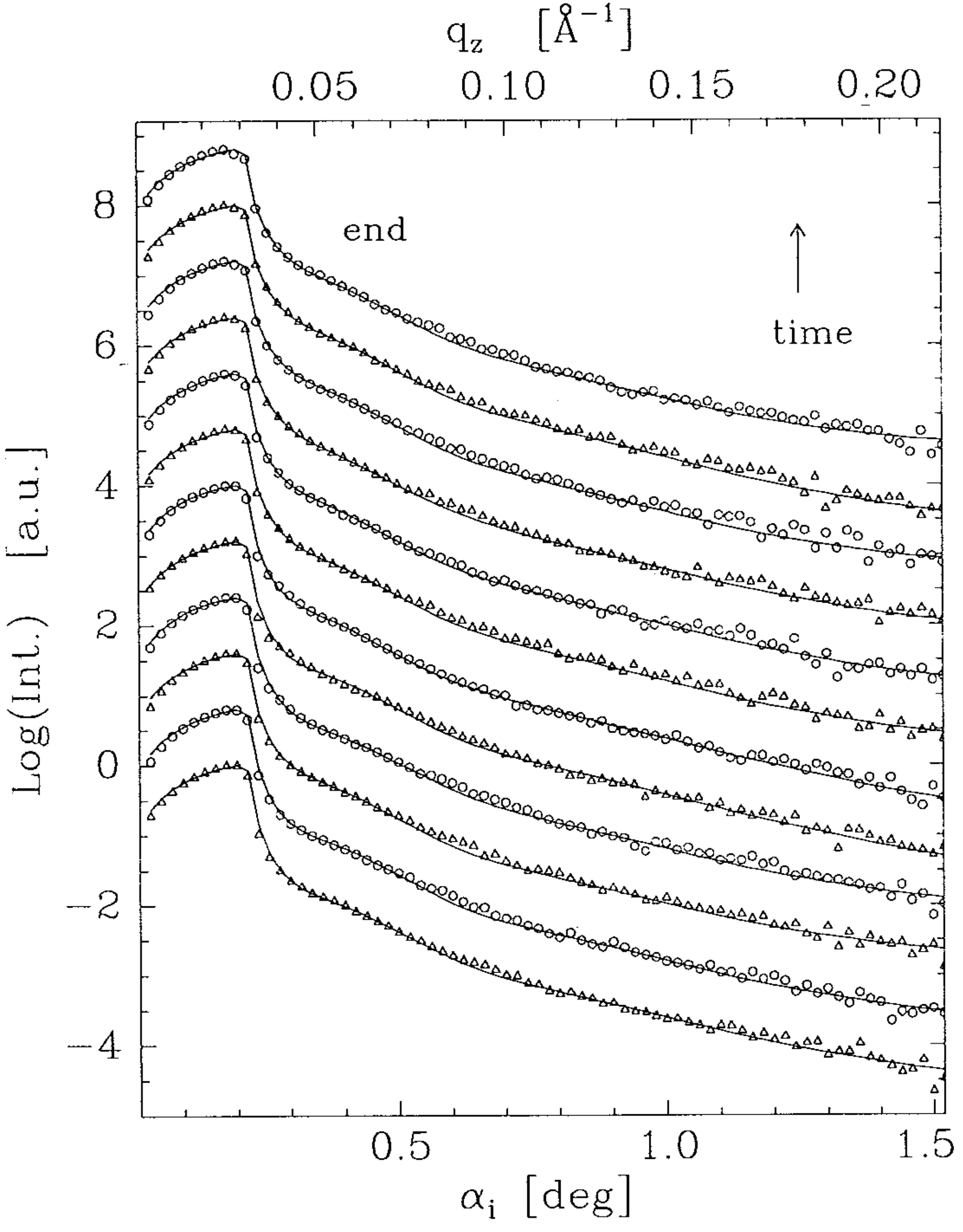

Figure 6.19: *Continuation of Fig.6.18.*

6.2.2 CCl_4 on CH_3/Si

Fit yield parameters are given in table 6.4. The roughness parameter shows an increase with increasing thickness and the density of the wetting liquid film gradually increases to the theoretical value of the bulk liquid CCl_4. The fit was done assuming a two layer model (CH_3 and CCl_4).

S.No	$\delta 10^6$	σ [Å]	l[Å]	S.No	$\delta 10^6$	σ [Å]	l[Å]	S.No	$\delta 10^6$	σ [Å]	l[Å]
1	3.0	12.0	43.0	12	4.4	32.0	138.0	23	4.8	36.0	245.0
2	3.0	13.0	44.0	13	4.7	35.0	155.0	24	4.9	35.0	260.0
3	3.0	14.0	45.5	14	4.7	33.0	180.0	25	4.8	36.0	258.0
4	3.0	14.0	47.0	15	4.9	37.4	179.0	26	5.0	37.0	267.0
5	3.1	18.0	51.0	16	4.9	34.0	185.0	27	5.0	37.0	263.0
6	3.0	17.0	54.0	17	4.8	36.0	218.0	28	4.9	38.0	270.0
7	3.2	25.0	60.0	18	4.9	37.0	232.0	29	5.0	38.0	267.0
8	3.3	25.0	64.0	19	4.7	38.0	211.5	30	5.0	38.0	266.0
9	3.3	30.0	84.0	20	4.8	38.0	253.0	31	5.1	38.0	270.0
10	3.6	32.0	93.0	21	4.6	38.0	238.0	32	5.1	37.0	273.0
11	4.0	32.0	118.0	22	4.6	36.0	250.0	33	5.0	37.0	270.0

Table 6.4: Fit parameters of the wetting film of CCl_4 on a CH_3/Si substrate.

An example of a density profile for this system is shown in Fig. 6.20. Figs. 6.21 and 6.22 show the transverse scans and the measured reflectivities over 17hrs and the film is stable after this time. The reflectivity measurements and fit curves of the system are shown in Figs. 6.23, 6.24, 6.25 and 6.26. These figures show a poor fitting but the thickness of the wetting film, which depends on the modulation of the curve, is exact within a range of errors. It was tried to get a good fit by dividing the liquid film into two layers and the thickness is almost the same as that obtained fitting the one-layer model. For comparison see appendix.

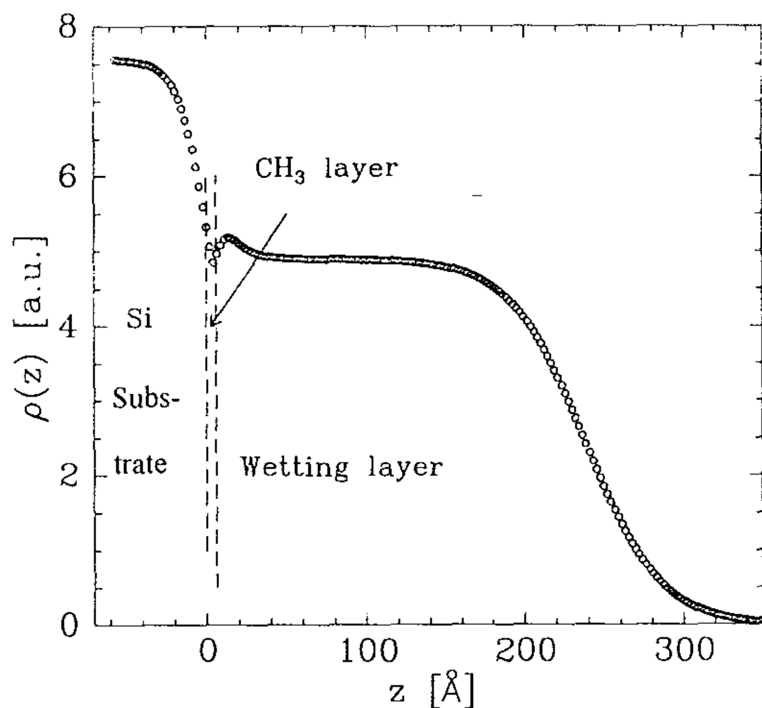

Figure 6.20: *An example of a density profile of the wetting film CCl_4 on CH_3/Si.*

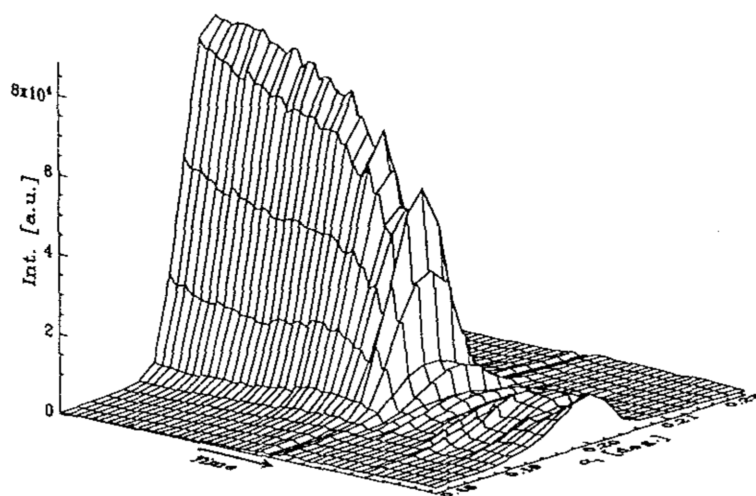

Figure 6.21: *Measured transverse scans at q_z = 0.03Å fixed for the system CCl_4 on CH_3/Si.*

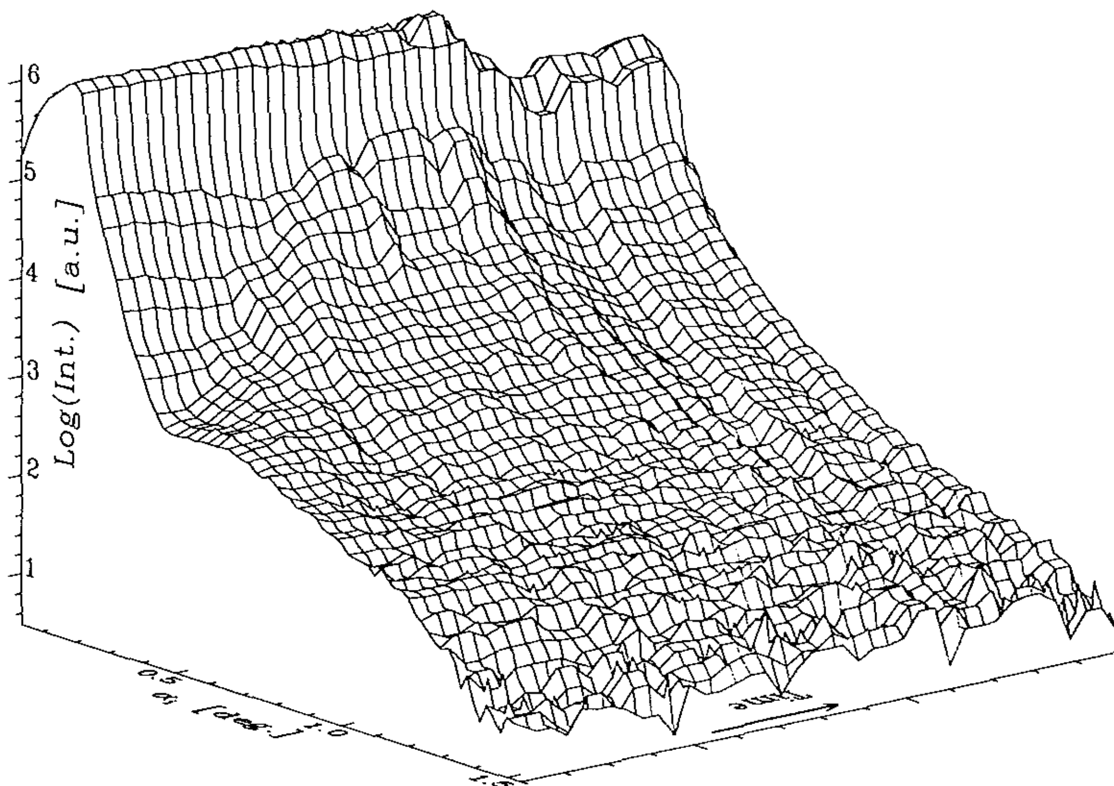

Figure 6.22: *Measured reflectivities over 17hrs for the system CCl_4 on CH_3/Si where the arrow shows time direction.*

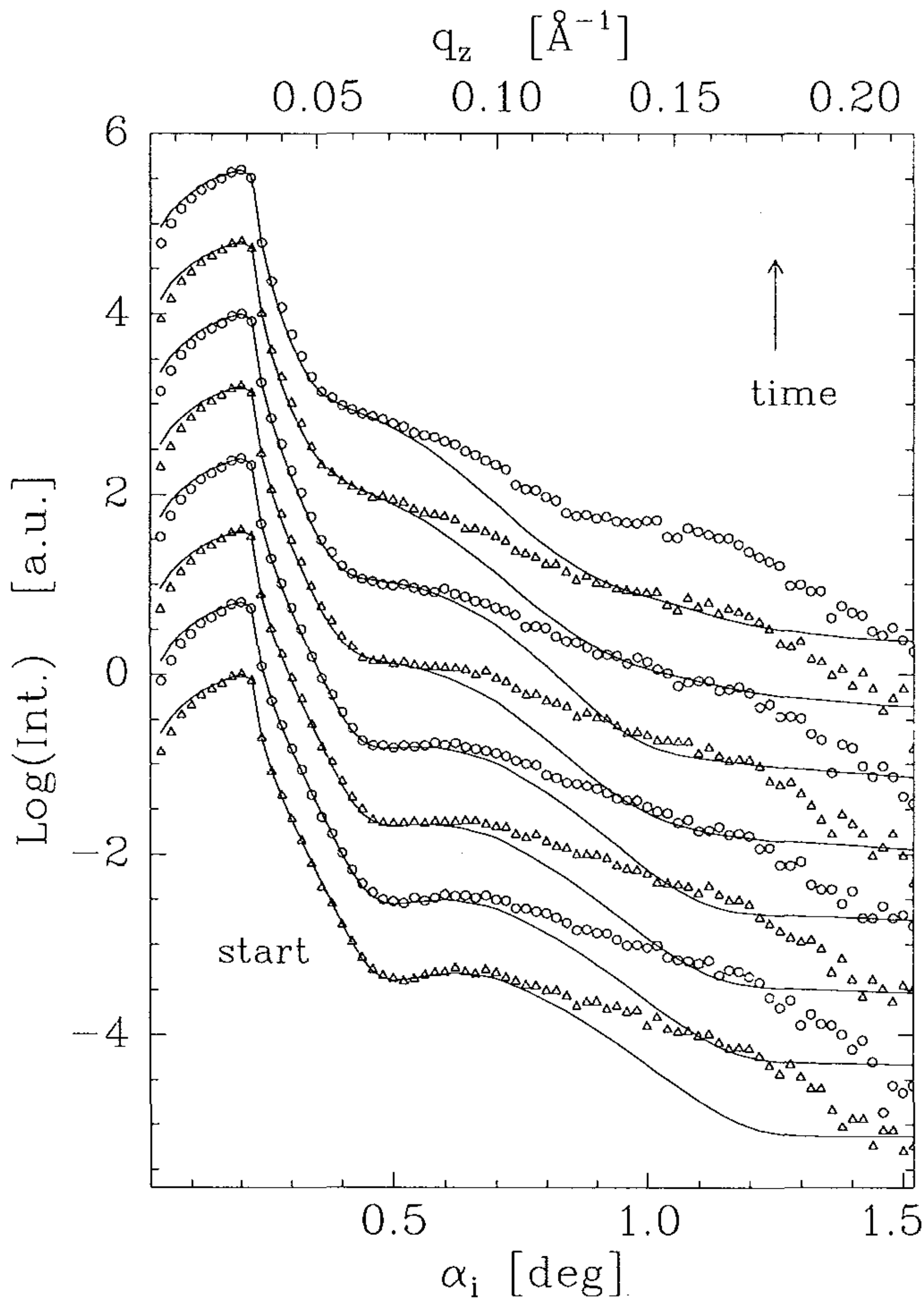

Figure 6.23: *Wetting reflectivities (open circles and triangles) and fit results (solid lines) of the system CCl_4 on CH_3/Si for the first 4.2hrs. The curves are shifted by a 0.8 order (log-scale) of magnitude against each other for clarity.*

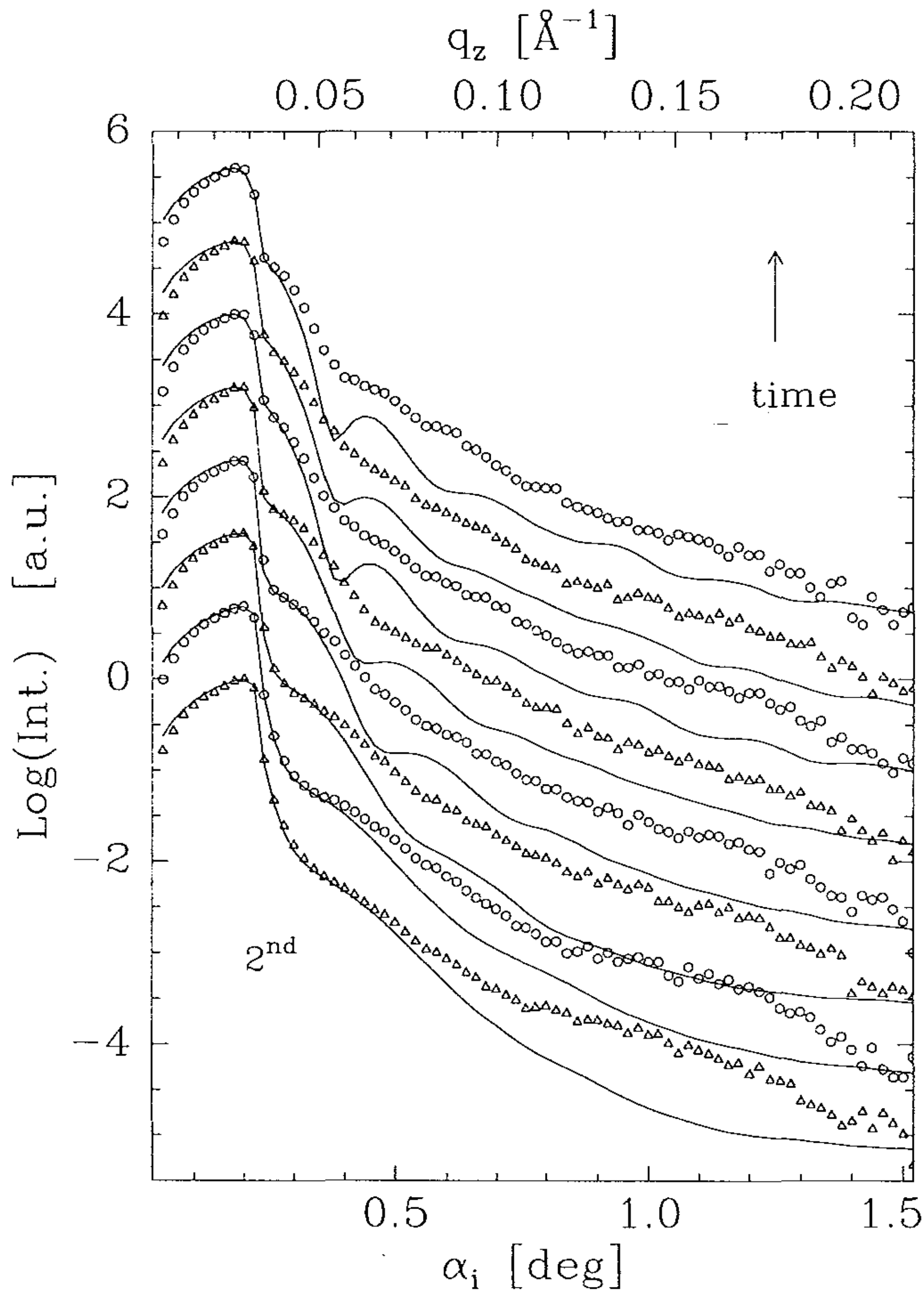

Figure 6.24: *Continuation of Fig.6.23 for the second 4.2hrs. The curves are shifted by a 0.8 order (log-scale) of magnitude against each other for clarity.*

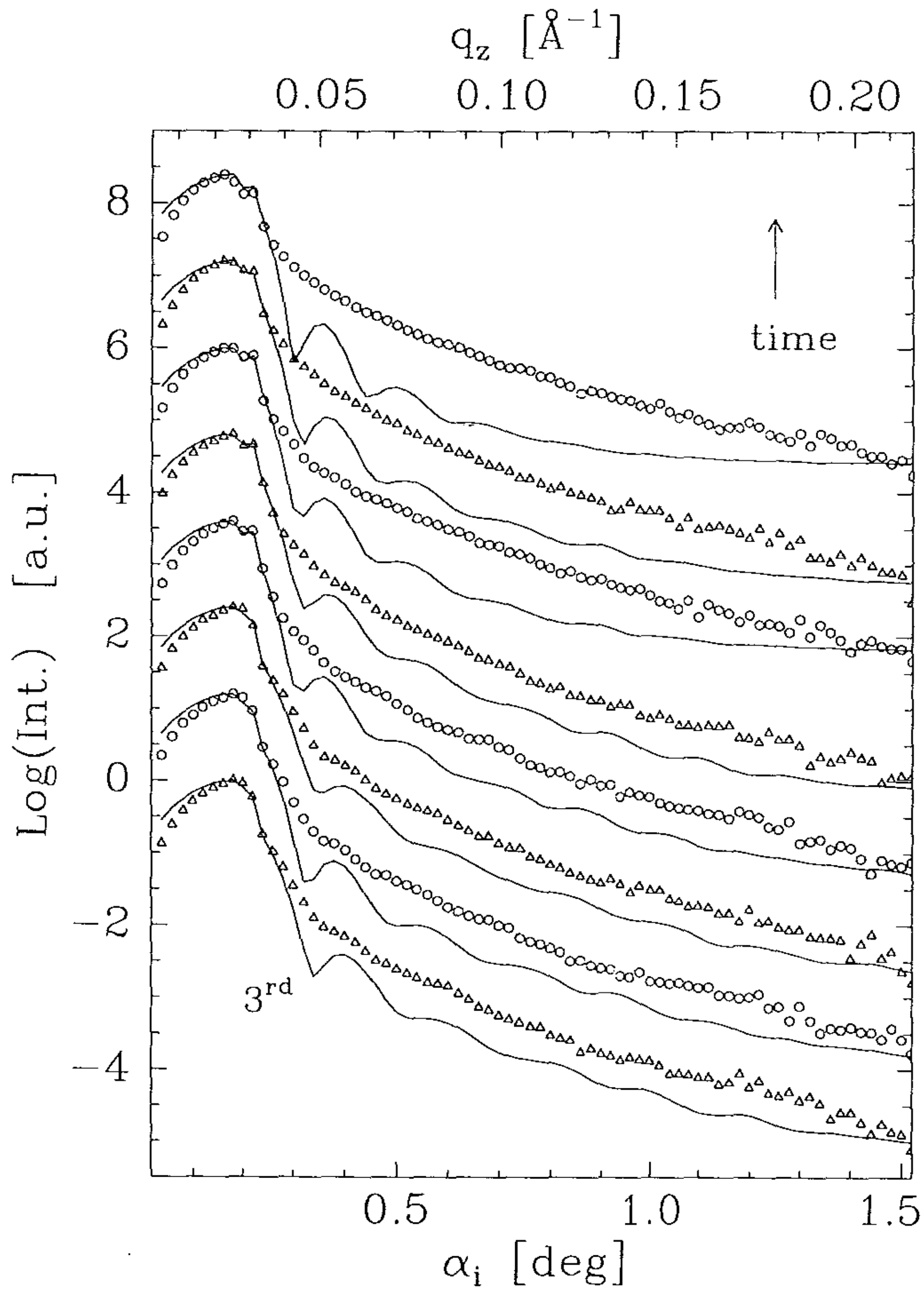

Figure 6.25: *Continuation of Fig.6.24 for the third 4.2hrs and the curves are shifted by a 1.2 order (log-scale) of magnitude against each other for clarity.*

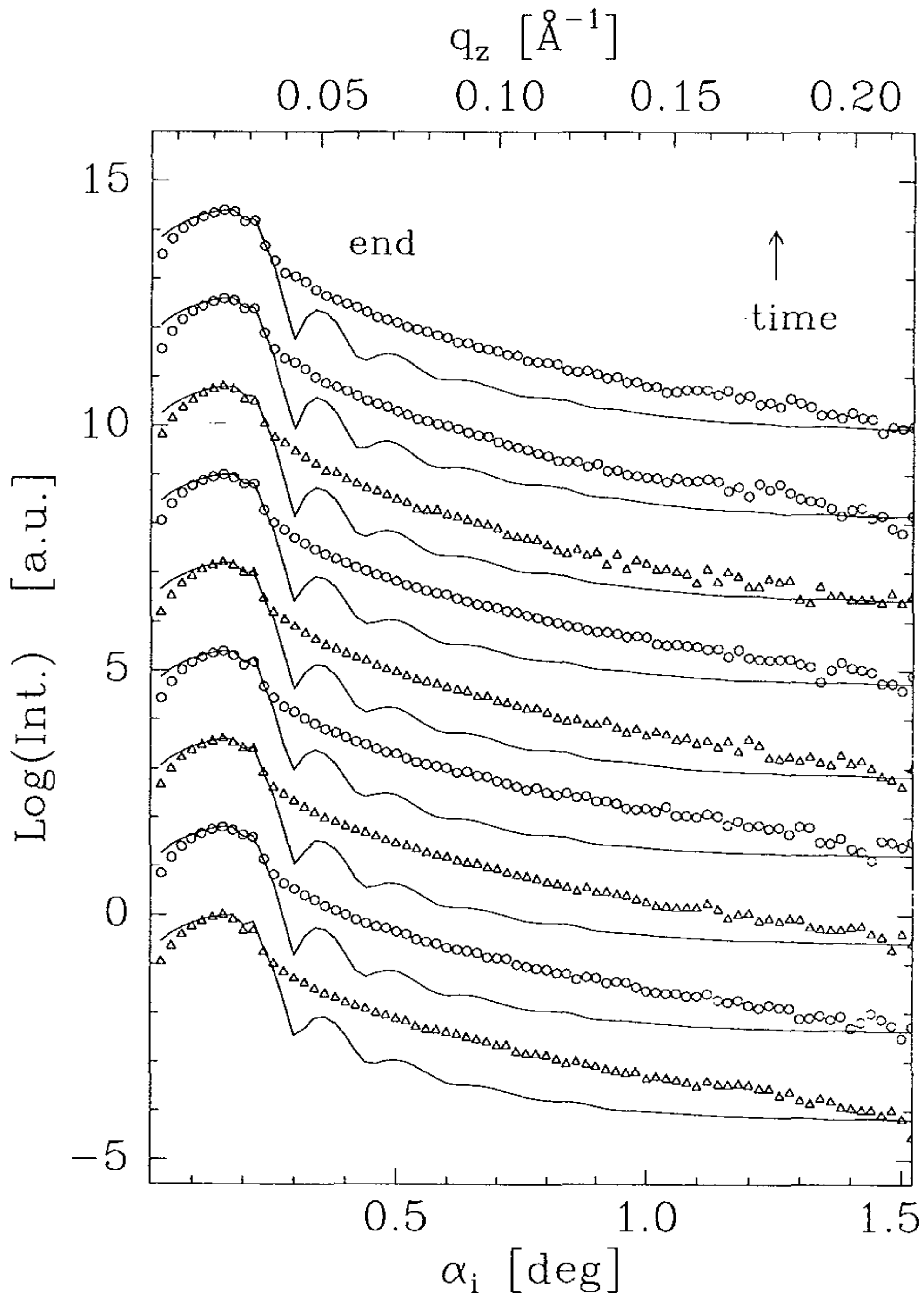

Figure 6.26: *Continuation of Fig.6.25 for the last 4.7hrs and the curves are shifted by a 1.8 order (log-scale) of magnitude against each other.*

6.2.3 CCl_4 on Ge/Si

The fit parameters of the system CCl_4 on Ge/Si are given in table 6.5. The measured transverse scans and a typical density profile of the system are shown in Figs. 6.27 and 6.28, respectively. Fig. 6.29 shows the reflectivities where the film is stable after 10hrs. The corresponding fitted reflectivity measurements (curves) are shown in Figs. 6.30 and 6.31 for a time width of 5.22hrs each and the curves are shifted by a unit order (log-scale) of magnitude against each other with the bottom as the starting point.

Sc.No.	$\delta \cdot 10^6$	$\sigma[\AA]$	$l[\AA]$	Sc.No.	$\delta \cdot 10^6$	$\sigma[\AA]$	$l[\AA]$
1	5.4	17.1	47.0	11	5.0	48.3	247.9
2	5.1	15.0	62.0	12	4.3	55.0	257.5
3	5.1	16.6	77.3	13	4.0	58.0	265.0
4	5.3	17.1	92.4	14	4.0	56.5	260.2
5	5.3	21.3	101.5	15	4.3	59.0	260.0
6	5.3	22.3	110.3	16	4.2	54.0	263.8
7	5.0	32.0	148.0	17	4.1	60.0	270.7
8	5.2	40.0	186.0	18	4.0	59.0	262.6
9	5.0	38.0	226.7	19	4.0	58.0	267.0
10	5.0	48.0	251.4	20	4.0	59.0	257.4

Table 6.5: Fit parameters of the system liquid film CCl_4 on Ge/Si substrate.

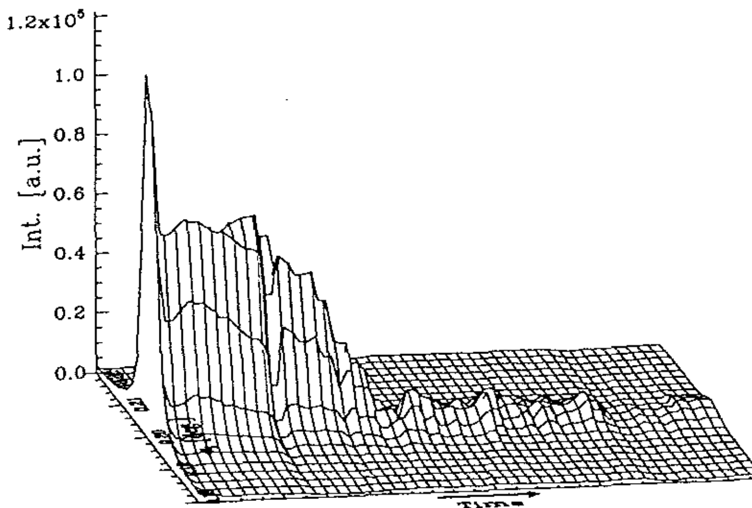

Figure 6.27: *Measured transverse scans at a $q_z = 0.03\AA$ fixed for the system CCl_4 on Ge/Si. The first scan, taken from the dry wafer, is introduced for comparison.*

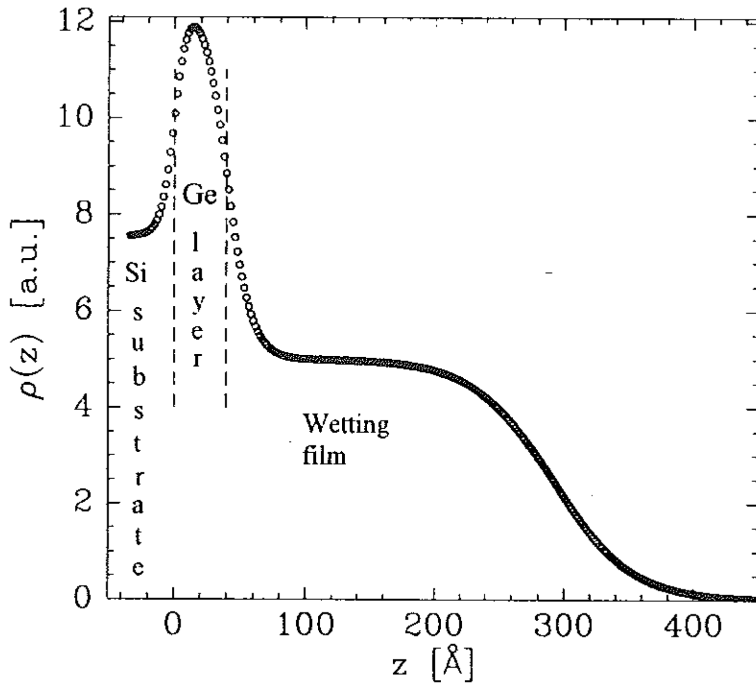

Figure 6.28: *An example of a density profile of a wetting film CCl_4 on Ge/Si.*

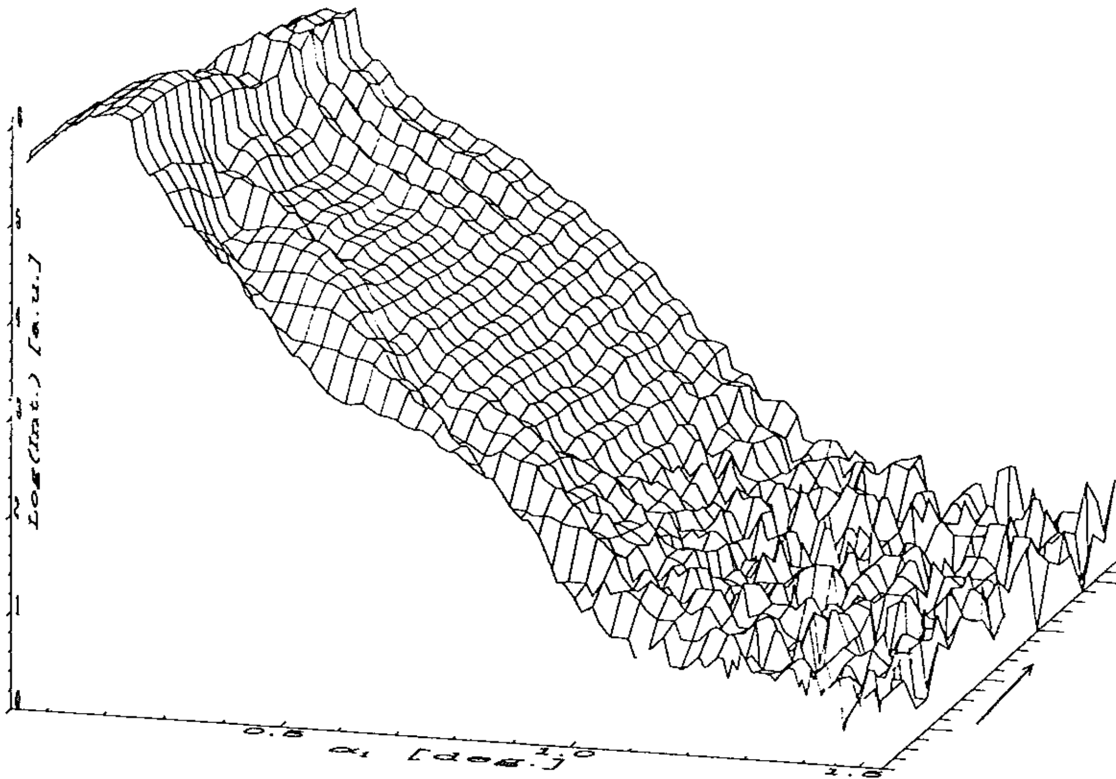

Figure 6.29: *Measured reflectivities over 10hrs for the system CCl_4 on Ge/Si (the arrow is for the time direction).*

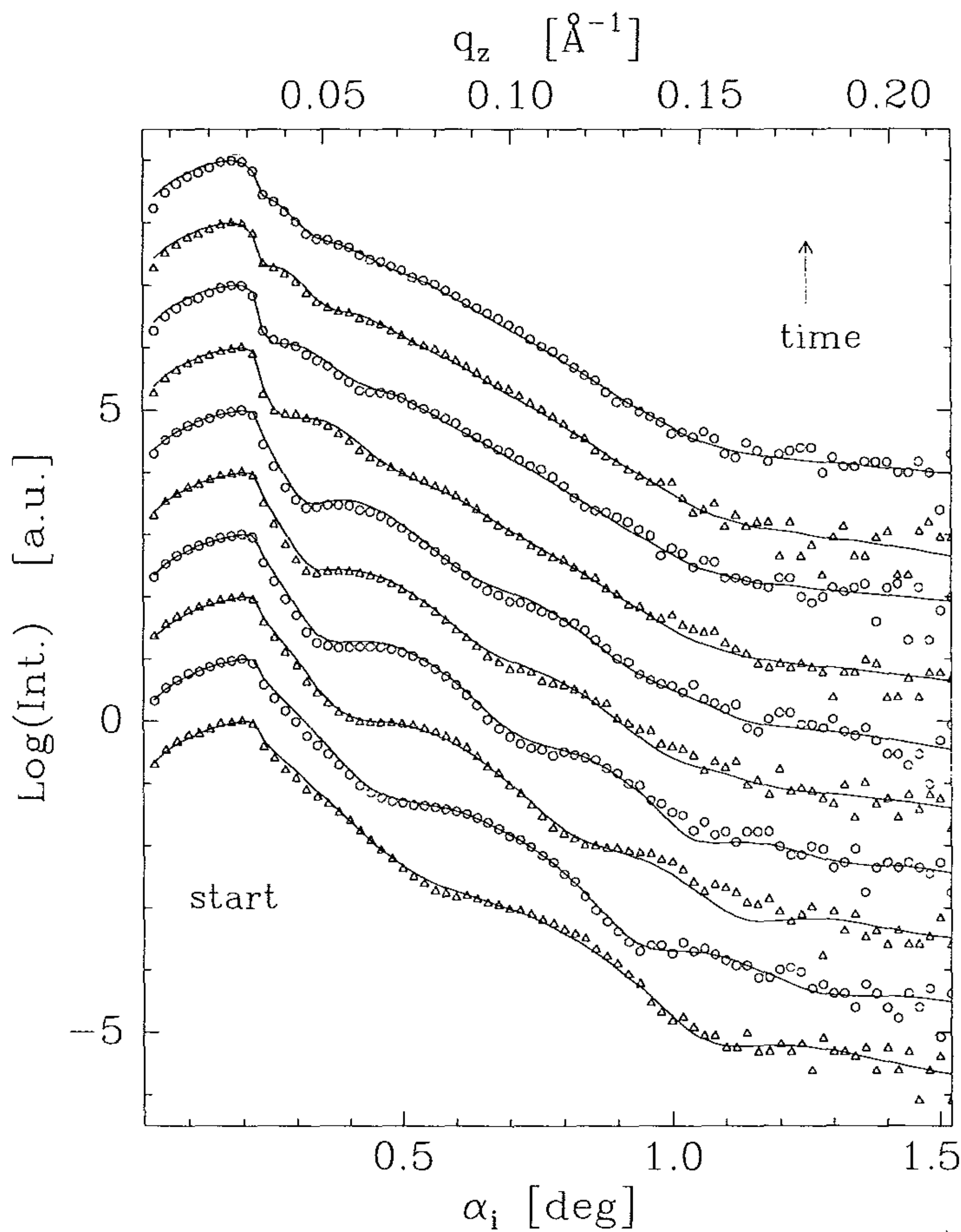

Figure 6.30: *Wetting reflectivity curves of the system CCl_4 on Ge/Si. Measured (open circles and triangles) and fit results (solid lines).*

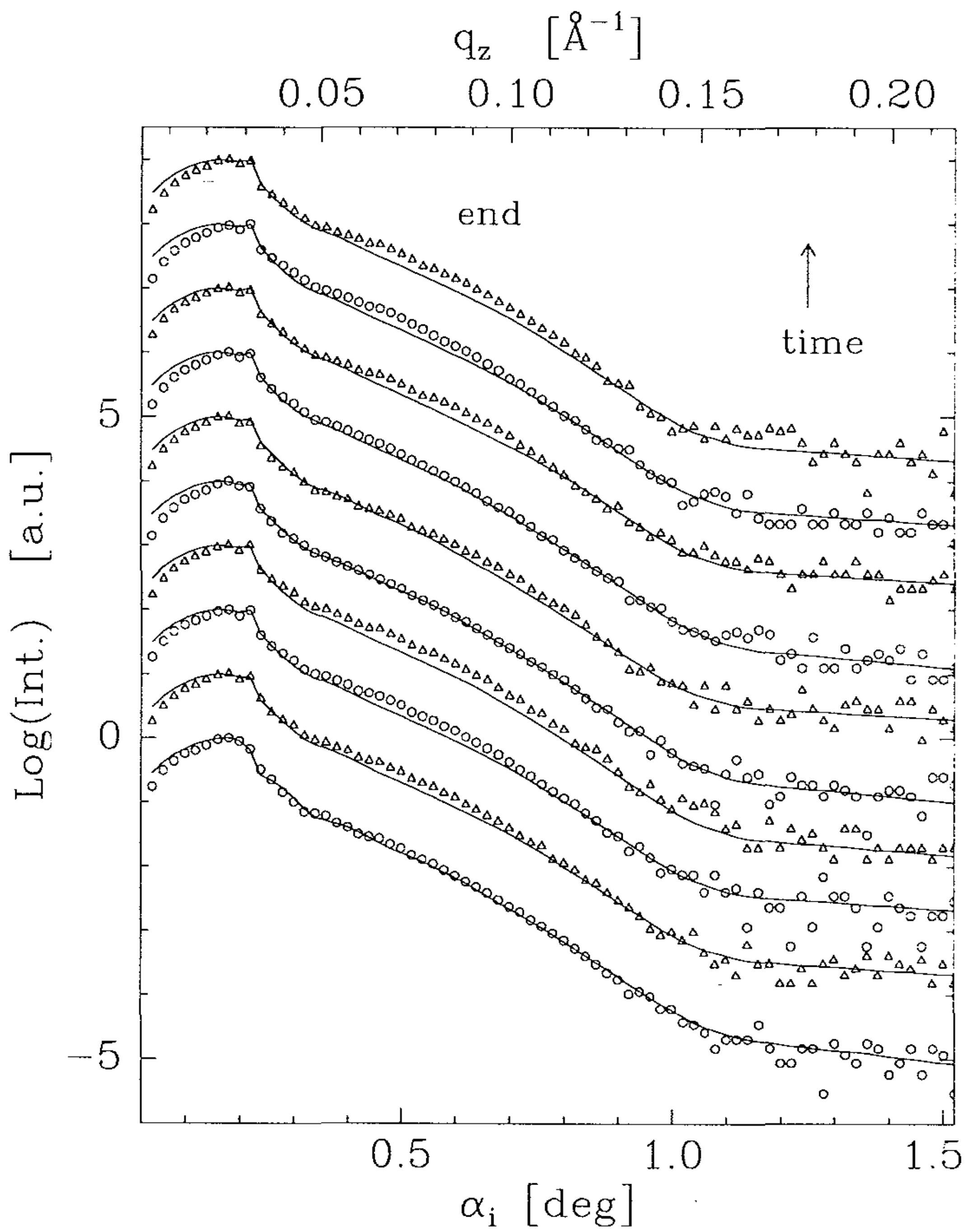

Figure 6.31: *Continuation of Fig.6.30.*

6.2.4 CCl_4 on a Quartz Glass

Table 6.6 shows the fit results of the wetting system where parameters of the dry substrate were kept constant. The roughness of the film is almost constant during its growth and the density gets its bulk value at the equilibrium thickness.

S.No	$\delta 10^6$	$\sigma[\AA]$	$l[\AA]$	S.No	$\delta 10^6$	$\sigma[\AA]$	$l[\AA]$	S.No	$\delta 10^6$	$\sigma[\AA]$	$l[\AA]$
1	4.0	8.0	64.8	16	4.5	8.9	163.4	31	5.0	9.3	215.5
2	4.1	8.0	65.3	17	4.5	8.7	168.7	32	5.1	9.2	223.5
3	4.3	8.2	67.0	18	4.6	8.7	171.0	33	5.0	9.3	226.9
4	4.5	9.3	72.5	19	4.6	8.4	175.1	34	5.0	9.2	228.0
5	4.7	9.6	75.0	20	4.7	8.8	176.2	35	5.0	9.2	228.3
6	4.9	10.0	82.0	21	4.7	8.9	182.2	36	5.0	9.1	225.8
7	4.1	8.5	103.5	22	4.8	8.9	186.9	37	5.0	8.9	225.0
8	4.1	8.7	114.4	23	4.8	8.7	190.1	38	5.0	9.3	226.5
9	4.1	8.2	122.4	24	4.9	8.9	191.1	39	5.0	9.1	227.2
10	4.3	8.6	135.3	25	4.9	9.0	193.1	40	5.0	8.8	222.3
11	4.4	8.8	141.6	26	4.9	9.1	196.9	41	5.0	8.7	222.6
12	4.4	9.0	145.4	27	4.9	8.8	204.0	42	5.0	9.0	225.0
13	4.4	9.0	152.5	28	5.0	9.2	212.9	43	5.0	8.6	225.7
14	4.5	8.8	157.0	29	5.0	9.4	212.7	44	5.0	8.9	223.9
15	4.6	9.3	162.3	30	5.0	9.5	211.8				

Table 6.6: Fit parameters of the reflectivity measurements of the system CCl_4 on a quartz glass substrate.

A typical density profile for this system are shown in Fig. 6.32 and the measured transverse scans during the growth process is shown in Fig. 6.33. The measured reflectivity curves over 20hrs are shown in a three dimensional picture. Fig. 6.34. The fitted reflectivity measurements are shown in Figs. 6.35, 6.36, 6.37 and 6.38 for a time width of 5.74hrs each, and the curves are shifted by a unit order (log-scale) of magnitude against each other.

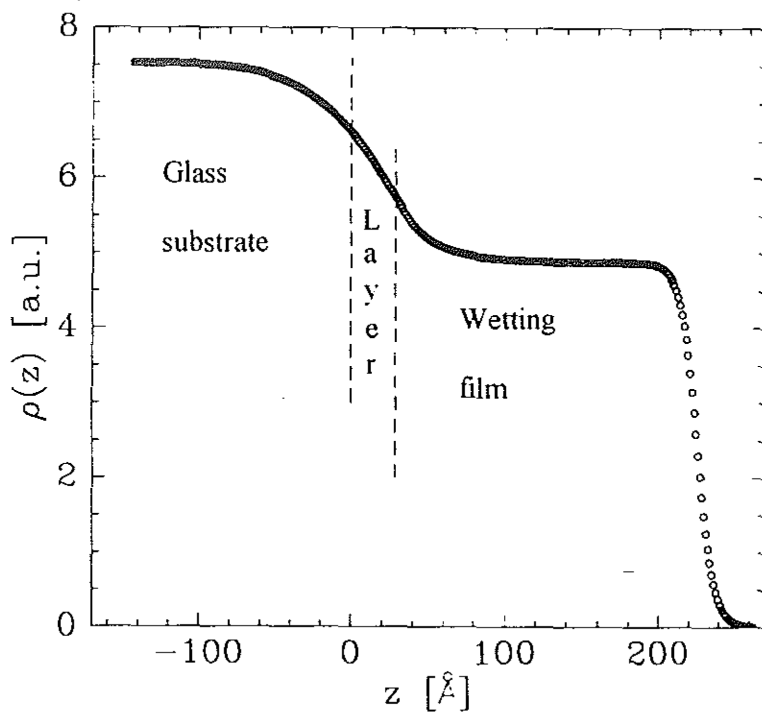

Figure 6.32: *An example of a density profile of a wetting film CCl_4 on a quartz glass.*

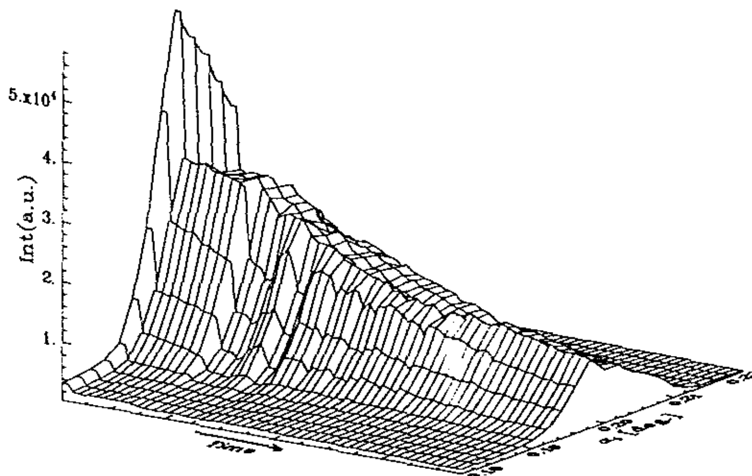

Figure 6.33: *Measured transverse -scans (q_x-scans at q_z = 0.03Å fixed for the system CCl_4 on a quartz glass where the first scan is referred to the dry substrate.*

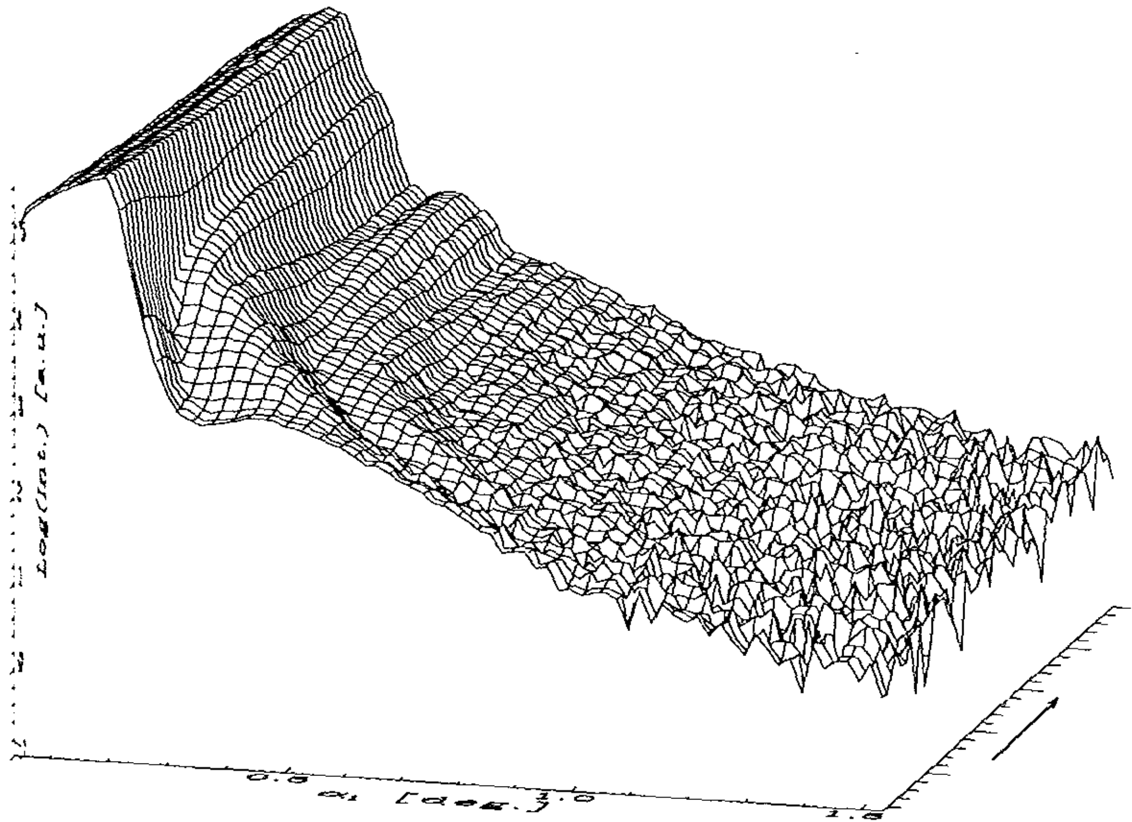

Figure 6.34: *Measured reflectivities over 23hrs for the system CCl_4 on a quartz glass where the arrow shows time direction.*

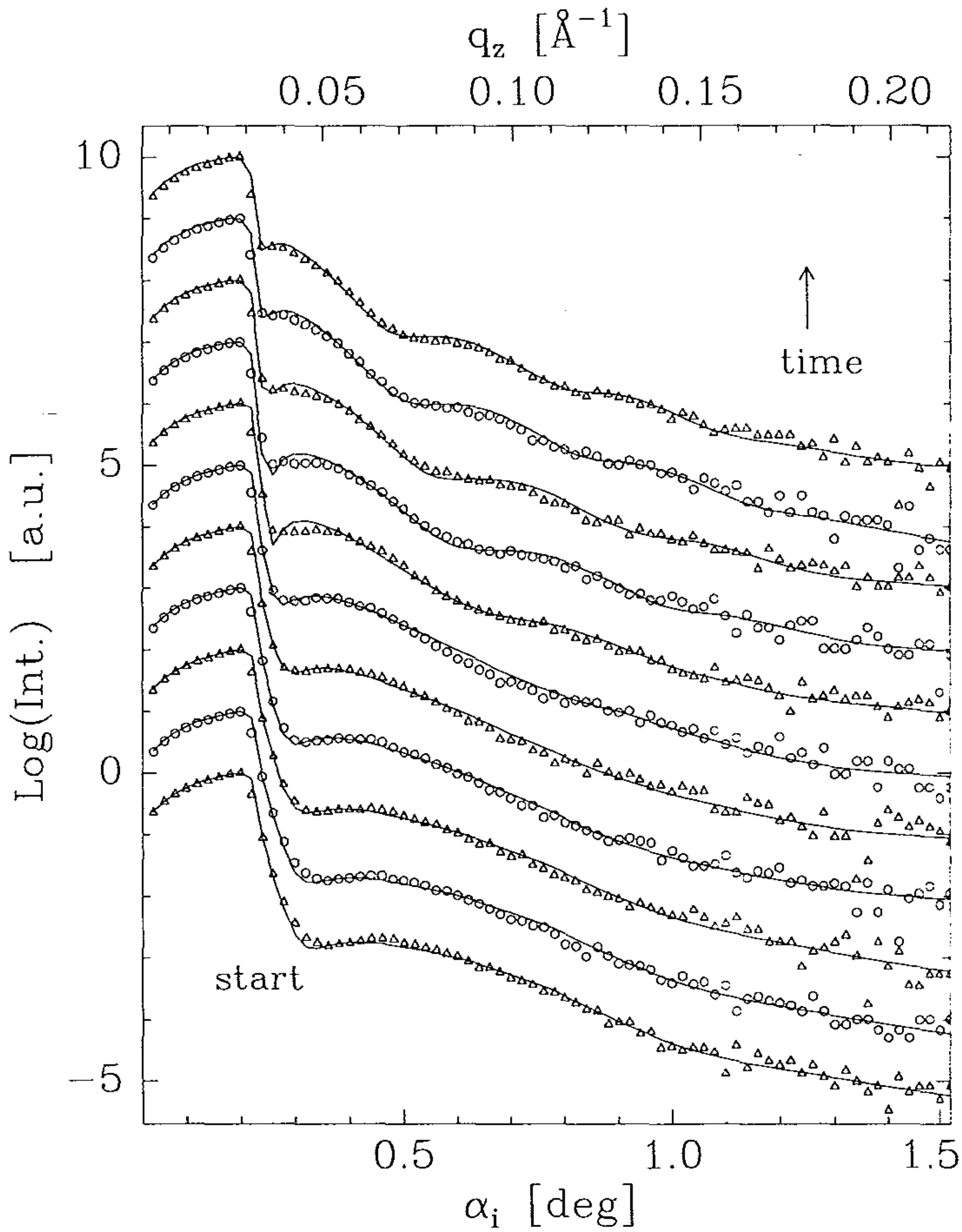

Figure 6.35: *Measured specular reflectivities (circles and triangles) and fit results (solid lines) for the system CCl_4 on a quartz glass.*

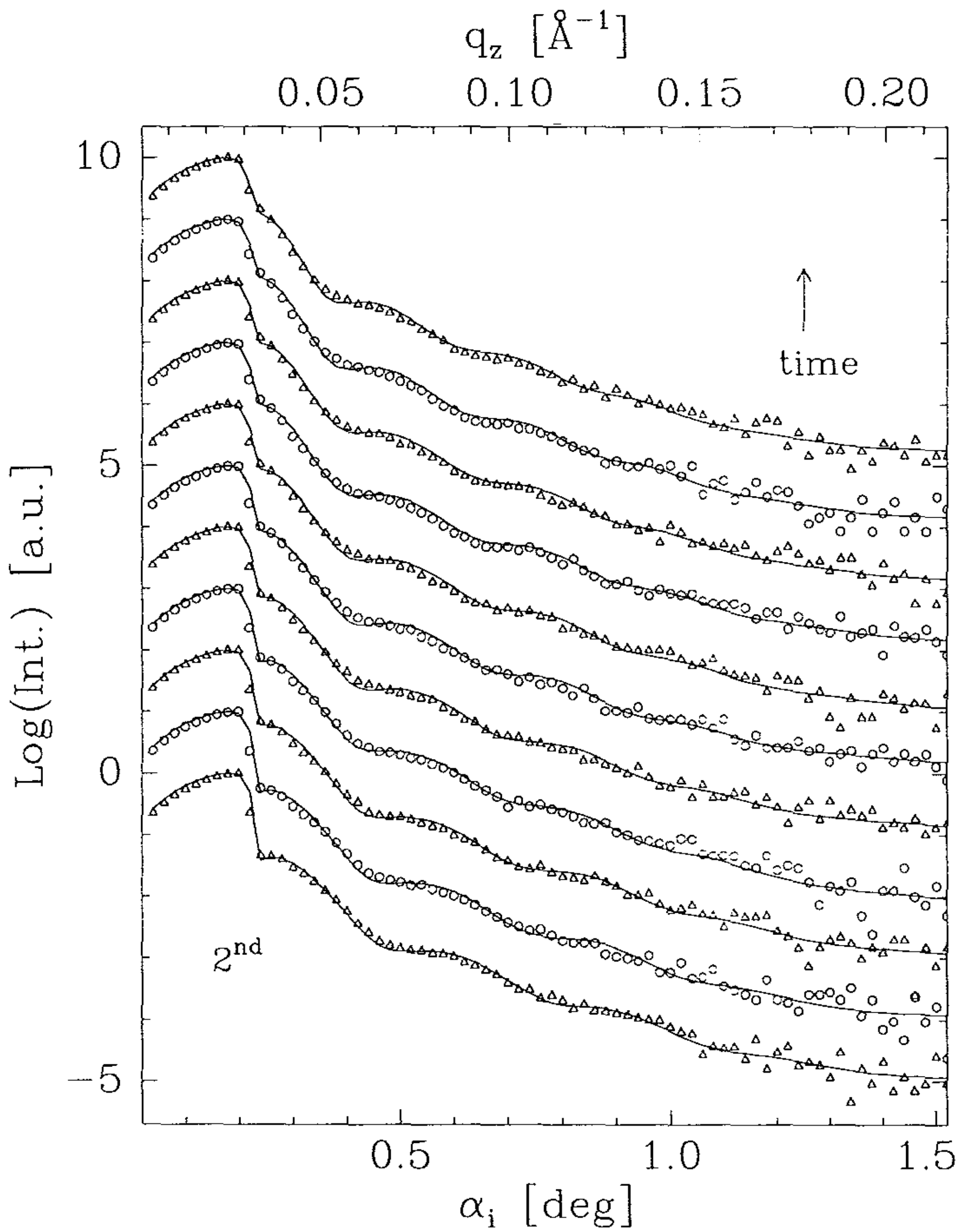

Figure 6.36: *Continuation of Fig.6.35.*

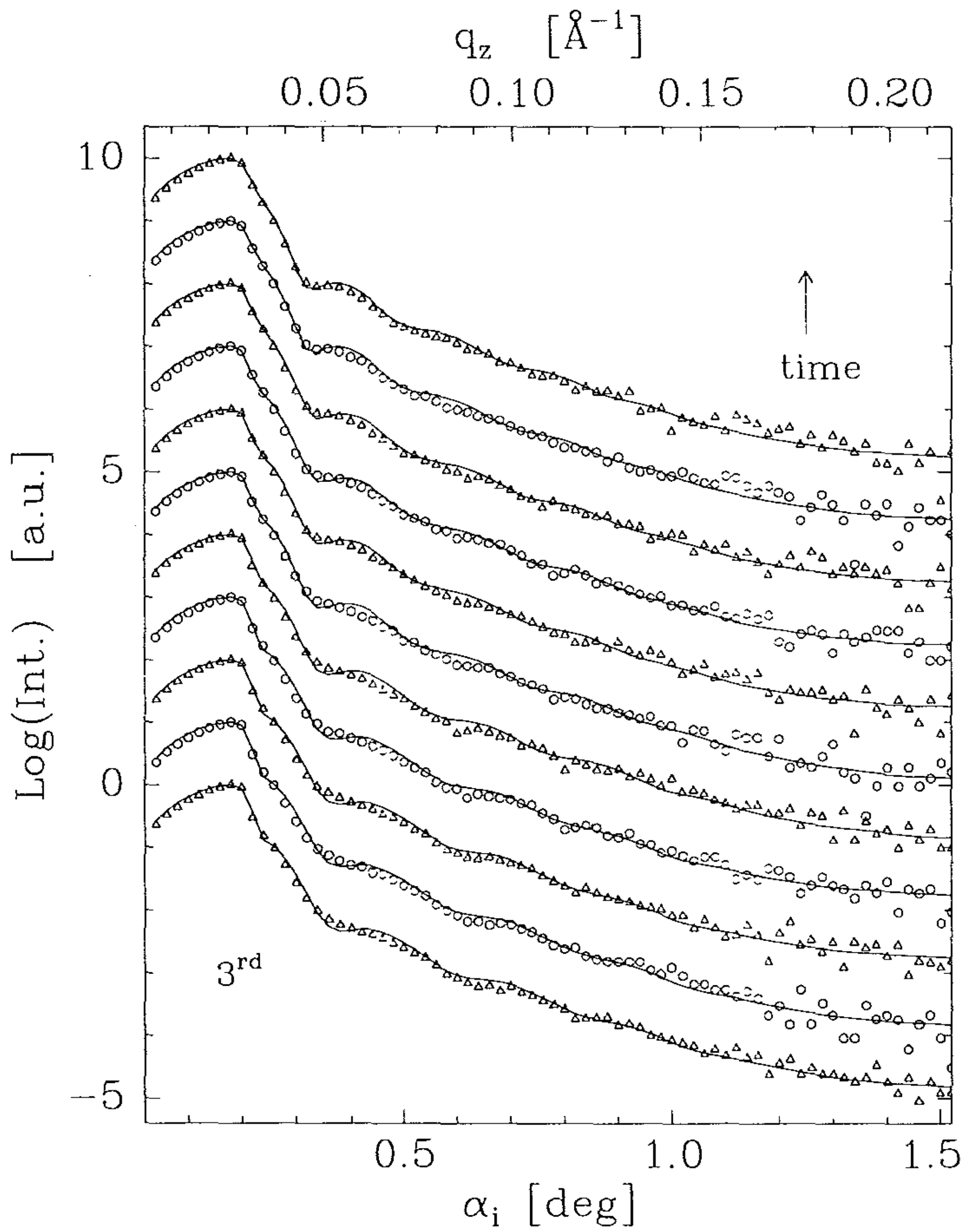

Figure 6.37: *Continuation of Fig.6.36.*

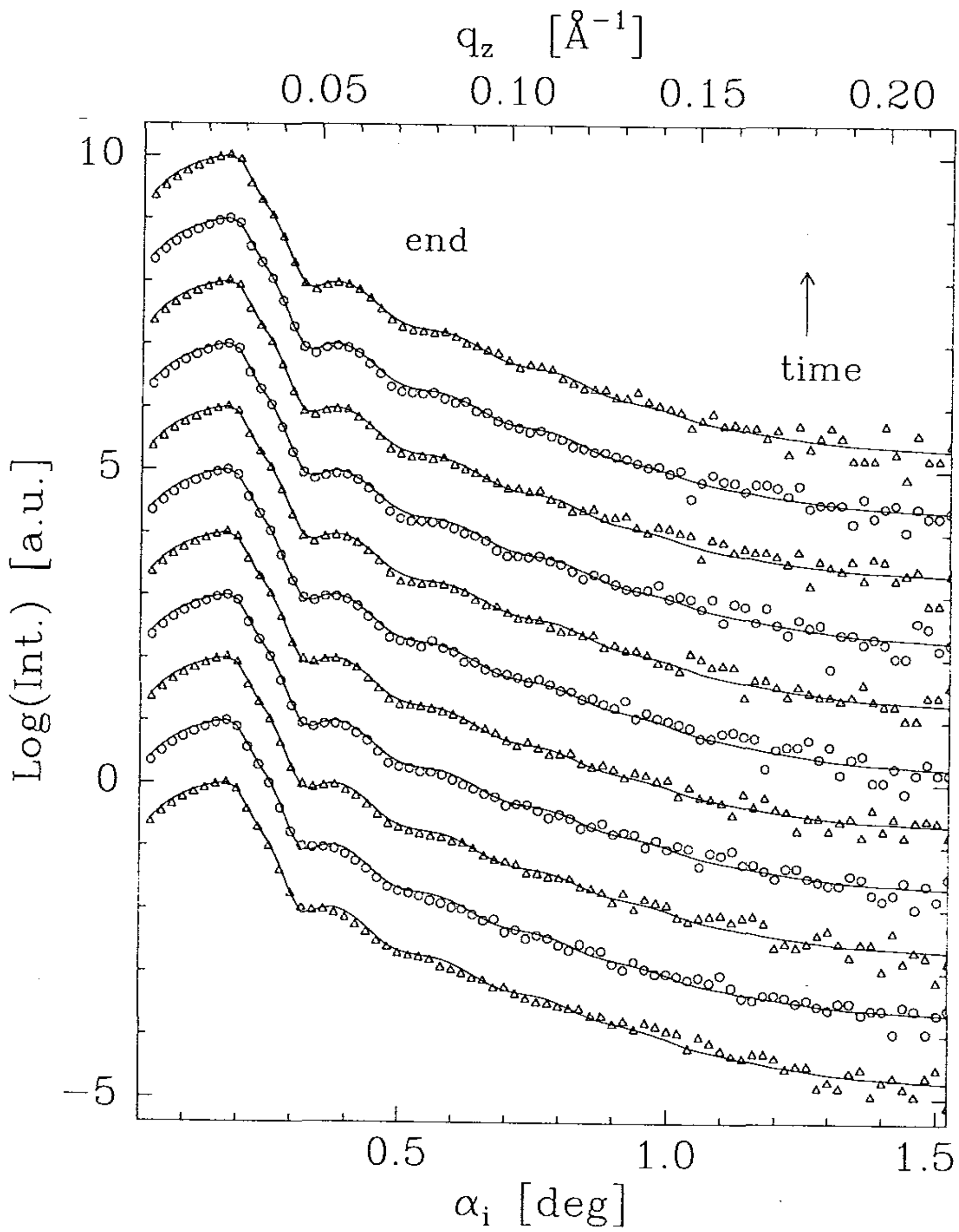

Figure 6.38: *Continuation of Fig.6.37.*

Chapter 7

Discussion

The observed growth kinetics of the wetting layers are adapted in this chapter in the framework of the model given in section 3.4. Thus, the growth parameters are obtained by fitting eq. (3.54).

7.1 Adaption of the growth measurements to the Kolmogorov Model

As was explained in chapter 3, the Kolmogorov model describes the time dependence of a first order phase transformation from a (metastable) phase A into a stable phase B. It contains two parameters: The rate of nucleation Γ of infinitesimally small new grains per unit volume of metastable material, and the velocity v of the isotropical growth of grains after nucleation until they are impeded by a neighboring grain. The parameters Γ and v are assumed as time independent constants. Thus, eq. (3.50) for $d = 2$ and $C_d = \pi$ can be reduced to

$$\Gamma v^2 = \frac{3}{\pi \tau^3}.$$

The constant C_d takes into account the geometry of the grain and depends on the dimension d of the growing mechanism[4]. Note, that the time constant τ depends on Γ and v. Therefore, a single experiment only yields the product Γv^d for a particular system. Results obtained from the fits of the data are given in table 7.1, and the measured and Kolmogorov-fitted time dependence of the wetting film thicknesses are

shown in Figs. 7.1, 7.2, 7.3 and 7.4 for the systems CCl_4 on H_2/Si, CH_3/Si, Ge/Si and on a quartz glass, respectively. Open circles are the measured thicknesses and the solid and broken lines represent fits with the Kolmogorov model for n variable and $n = 3$, respectively.

System	H_2/Si	CH_3/Si	Ge/Si	Q.Glass
τ[hrs] ($n = 3$)	11.49	7.45	3.62	7.79
l_0[Å]	33.0	43.0	55.0	65.0
l_{max}[Å]	88.0	269.0	265.0	225.0
$\Gamma v^2[10^{-3}(hrs)^{-3}]$	0.63	2.20	20.13	2.02
τ[hrs]	13.57	7.57	3.57	8.57
(n variable)	1.18	2.53	2.64	1.35
l_0[Å]	25.0	43.0	50.0	65.0
l_{max}[Å]	101.0	271.0	264.0	233.0

Table 7.1: Parameters obtained fitting the Kolmogorov model to the examined liquid film CCl_4 on the four bare substrates.

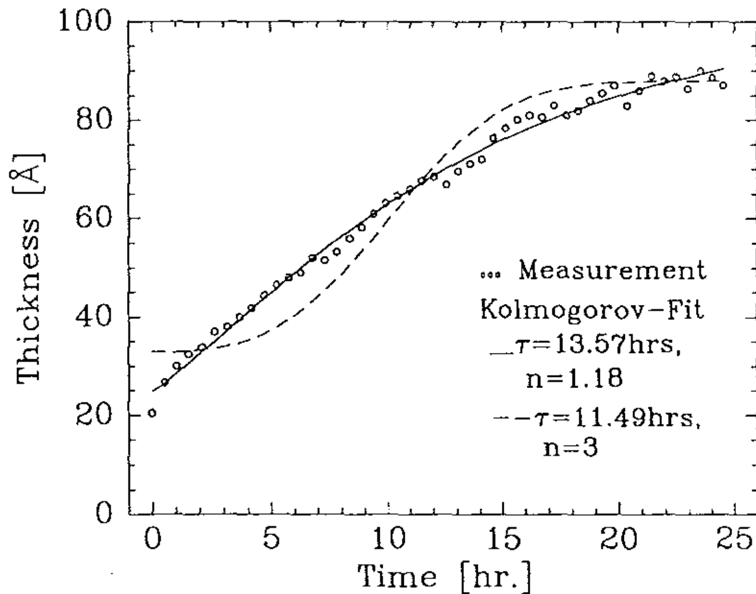

Figure 7.1: *Time dependent measurement and Kolmogorov -fitted results of the wetting film CCl_4 on H_2/Si.*

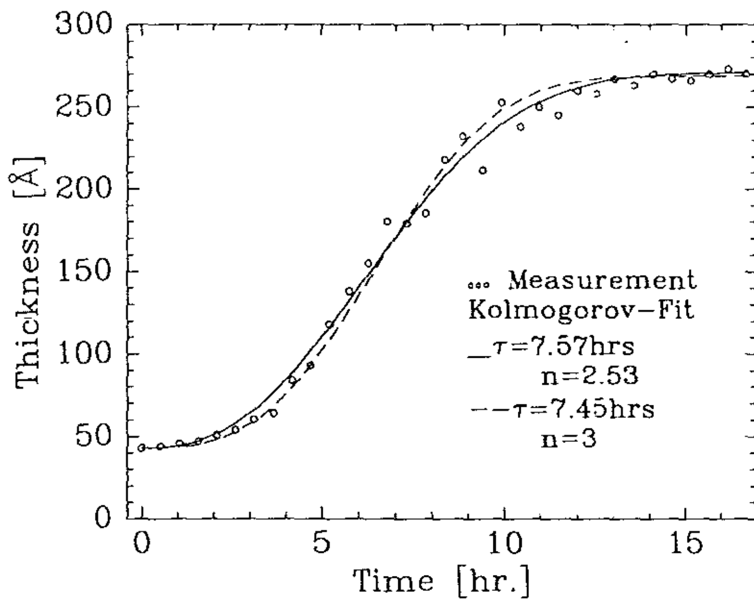

Figure 7.2: *Measured and Kolmogorov -fitted results of the system CCl_4 on CH_3/Si.*

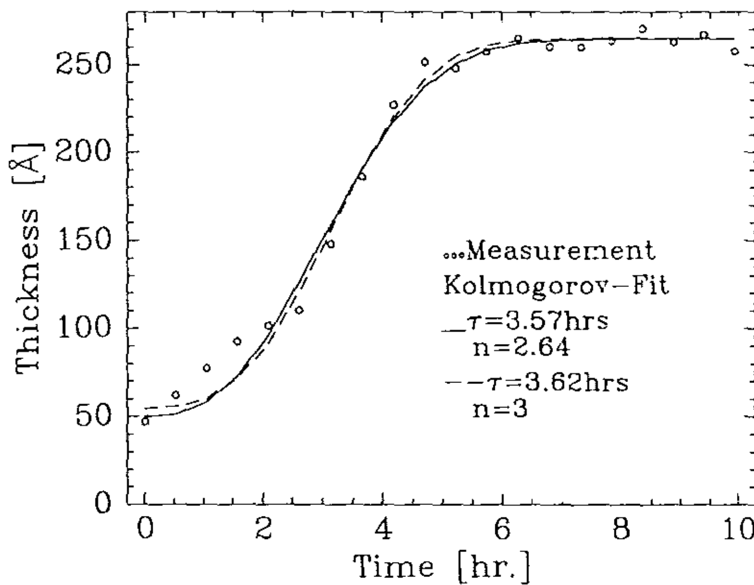

Figure 7.3: *Time dependent measurements and fit results of the Kolmogorov model for the system CCl_4 on Ge/Si.*

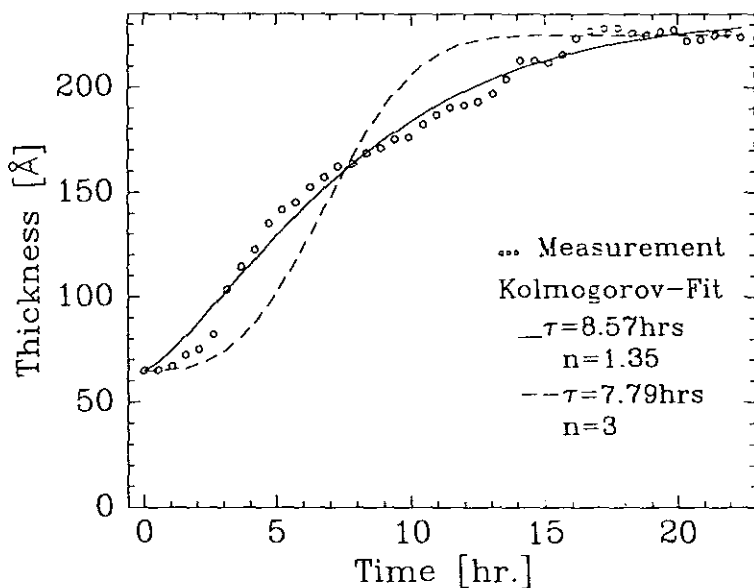

Figure 7.4: *Measured and Kolmogorov-fit results of the system CCl_4 on a quartz glass.*

7.2 Concluding Remarks

Experiments in which the wetting of silicon (coated with H_2, CH_3 and Ge) and a quartz glass by a liquid CCl_4 determined by x-ray specular reflection have been described with the Kolmogorov model. The aim of this work is to study the dynamics of growing wetting films. Gravitational effects as well as temperature stability of the system lead to a finite value l_{max}[26,37]. The temperature pulse ΔT at the time t=0 reduces the thickness l_{max} to a value l_o. Then the film starts to grow and for $t \gg \tau$ again reaches a thickness l_{max}.

From Figs. 7.1 to 7.4 it can be seen that the model is able to explain the data for all investigated systems with different dimensionalities. Although it is difficult to measure Hamaker constants accurately, it seems to follow from all measurements (see [27,37]) that the effective Hamaker constant of the system CCl_4/Ge/Si is larger than the others. This may explain the smaller value of the time constant: A larger Hamaker constant, i.e. a large substrate-adsorbate interaction leads to a quicker film growth. This argument is supported by an analysis of the off-specular x-ray scattering of the bare substrate Ge/Si (see table 6.2). Fit of a data using a fractal height-height correlation function Eq. (2.30) yields extremely jagged surfaces for small values of h the Hurst parameter) and the in-plane correlation length ξ, Fig. 2.7. The smaller value of h provides a relatively larger effective surface area which is more attractive, i.e. it gives a smaller value of τ. From table 7.1 the growth seems two-dimensional. However, for an extremely jagged surface a pure two-dimensional growth of the wetting film is not possible. Nevertheless, the experimental data shows nearly a two-step (fast-slow-fast) growth of the film and the fit yields an average value of the parameters (nearly two-dimensional) because in the Kolmogorov model the exponent n is related to the dimension of the growth process. Additionally, a greater roughness enlarges the film thickness (at a fixed chemical potential difference $\delta\mu$) because the free energy is reduced[30]. Therefore the roughness of the substrate can cause an acceleration of the growth process and leads to a smaller value of the time constant τ.

The time constants of the systems CCl_4/CH_3/Si and CCl_4/quartz glass are not far apart. The substrate CH_3/Si matches with the theory that the average roughness with a greater value of h(smooth hills and valleys) explains nearly a two dimensional growth.

However, the dimensionality n of the quartz glass substrate is smaller which results from the surface roughness and small value of h.

The fact that small roughnesses yield large time constants, can also be seen from the dynamics of the system $CCl_4/H_2/Si$ where the smaller value of n is related with the value of the Hurst parameter. Although the roughness of the substrate is small, the dimensionality n of the growth is small, where in this system is related with the parameter h, such that the jagged surface does not support a pure two-dimensional growth.

The obtained time constants of the examined systems are in the range of 3.5hrs to 13.5hrs. Comparably long τ-values for other systems were observed[26]{CCl_4 on SiO_2/Si with τ =22hrs}, [34]{the polymer $(C_4H_8)_x$ -$[C_2H_3(C_2H_5)]_{1-x}$ on SiO_2/Si with $\tau \approx$48hrs} and [29]{H_2O on quartz with $\tau \approx$3days}. Moreover, the effective dimensionality for the growth process ranges approximately from 1.2 to 3.0. Although some of these dimensionalities n are smaller than what one would expect from the theory, the quality of the fits suggests that the theory is still relevant, and that some explanation for the small measured values of n should first be sought within the context of the general Kolmogorov-Avrami theory. Several systems appear to have the expected integer values of n, but in many other systems the value of n is smaller and not necessarily integer[39]. A number of explanations have been offered, many of which are specific to the particular system, see for example[4,15,35].

In general the time constant and hence the growth process seems to depend on the surface roughness, the real in-plane structure(jagged or smooth) of the substrate and the Hamaker constant of the system. Therefore, a better information about the growth process can be obtained measuring a substrate with different surface roughnesses or carrying out set of experiments with the same substrate and different liquids.

Appendix A

As was mentioned in section 6.2.2 the wetting liquid film of the system CCl_4 on CH_3/Si was fitted assuming a two CCl_4 layer model. The parameters obtained from the fits are tabulated below and note that the thickness of the CH_3 layer must be subtracted to get the actual thickness of the wetting layer. Parameters found from fitting the wetting reflectivities and the growth model is given in tables A.1 and A.3, respectively. The assumed density profile is shown in Fig. A.1, and Figs. A.2, A.3 and A.4 are the measured reflectivities with their fits 5.74hrs each. Each of the reflectivity curves are shifted by a unit order (log-scale) of magnitude against each other. Fig. A.5 shows the x-ray measured thickness with the model fit results.

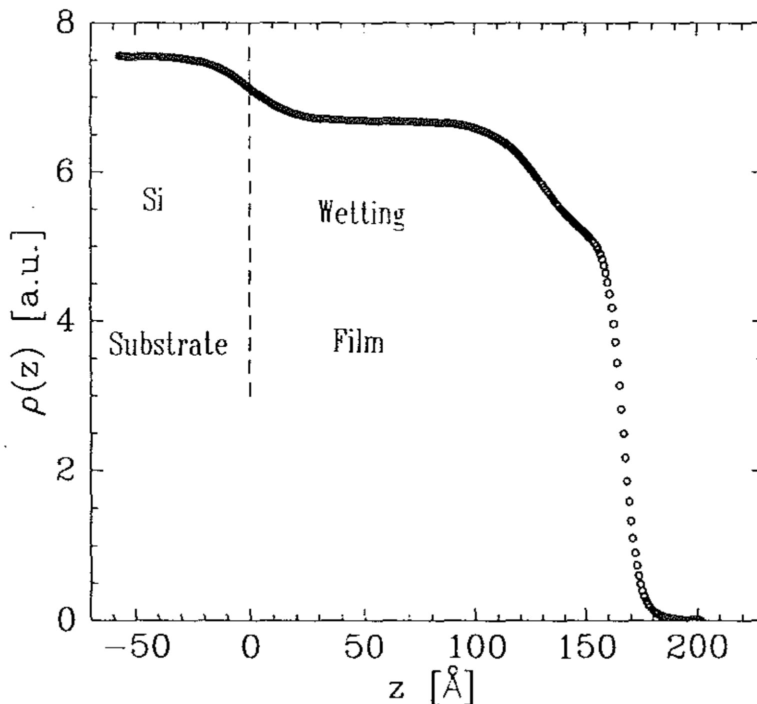

Figure A.1: *A typical example of the density profile found during the fit for the system CCl_4 on CH_3/Si assuming two layers of the film.*

Sc.No.	$\delta_1 \cdot 10^6$	$\sigma_1[\AA]$	$l_1[\AA]$	$\delta_2 \cdot 10^6$	$\sigma_2[\AA]$	$l_2[\AA]$	$(l_1 + l_2)[\AA]$
1	4.2	5.0	20.0	4.2	5.0	27.0	47.0
2	4.2	5.0	19.0	4.3	5.0	28.0	47.0
3	4.6	5.5	19.0	4.3	4.6	31.0	50.0
4	4.8	7.0	21.0	4.3	4.7	32.0	53.0
5	5.1	4.2	21.0	4.5	5.8	35.0	56.0
6	5.6	3.0	24.0	4.5	5.0	39.0	63.0
7	6.0	4.7	29.0	4.7	5.2	41.0	70.0
8	6.0	4.7	31.7	4.8	5.6	40.6	72.3
9	6.4	9.0	48.8	4.9	4.4	39.0	87.8
10	6.9	35.0	55.0	5.0	6.0	46.0	101.0
11	6.9	35.0	87.0	5.0	6.0	40.0	127.0
12	6.8	31.5	120.7	5.0	4.5	26.1	146.8
13	6.7	17.1	130.0	5.0	5.2	36.6	166.6
14	7.1	19.1	150.0	5.0	4.4	35.8	185.8
15	6.9	19.7	150.2	4.9	4.5	34.6	184.8
16	7.1	26.1	165.0	5.1	4.3	33.4	198.4
17	7.4	26.4	195.0	5.0	4.0	34.4	229.4
18	7.5	33.8	219.2	5.0	3.2	30.6	249.8
19	7.3	25.9	190.0	4.9	4.2	34.9	224.9
20	7.6	34.6	220.0	5.4	3.3	36.7	256.7
21	7.6	43.9	224.8	5.4	2.91	28.2	253.0
22	7.4	16.4	198.0	6.7	1.7	64.1	262.1

Table A.1: Parameters obtained fitting the system CCl_4 on CH_3/Si with two CCl_4 layers.

Sc.No.	$\delta_1 \cdot 10^6$	$\sigma_1[\AA]$	$l_1[\AA]$	$\delta_2 \cdot 10^6$	$\sigma_2[\AA]$	$l_2[\AA]$	$(l_1+l_2)[\AA]$
23	7.3	4.0	220.0	6.7	3.0	40.1	260.1
24	7.4	1.3	140.0	7.2	0.1	130.0	270.0
25	7.6	23.3	170.0	7.2	0.1	95.0	265.0
26	7.5	3.0	220.0	7.1	0.2	55.0	275.0
27	7.3	8.9	210.0	7.2	0.1	60.0	270.0
28	7.4	14.5	208.0	7.2	0.1	70.0	278.0
29	7.3	2.4	230.0	6.9	3.3	41.2	271.2
30	7.4	3.0	226.0	7.1	1.8	43.2	269.2
31	7.3	38.8	230.0	6.5	3.4	46.9	276.9
32	7.4	31.3	229.0	6.6	3.9	53.0	282.0
33	7.4	21.1	220.0	6.4	3.2	57.0	277.0

Table A.2: Continuetion of Table A.1

n	τ[hrs]	$l_o[\AA]$	$l_{max}[\AA]$	$\Gamma \cdot [10^{-3}(hrs)^{-3}]$
3.0	7.21	47	274	2.55
2.6	7.33	47	277	–

Table A.3: Parameters obtained fitting the model (with n = 3 and 2.6) for the system CCl_4 on CH_3/Si with two CCl_4 layers.

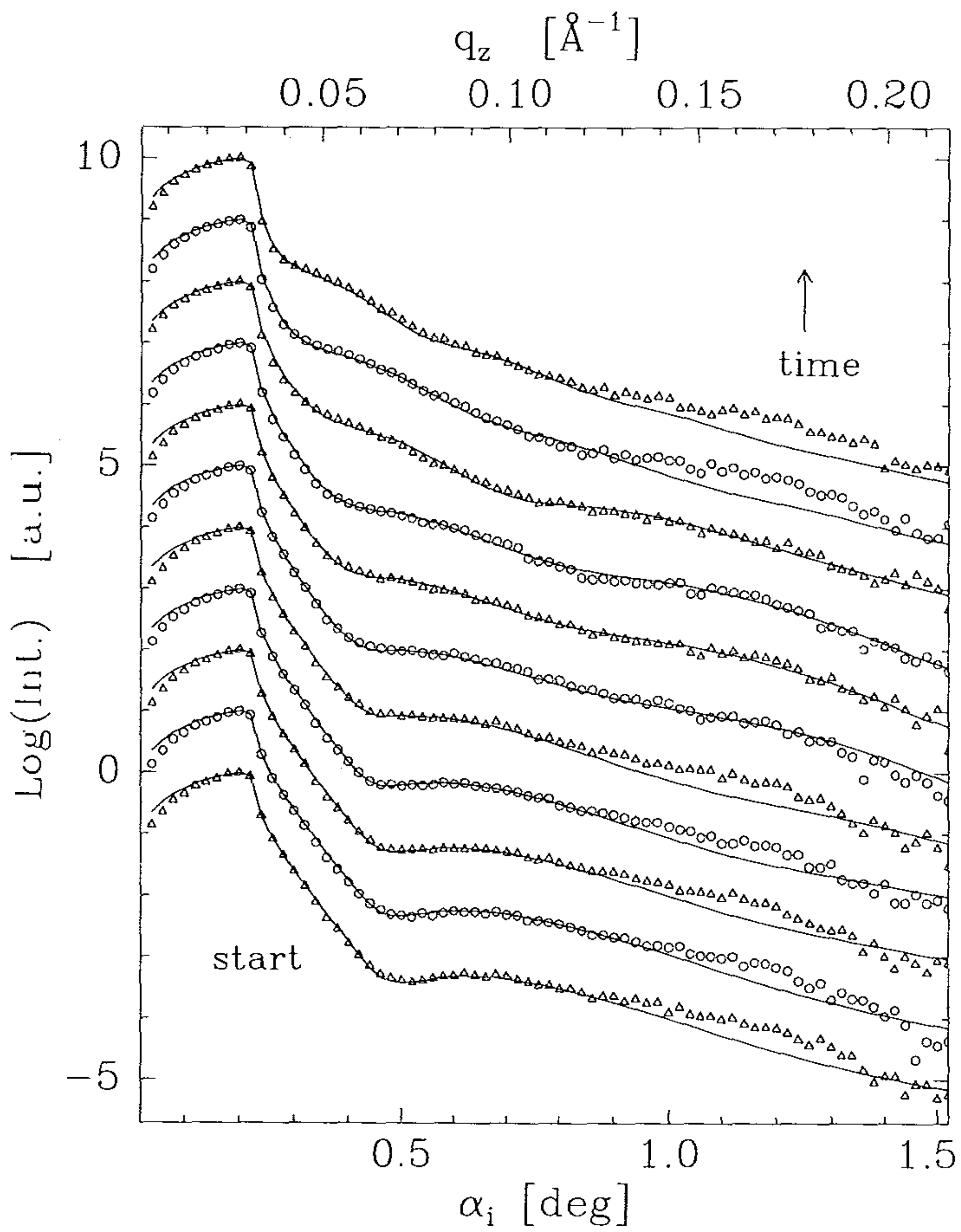

Figure A.2: *Wetting reflectivities (open circles and triangles) and fit results of the system CCl_4 on CH_3/Si for the first 5.74hrs assuming a two layer of the wetting film.*

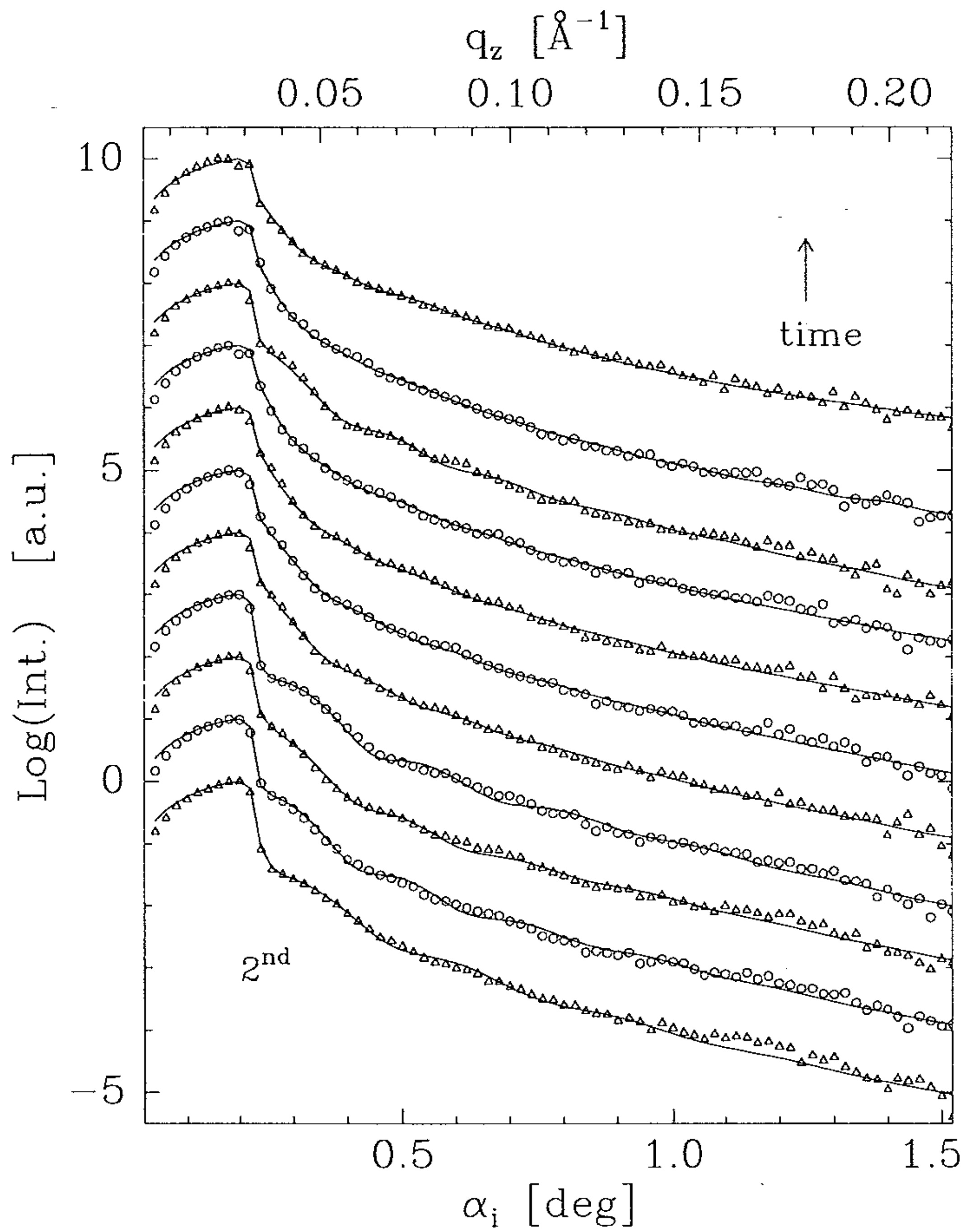

Figure A.3: *Continuation of Fig.(A.2) for the second 5.74hrs.*

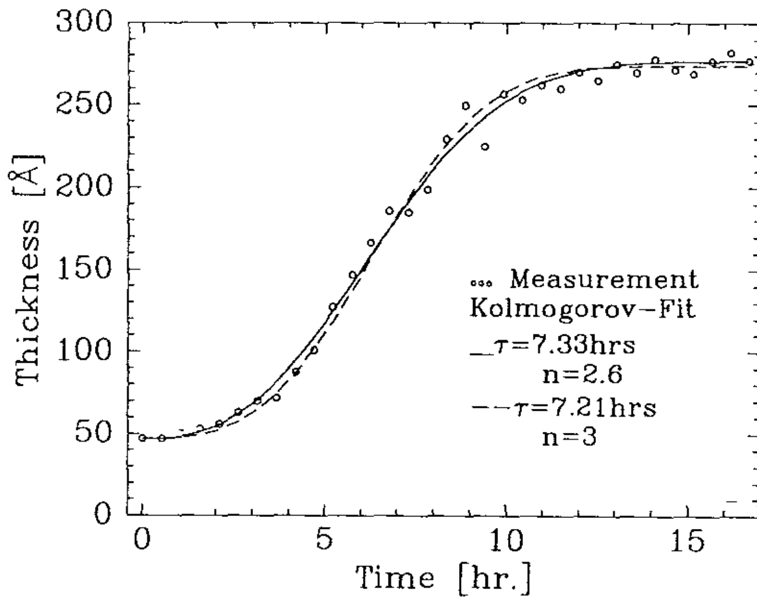

Figure A.5: *Measured and the Kolmogorov fit results for the system CCl_4 on CH_3/Si assuming a two CCl_4 layers.*

References

[1] M.Avrami: Kinetics of phase change.I. J.Chem.Physics. **7**: 1103(1939).

[2] M.Avrami: Kinetics of phase change.II. J.Chem.Physics. **8**: 212(1940).

[3] J.H.Awbery: A university text-book of physics, vol.**III**. Heat, Charles Griffin and Company Limited. London(1952).

[4] J.D.Axe and Y.Yamada: Scaling relations for grain autocorrelation functions during nucleation and growth. Phys.Rev.B **34**: 1599(1986).

[5] L.Bruegemann, R.Bloch, W.Press and M.Tolan: Resolution investigations of x-ray three-crystal diffractometers. Acta.Cryst.A **48**: 688(1992).

[6] CRC: Handbook of chemistry and physics. 66th edition. CRC press, Boca Raton(1986).

[7] M.D.Croucher: A simple expression for the Hamaker Constant of liquid like materials. Colloid and Polymer Sci., **259**: 462(1981).

[8] S.Dietrich: Wetting Phenomena. in: Phase transition and critical phenomena, edited by C.Domb. J.L.Lebowitz, vol.12. Academic Press. New York(1988).

[9] H.Dosch, in Critical Phenomena at Surfaces and Interfaces (Evanescent X-Ray and Neatron Scattering). edited by G.Hhler. Springer Tracts in Modern Physics Vol. 126 Springer-Verlag, Berlin(1992)

[10] J.Frenkel: Kinetic theory of liquids, Dover, New York(1955).

[11] P.G.de Gennes: Wetting statics and dynamics, Revs. Mod. Phys.,**57**: 827(1985).

[12] Gmelin: Gmelins Handbuch der anorganischen chemie. vol. C D2. Hrsg.vom Gmelin-Institut, 8.Auflage. Weinheim: Verlag-Chemie(1950).

[13] J.Gregory: The calculation of Hamaker Constants, Adv.Coll.Int.Sci., **2**: 396(1969).

[14] H.C.Hamaker: Physica **4**: 1058(1937).

[15] N.Hamaya, Y.Yameda, J.D.Axe, D.P.Belanger and S.M.Shapiro: Neutron

scattering study of the nucleation and growth process at the pressure-induced first order phase transformation of RbI. Phys.Rev.B **33**: 7770(1986).

[16] International tables for x-ray crystallography. vol.3, Kynoch press. Birmingham (1974).

[17] J.Israelechvili: Intermolecular and surface forces, second edition. Academic press. London(1991).

[18] R.W.James: The optical principles of the diffraction of x-rays. Woodbridge Connecticut Ox-Bow Press(1962).

[19] A.N.Kolmogorov: On the statistical theory of metal crystallization. Bull. Acad. Sci. U.S.S.R., Phys. Ser. **3**: 355(1937).

[20] Landolt-Boernstein: Zahlenwerte und Funktionen aus Physik. Chemie. Astronomie. Geophysik und Technik. Springer Verlag: Berlin, Heidelberg. New York(1950).

[21] J.Lekner: Theory of reflection. Martinus Nijhoff Publisher. Dordrecht/Boston/ Lancaster(1987).

[22] E.M.Lifshitz: The theory of molecular attractive forces between solids. Zh.Eksperim. i Teor.Fiz. **29**: 94(1955).

[23] J.Mahanty and B.W.Ninham: Dispersion forces. Academic Press. New York(1976).

[24] A.D. McLachlan: Proc. R.Soc.Lond.Ser.A **202**: 224(1963).

[25] P.Mueller-Buschbaum: Untersuchung des Benetzungsverhalten von Tetrachlorkohlenstoff auf Si(100) mittels Roentgenbeugung, Diploma Thesis. University Kiel(1992).

[26] P.Mueller-Buschbaum, M.Strzekzyk. M.Tolan and W.Press: X-ray study of growing wetting films, Z.Phys.B **98**: 89(1995).

[27] P.Mueller-Buschbaum, M.Tolan. W.Press: X-ray study of the wetting behaviour of CCl_4 on Si/SiO_2 surfaces. Z.Phys.B **95**: 331(1994).

[28] L.G.Parratt: Surface studies of solids by total reflection of x-rays. Phys.Rev. **95**: 359(1954).

[29] R.M.Pashley, J.A.Kitchener: Surface forces in adsorbed multilayers of water on quartz, J.Coll.Int.Sci., **71**: 491(1979).

[30] M.O.Robbins, D.Andelman. J.F.Joanny: Phys.Rev.A **43**: 4344(1991).

[31] J.-p.Schlomka, M.Tolan, L.Schwalowsky, O.H.Seek, J.Stettner, and W.Press: X-ray diffraction from Si/Ge layers: Diffuse scattering in the region of total external

reflection. Phys.Rev.B **51**: 2311(1995).

[32] O.H.Seek. P.Mueller-Buschbaum. M.Tolan and W.Press: Diffuse x-ray scattering in the specular direction. Europhys.Lett., **29**: 699(1995).

[33] S.K.Sinha. E.B.Sirota and S.Garoff: X-ray and Neutron scattering from rough surfaces, Phys.Rev.B **38**: 2297(1988).

[34] U.Steiner, J.Klein. E.Eisen. A.Budkowski. L.J.Fetters: Complete wetting from polymer mixtures. Science **258**: 1126(1992).

[35] M.Strzelczyk: Realzeituntersuchung des Wachstums von Benetzungsfilmen. Diploma Thesis. University Kiel(1995).

[36] J.Sueßenbach: Phasendiagramme von Metall-Tetramethylverbindungen adsorbiert auf Graphit(001) im Submonolagenbereich. Dissertation. University Kiel(1995).

[37] I.M.Tidswell. T.A.Rabedeau. and P.S.Pershan: Wetting films on chemically modified surfaces. Phys.Rev.B **44**: 10869(1991).

[38] J.Visser: On Hamaker Constants: A comparison between Hamaker constants and Lifschitz-van der Waals constants. Adv.Coll.Int.Sci. **3**: 331(1972).

[39] C.P.Yang and J.F.Nagle: Phase transformations in lipids follow classical kinetics with small fractional dimensionalities. Phys. Rev.A **37**: 3993(1988).

[40] Y.Yoneda: Anomalous surface reflection of x-rays. Phys.Rev. **131**: 2010(1963).

[41] T.Young: Philos. Trans. R.Soc.Lond. **35**: 95(1805).